

Julius-Maximilians-Universität Würzburg

Fakultät für Biologie



**Vaccinia Virus-mediated Therapy of Solid Tumor
Xenografts: Intra-tumoral Delivery of Therapeutic
Antibodies**

Dissertation

zur Erlangung des naturwissenschaftlichen Doktorgrades der

Julius-Maximilians-Universität Würzburg

vorgelegt von

Ting Huang

aus China

Würzburg, 2013



Eingereicht am: _____

Mitglieder der Promotionskommission:

Vorsitzender: _____

Prof. Dr. W Rössler

Erstgutachter : _____

Prof. Dr. A. A. Szalay

Zweitgutachter: _____

Prof. Dr. G. Krohne

Tag des Promotionskolloquiums: _____

Doktorurkunde ausgehändigt am: _____

Contents

Summary	1
Zusammenfassung	4
Introduction	7
1.1 Cancer	7
1.1.1 Concept and Epidemiology	7
1.1.2 Classification and Morphology	9
1.1.3 Causes of Cancer	10
1.1.4 Stroma in Cancer	13
1.1.5 Conventional and New Oncolytic Therapy	16
1.2 Fibroblast Activation Protein	19
1.2.1 History and Concept	19
1.2.2 Structure, Bio-Distribution and Function	19
1.2.3 Clinical Implication of FAP in Patients	20
1.2.4 Strategies of Targeting FAP	21
1.3 Epithelial Growth Factor Receptor	22
1.3.1 Concept	22
1.3.2 Structure, Bio-distribution and Function	22
1.3.3 Clinical Implication of EGFR in Patients	24
1.3.4 Strategies of Targeting EGFR	25
1.4 Vascular Endothelial Growth Factor	26
1.4.1 Concept	26
1.4.2 Structure, Bio-distribution and Function	26
1.4.3 Clinical Implication of VEGF in Patients	27
1.4.4 Strategies of Targeting VEGF	28
1.5 Vaccinia Virus	30
1.5.1 Nomenclature	30
1.5.2 Taxonomy and Morphology	30

1.5.3 Vaccinia Virus Replication Cycle	32
1.5.4 Recombinant VACV Used in This Study	34
1.6 Aims of the Study	38
Materials.....	40
2.1 Antibodies	40
2.2 Buffers.....	41
2.3 Cell Lines and Cell Culture Media	48
2.4 Chemicals and Enzymes.....	49
2.5 Kits	54
2.6 Laboratory Animals	55
2.7 Laboratory Equipment and Other Materials	56
Methods	60
3.1 Generation of Recombinant Vaccinia Viruses (VACVs).....	60
3.1.1 Cloning of Plasmids Encoding anti-EGFRVHHFLAG	60
3.1.2 Co-transfection of Plasmids with the Parental Virus GLV-1h68 or GLV-1h164.....	61
3.1.3 Plaque Selection.....	61
3.1.4 Screening for Marker Gene Expression	62
3.1.5 Screening for GPT	63
3.1.6 DNA Extraction from Viruses	63
3.1.7 Amplification and Purification of Recombinant Viruses	64
3.2 Virological Methods.....	65
3.2.1 Infection of Cells with Vaccinia Virus	65
3.2.2 Determination of Viral Titers by Standard Plaque Assay	65
3.2.3 Viral Replication Assay	66
3.2.4 Viral Cell Killing Ability Assay.....	66
3.3 Molecular Methods.....	67
3.3.1 Polymerase Chain Reaction (PCR)	67
3.3.2 Agarose Gel Electrophoresis	67

3.4 Protein Analytical Methods.....	68
3.4.1 Preparation of Soluble Protein from Mammalian Cells	68
3.4.2 Protein Quantification	68
3.4.3 SDS-PAGE	69
3.4.4 Transfer Protein to PVDF Membrane (Western blot)	69
3.4.5 Colorimetric Immunodetection	70
3.4.6 ELISA	70
3.5 <i>In Vivo</i> and <i>Ex Vivo</i> Studies	72
3.5.1 Establishment of Xenograft Tumor Models	72
3.5.2 Antibody Injection (Avastin and Erbitux)	73
3.5.3 Anesthesia and Blood Collection from Orbital Sinus.....	73
3.5.4 Detection of Virus-encoded Marker Gene RUC-GFP Expression.....	74
3.5.5 Tumor and Organ Preparation for Virus Titration.....	74
3.5.6 Histology Analysis of Tumors - Paraffin Embedded Slides	75
3.5.7 Histological Analysis of Tumors - Agarose Embedded Slides.....	75
Results	77
4.1 Anti-fibroblast Activation Protein Single Chain Antibody GLAF-5 Encoded by Oncolytic Vaccinia Virus Significantly Increases Antitumor Therapy (Part 1).....	77
4.1.1 Construction of Recombinant VACVs Encoding GLAF-5.....	77
4.1.2 Expression of GLAF-5	79
4.1.3 Purification of GLAF-5	80
4.1.4 GLAF-5 Does Not Inhibit DPP Activity of FAP	81
4.1.5 GLAF-5 Shows Increased Viral Replication Efficiency.....	83
4.1.6 GLAF-5 Shows Increased Cell Killing Ability.....	84
4.1.7 GLAF-5 Enhances VACV-mediated Antitumor effects in “Responder” Tumor Xenograft Models	85
4.1.8 GLAF-5 Enhances VACV-mediated Antitumor effects in “Non-responder” Tumor Xenograft Model	86
4.1.9 GLAF-5 is Present in Mouse Serum	87

4.1.10 GLAF-5 Does Not Cause Toxicity.....	88
4.1.11 Virally Expressed GLAF-5 Enhances VACV Replication in Tumors	89
4.1.12 Virally Expressed GLAF-5 Reduces Tumor Vascularity and Stromal Cellularity.....	96
4.2. Anti-EGFR Nanobody Encoded by Vaccinia Virus Significantly Enhances Antitumor Therapy (Part 2).....	100
4.2.1 Combined Treatment of GLV-1h68 with Erbitux Enhances Antitumor Therapy in A549 Xenograft Model	100
4.2.2 Construction of GLV-1h442 Encoding the Anti-EGFRVHHFLAG Nanobody	101
4.2.3 Expression of Anti-EGFRVHHFLAG Nanobody in GLV-1h442-infected Cells.....	102
4.2.4 Purification of Anti-EGFRVHHFLAG Nanobody.....	103
4.2.5 Purified Anti-EGFRVHHFLAG Nanobody Decreases Phosphorylation of EGFR in Cells.....	104
4.2.6 Anti-EGFRVHHFLAG Nanobody Does Not Alter Viral Replication Efficiency	105
4.2.7 Anti-EGFRVHHFLAG Nanobody Does Not Alter Cell Killing Activity	106
4.2.8 Anti-EGFRVHHFLAG Nanobody Enhances Antitumor Effects in A549 and DU145 Human Xenograft Models	107
4.2.9 Anti-EGFRVHHFLAG Nanobody Does Not Cause Toxicity in A549 and DU145 Human Xenografts.....	109
4.2.10 Virally Expressed Anti-EGFRVHHFLAG Nanobody is Present in Serum of GLV-1h442-treated Mice	110
4.2.11 Virally Expressed Anti-EGFRVHHFLAG Nanobody Does Not Change Viral Distribution.....	111
4.2.12 Virally Expressed Anti-EGFRVHHFLAG in GLV-1h442-colonized Tumors Inhibits Cell Proliferation	114
4.3 Expression of Anti-VEGF Antibody Together with Anti-EGFR or Anti-FAP Drastically Enhances Tumor Regression As a Result of Vaccinia Virotherapy (Part 3).....	116

4.3.1 Construction of Two Antibodies Expressing VACVs	116
4.3.2 Expression of Two Antibodies.....	117
4.3.3 Two Antibodies Expressing VACVs Exhibit Reduced Virus Replication Efficiency	119
4.3.4 Two Antibodies Expressing VACVs Exhibit Reduced Viral Cell Killing Efficiency	120
4.3.5 Two Antibodies Expressing VACVs Reduce Tumor Growth in Human Xenograft Models.....	122
4.3.6 Virally Expressed Antibodies are Detectable in Serum of Mice.	126
4.3.7 Expression of Two Antibodies by VACVs Does Not Alter Viral Tissue Distribution in Mice	128
4.3.8 Two Antibodies Expressing VACVs Suppress Cell Proliferation.....	131
4.3.9 Two Antibodies Expressing VACVs Suppress Angiogenesis.....	132
Discussion.....	135
5.1 Against FAP scAb Encoded by VACV Significantly Enhances Virotherapy ..	135
5.2 Against EGFR Nanobody Encoded by VACV Significantly Enhances Virotherapy	139
5.3 Expression of Anti-VEGF Antibody in Combination with Anti-EGFR or Anti-FAP Dastically Improves Virotherapy.....	142
5.4 Conclusion	145
References	149
Abbreviations	156
Publication.....	161
Curriculum Vitae.....	162
Acknowledgements	163
Eidestättliche Erklärung.....	165

Summary

Over the past 30 years, much effort and financial support have been invested in the fight against cancer, yet cancer still represents the leading cause of death in the world. Conventional therapies for treatment of cancer are predominantly directed against tumor cells. Recently however, new treatments options have paid more attention to exploiting the advantage of targeting the tumor stroma instead.

Vaccinia virus (VACV) has played an important role in human medicine since the 18th century as a vaccination against smallpox. In our laboratory, the recombinant, replication-competent vaccinia virus, GLV-1h68, was shown to enter, colonize and destroy cancer cells both in cell culture, and *in vivo*, in xenograft models (Zhang, Yu et al. 2007). In addition, combined therapy of GLV-1h68 and anti-VEGF immunotherapy significantly enhanced antitumor therapy *in vivo* (Frentzen, Yu et al. 2009).

In this study, we constructed several new recombinant VACVs carrying genes encoding different antibodies against fibroblast activation protein (FAP) in stroma (GLV-1h282), nanobody against the extracellular domain of epidermal growth factor receptor (EGFR, GLV-1h442) or antibodies targeting both vascular endothelial growth factor (VEGF) and EGFR (GLV-1h444) or targeting both VEGF and FAP (GLV-1h446).

The expression of the recombinant proteins was first verified using protein analytical methods, SDS-gel electrophoresis, Western blot analysis, immunoprecipitation (IP) assays and ELISA assays. The proteins were detected after infection of the cells with the different VACVs and the recombinant proteins purified by affinity adsorption. The purified antibodies were shown to specifically bind to their respective antigens.

Secondly, the infection and replication capability of all the virus strains was analyzed in cell culture using several human tumor cell lines (A549, FaDu or DU145), revealing that all the new recombinant VACVs were able to infect cancer cells with comparable efficiency to the parental viruses from which they were derived.

Thirdly, the antitumor efficacy of the new recombinant VACVs was evaluated *in vivo* using several human cancer xenograft models in mice. In A549 and DU145 xenografts, the new recombinant VACVs exhibited an enhanced therapeutic efficacy compared to GLV-1h68 with no change in toxicity in mice. In the FaDu xenograft, treatment with GLV-1h282 (anti-FAP) significantly slowed down the speed of tumor growth compared to GLV-1h68. Additionally, treatment with the recombinant VACVs expressed the various antibodies achieved comparable or superior therapeutic effects compared to treatment with a combination of GLV-1h68 and the commercial therapeutic antibodies, Avastin, Erbitux or both.

Next, the virus distribution in tumors and organs of treated mice was evaluated. For most of the viruses, the virus titer in tumors was not significantly different than GLV-1h68. However, for animals treated with GLV-1h282, the virus titer in tumors was significantly higher than with GLV-1h68. This may be the reason for enhanced antitumor efficacy of GLV-1h282 *in vivo*.

Lastly, the underlying mechanisms of therapeutic antibody-enhanced antitumor effects were investigated by immunohistochemistry. Blood vessels density and cell proliferation in tumors were suppressed after treatment with the antibody-encoded VACVs. The results indicated that the suppression of angiogenesis or cell proliferation in tumors may cause the observed therapeutic effect.

In conclusion, the results of the studies presented here support the hypothesis that the treatment of solid tumors with a combination of oncolytic virotherapy and immunotherapy has an additive effect over each treatment alone. Moreover, expression of the immunotherapeutic antibody by the oncolytic VACV locally in the tumor enhances the antitumor effect over systemic treatment with the same antibody.

Summary

Combined, these results indicate that therapy with oncolytic VACVs expressing-therapeutic antibodies may be a promising approach for the treatment of cancer.

Zusammenfassung

In den letzten 30 Jahren wurde viel Aufwand und finanzielle Unterstützung in den Kampf gegen Krebs investiert, doch das Resultat ist limitiert, da Krebs immer noch die zweithöchste Todesursache in der Welt darstellt. Zusätzlich zu gegenwärtig verwendeten Therapien, die vorwiegend gegen Tumorzellen gerichtet sind, wird neuen Therapien mehr Aufmerksamkeit gewidmet, die stattdessen direkt auf das Tumorstroma zielen.

Onkolytische Vaccinia Viren haben seit dem 18ten Jahrhundert als Impfstoff gegen Pocken in der Humanmedizin eine wichtige Rolle gespielt. In unserem Labor hat das rekombinante, replikationskompetente Vaccinia Virus GLV-1h68 gezeigt, dass es in Zellkultur und in Xenograft Modellen in Krebszellen eindringen sowie diese kolonisieren und zerstören kann (Zhang, Yu et al. 2007). Zusätzlich verbessert die kombinierte Therapie von GLV-1h68 und anti-VEGF Immunotherapy signifikant die Antitumortherapie *in vivo* (Frentzen, Yu et al. 2009).

In dieser Studie haben wir mehrere neue rekombinante VACVs konstruiert, die die Gene für verschiedene Antikörper gegen das Fibroblasten Aktivierungs Protein (FAP) im Stroma (GLV-1h282) oder einen Nanobody gegen die extrazelluläre Domäne des Epidermalen Wachstumsfaktor (EGFR; GLV-1h442) kodieren. Ausserdem wurden Viren konstruiert, die eine Ko-Expression von Antikörpern gegen sowohl vaskulären Endothelwachstumsfaktor (VEGF) als auch EGFR (GLV-1h444) oder gegen sowohl VEGF als auch FAP (GLV-1h446) erlauben.

Zunächst wurden SDS-Gelelektrophorese, Western Blot Analyse, Immunpräzipitation (IP) und ELISA Assays durchgeführt, um die Expression der rekombinanten Proteine in Zellen mit proteinanalytischen Methoden zu untersuchen. Die Proteine waren nach Infektion der Zellen mit den verschiedenen VACVs nachweisbar und wurden mittels

des FLAG Tags mit einem IP Kit aufgereinigt. Es konnte gezeigt werden, dass die aufgereinigten Antikörper spezifisch an ihr jeweiliges Antigen binden.

Zweitens wurde die Infektion und Replikationsfähigkeit aller Virusstämme in Zellkultur untersucht (A549, FaDu oder DU145) und mit ihrem jeweiligen Ausgangsstamm GLV-1h68, GLV-1h164, GLV-1h282 oder GLV-1h442 verglichen. Die Ergebnisse zeigten, dass alle neuen rekombinanten VACVs Zellen mit vergleichbarer Effizienz infizieren konnten wie ihre Ausgangsstämme.

Drittens, um die Antitumoreffizienz der neuen rekombinanten Stämme *in vivo* zu testen, wurden verschiedene humane Tumor Xenotransplantat-tragende Nacktmäuse mit verschiedenen VACVs behandelt. In A549 und DU145 Xenotransplantaten zeigten die neuen rekombinanten VACVs erhöhte therapeutische Effizienz verglichen mit dem Ausgangsstamm GLV-1h68, ohne Veränderung der Toxizität in Mäusen. Im FaDu Xenotransplantat verursachte die Behandlung mit GLV-1h68 keine Tumorregression, wohingegen die Behandlung mit GLV-1h282 (anti-FAP) die Geschwindigkeit des Tumorwachstums signifikant verlangsamte sowie das Überleben verlängerte. Zusätzlich haben wir herausgefunden, dass die Behandlung mit Antikörpern, die mittels Virus geliefert wurden, einen identischen oder sogar erhöhten inhibitorischen Effekt erzielen können, wie in einer Kombinationstherapie von GLV-1h68 und kommerziell erhältlichen Antikörpern, wie Avastin, Erbitux oder beidem.

Um die virale Verteilung *in vivo* zu untersuchen, wurden Tumore und Organe von Mäusen seziiert und homogenisiert, gefolgt von Titration der Virusmenge. Die Virus-Titer in Tumoren waren signifikant höher in Tieren, die mit GLV-1h282 behandelt wurden als solche, die mit GLV-1h68 behandelt wurden. Dies mag den Grund für die erhöhte Antitumoreffizienz von GLV-1h282 *in vivo* darstellen. Die Virus-Titer in allen anderen Gruppen zeigten keinen signifikanten Unterschied.

Um den Mechanismus der durch therapeutische Antikörper erhöhten Antitumorthherapie zu untersuchen, wurde Immunohistochemie durchgeführt. Nach

Behandlung mit den Antikörper-kodierenden VACVs waren die Blutgefäßdichte und Zellproliferation in Tumoren reduziert, nachgewiesen durch die jeweilige CD31 and Ki67 Färbung. Die Resultate deuteten an, dass die Suppression der Angiogenese oder der Zellproliferation in Tumoren den beobachteten Effekt verursachen könnte.

Zusammenfassend zeigen die hier präsentierten Daten dass die Kombination der Behandlung von onkolytischer Virotherapie mit Immunotherapie durch Virus-gelieferte Antikörper einen vielversprechenden Ansatz für Krebstherapie darstellt.

Introduction

1.1 Cancer

1.1.1 Concept and Epidemiology

Cancer consists of a group of diseases involving unregulated cell growth, known as malignant neoplasm (<https://en.wikipedia.org/wiki/Cancer>). And it has the ability to become anaplastic, invasive and metastatic (in most cases metastasis to other locations via blood vessels or lymph node vessels).

Cancer is a worldwide disease and GLOBOCAN estimates that 12.7 million new cancer cases occurred worldwide in 2008. (<http://www.cancerresearchuk.org/cancer-info/cancerstats/world/the-global-picture/cancer-overall-world>). The variation in cancer incidence and mortality statistics across different regions of the world are shown (Figure.1). Figure 2 projects the numbers of new cancer cases and deaths in 2013, about 1,660,290 new cancer cases are expected to be diagnosed in 2013. From the above, it would be concluded that cancer is an endemic disease that occurs in populations throughout the world. While the incidence in developed countries appears to be greater than in underdeveloped countries, this could be a reflection of underreporting in countries with limited health care services.

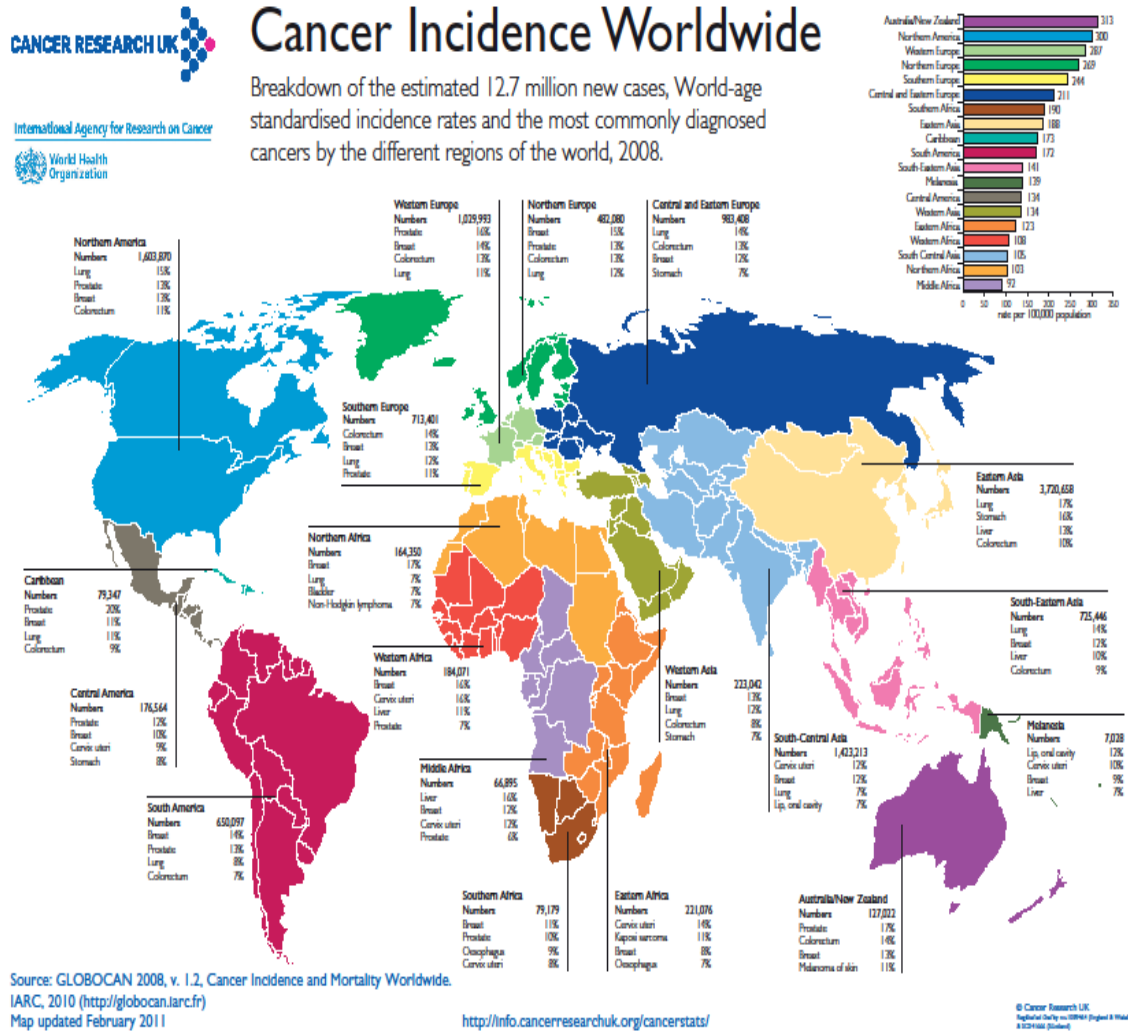


Figure 1 Cancer incidence worldwide

<http://kch.illinois.edu/Research/Labs/CancerEpidemiology/>

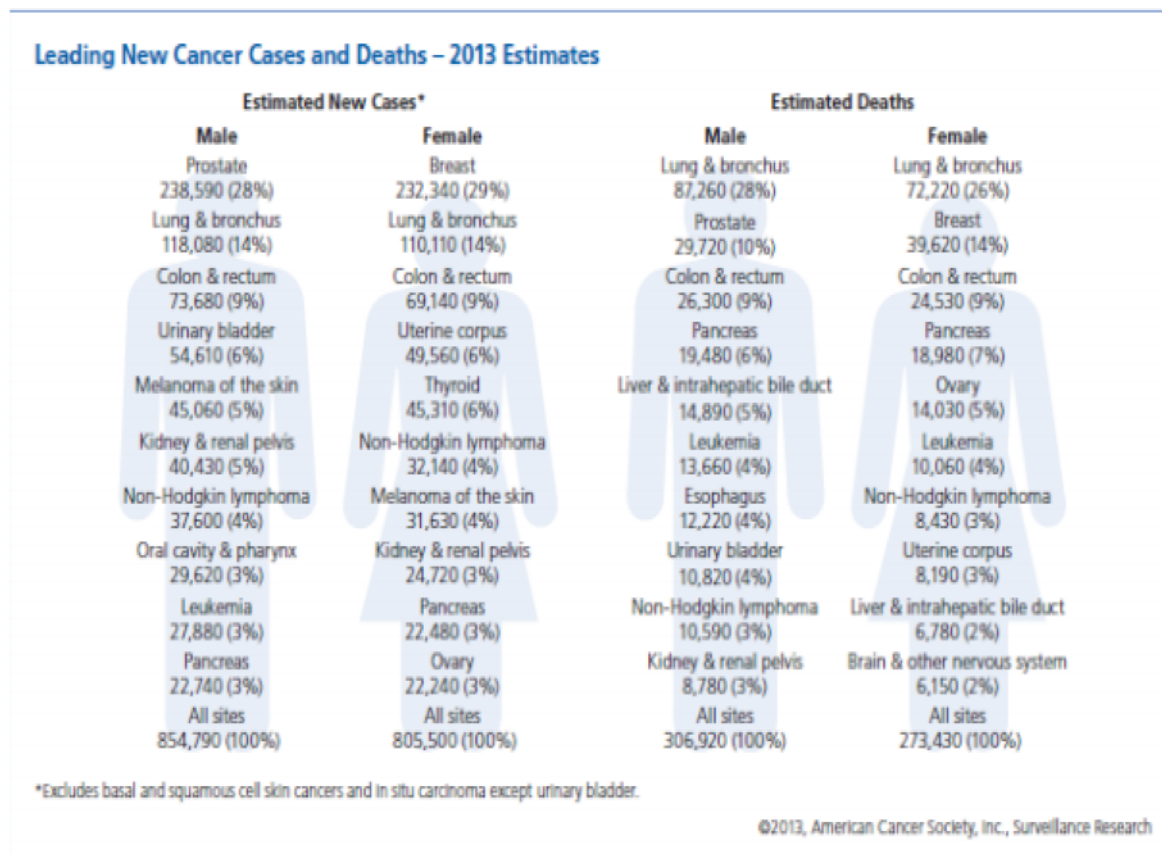


Figure 2 Estimates for new cancer cases and deaths in 2013 (from Cancer Facts & Figures 2013).

1.1.2 Classification and Morphology

Classification of cancer may be based on their primary site of origin or their histological or tissue types.

Classification by Site of Origin: This classification indicates the tissue or organ in which the cancer originated, such as breast cancer, lung cancer, colon cancer, etc.

Classification by Tissue Types: This classification indicates the cell type from which the cancer is derived. For example, carcinoma is derived from the epithelial layer of cells and represents the most common forms of cancer. Sarcoma is derived from cells of connective and supportive tissues including muscles, bones, cartilage and fat or mesenchymal cells. Lymphoma and leukemia are malignancies derived from hematopoietic (blood-forming) cells and myeloma is derived from the plasma cells of bone marrow. Cancers classified as mixed types may be derived from multiple cell types.

Classification by Grade: This classification ranks the cancer with respect to the degree of abnormality of the cancer tissue in comparison with normal tissues. Low to high abnormality is considered as grade 1 to 4.

1.1.3 Causes of Cancer

Today it is well known that cancer is a disease involving both structural and dynamic changes in the genome of the transformed cell, resulting in the cell losing its control over proliferation and growth. However the causes of these changes which are not fully defined are complex and diverse. For example, factors which can increase the risk of cancer range from lifestyle factors such as tobacco use, diet, physical activity and psychological status; certain types of infections like human papillomavirus (HPV) in cervical cancer, hepatitis virus in liver cancer; environmental exposures to different types of chemicals and radiation; and other carcinogens.

Unlike external factors which can be avoided, reduced or used to prevent the development of cancer, there are internal factors that are known to contribute to the cause and development of cancer, including inherited genetic factors (some types of cancer run in certain families), genetic mutations, hormones, immune conditions and effects from dysfunctional metabolic pathways. Oftentimes external and internal

effects act together or in sequence to affect the initiation and development of cancer. Ten years ago, Hanahan and Weinberg proposed that all cancers share six common traits ("hallmarks") that govern the transformation of normal cells to cancerous (malignant or tumor) cells, albeit through various mechanistic strategies (Hanahan and Weinberg 2000). As shown in figure 3, these hallmarks are (clockwise direction): cancer cells stimulate their own growth; they resist inhibitory signals that might control their growth; they invade local tissues and spread to distant sites (metastasis); they acquire the limitless ability to multiply; they stimulate the growth of blood vessels to supply nutrients and assist the growth of tumors (angiogenesis); and they evade their own programmed cell death (apoptosis).

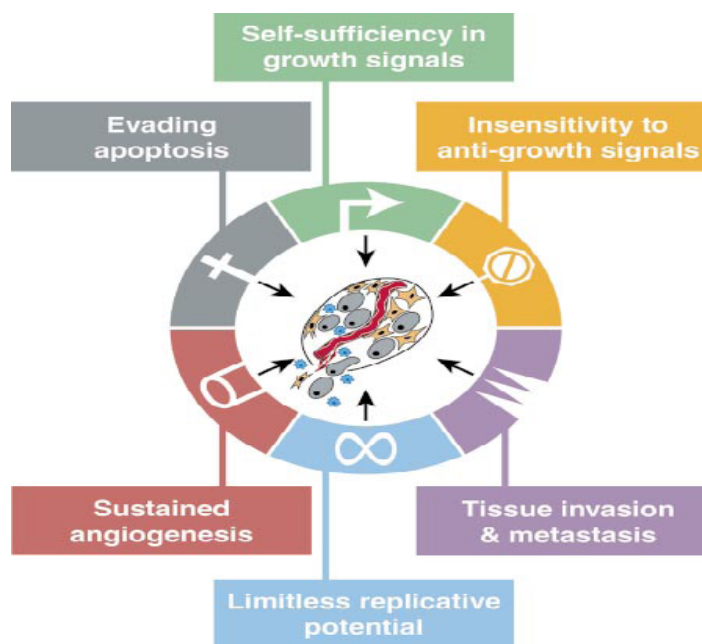


Figure 3 The six hallmarks of cancer (Hanahan and Weinberg 2000).

In 2011, Weinberg and Hanahan proposed 4 new hallmarks: deregulating cellular energy; avoiding immune destruction; tumor promoting inflammation; genome instability (Hanahan and Weinberg 2011) (figure 4). However, initiation and development of cancer is not only the act of tumor cells alone, but rather is

dependent on the assistance of a rich microenvironment in which the microenvironment co-evolves into an activated state through continuous paracrine communication, thus creating a dynamic signaling circuit that promotes cancer initiation and growth, and ultimately leads to a fatal disease (Pietras and Ostman 2010). Indeed, many of the hallmarks of the cancer are provided by various stroma components.

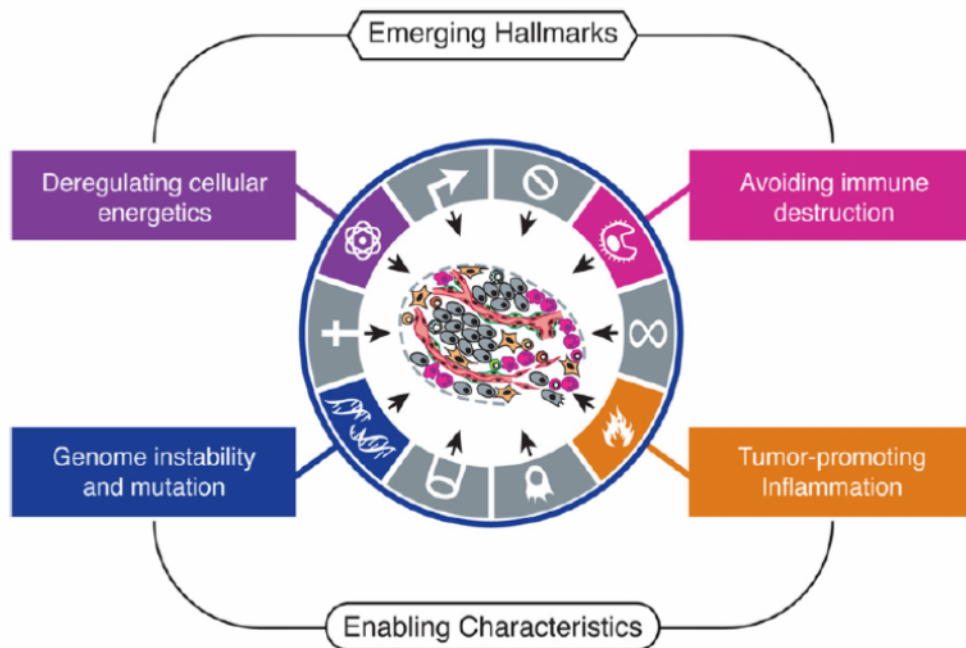


Figure 4 Emerging hallmarks and enabling characteristics (Hanahan and Weinberg 2011).

1.1.4 Stroma in Cancer

Stroma in tumor or cancer comprises a microenvironment consisting of various types of mesenchymal cells and the extracellular matrix (ECM). Within this microenvironment the formation of blood vessels, production of enzymes and regulation of inflammation occurs. It was proven that a solid tumor cannot grow bigger than 1-2 mm in diameter without support of the microenvironment (Folkman, Watson et al. 1989). Cancer cells alter their adjacent stroma to form a permissive and supportive environment for tumor progression, known as the 'reactive' tumor stroma (Mueller and Fusenig 2004).

The stroma in the epithelial parenchyma of carcinomas consists of ECM as well as cellular components such as fibroblasts, immune cells, inflammatory cells, blood-vessel and lymph-vessel cells (Mueller and Fusenig 2004). Figure 5 shows the complex composition in a representative carcinoma tissue (Nyberg, Salo et al. 2008).

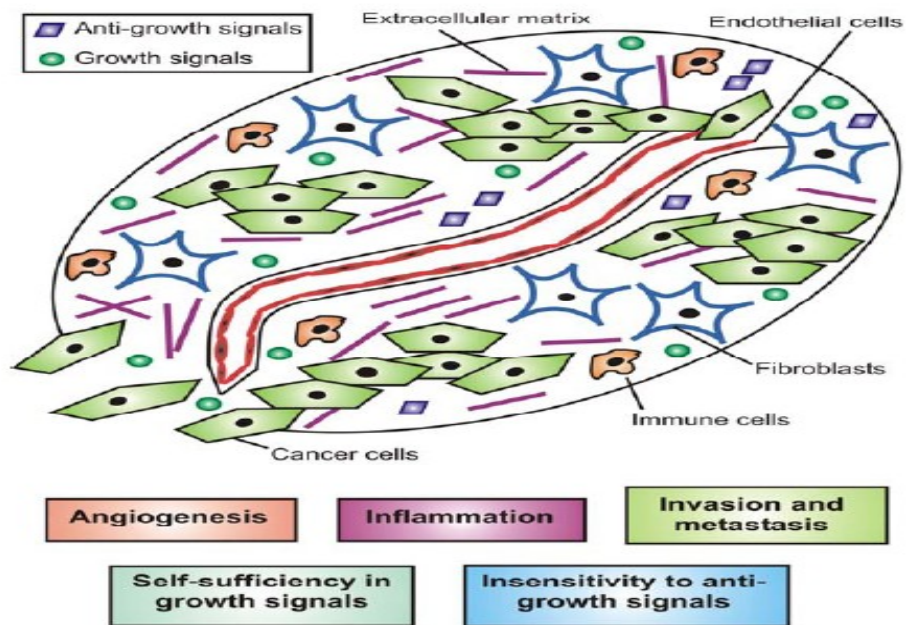


Figure 5 Characteristics of the carcinoma tissue (Nyberg, Salo et al. 2008).

As the importance of the stroma in carcinoma development became more clear, more research focused on the characterization and function of this essential tissue.

Compared to conventional treatments that target only the tumor cells themselves, therapies targeting the stroma have some potential advantages (Pure 2009). The non-transformed cellular components of the stroma are likely to be more genetically stable, thus less prone to develop drug resistance. The stroma promotes tumorigenesis through common mechanisms irrespective of the tumor type, thus providing targets for therapy with the potential to be applied to a broader population of cancer patients. Furthermore, an integrated approach to treating cancer that combines tumor cell-targeted therapies with therapies that act on components of the stroma has the potential for synergistic efficacy without overlapping toxicity. Lastly, therapies targeting the components of host-derived stroma can be studied and developed in human tumor xenograft mouse models.

Consequently, considerable new research and effort to study, design and characterize new cancer treatment strategies have been applied to the cancer stroma. Table 1 shows the recent clinical trials designed to target the stroma (Mueller and Fusenig 2004).

Table 1 Clinical trials designed to target the stroma (Mueller and Fusenig 2004).

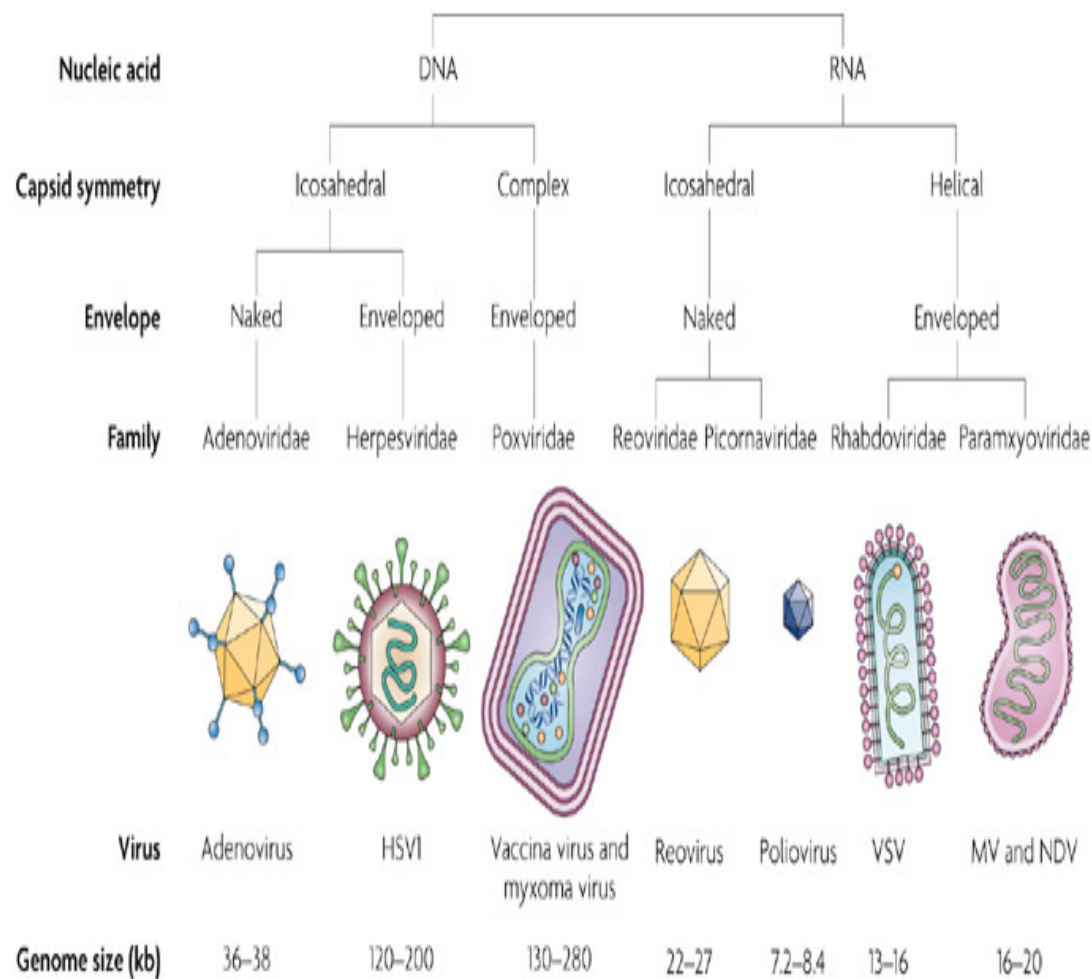
Table 1 Cancer clinical trials designed to target the tumour stroma			
Target	Approach	Clinical trial	Outcome/status
Endothelial cells	Inhibition of VEGF signalling	Phase III for colon carcinoma, lung carcinoma and renal-cell carcinoma; Phase II for lung carcinoma and renal-cell carcinoma	Improved survival for colon carcinoma ¹¹⁰ ; Phase II studies for lung and renal-cell carcinoma show slightly improved survival ^{111,112} , and Phase III trials for these are ongoing*†
	Inhibition of endothelial-cell proliferation by TNP 470, a fumagillin analogue	Phase I/II for lung carcinoma and advanced solid tumours	Drug well tolerated; some patients with partial response ¹¹¹
	Induction of apoptosis in proliferating endothelial cells with tubulin-binding agents	Phase I for thyroid cancer	Ongoing*
Inflammatory cells	NSAIDs	Phase II for colon carcinoma	Ongoing with first beneficial results ¹¹³
ECM components	Local injection of radiolabelled antibodies against tenascin	Phase I and II for glioma	Increased survival ¹¹⁴
ECM/basement-membrane signalling	Antibodies against integrin	Phase I and II for lymphoma, melanoma and glioblastoma	Ongoing*
ECM integrity	MMP inhibitors	Phase I, II, III	Initial results were negative ⁵⁹ ; new components and combinations are in Phase I*
ECM fragments	Injection of endostatin	Phase I	Ongoing ¹¹¹

*For further information, see the National Cancer Institute's Angiogenesis Inhibitors in Clinical Trials web page in the online links box. †For further information, see the Special Project Angiogenesis web page in the online links box. ECM, extracellular matrix; MMP, matrix metalloproteinase; NSAIDs, non-steroidal anti-inflammatory drugs; VEGF, vascular endothelial growth factor.

1.1.5 Conventional and New Oncolytic Therapy

There are a number of methods of treatment of cancer, such as: surgery, chemotherapy, radiation therapy, and immunotherapy. The choice of the treatments depends on the type, location, grade and stage of the cancer as well as the general state, health and financial situation of the patient. Much success in the treatment of cancer has been achieved over the past 30 years, but cancer is still the second greatest cause of mortality in the world. The pursuit and development of new effective methods to treat cancer is still very important and urgent. Conventional therapies oftentimes have severe negative side effects on healthy cells and tissues. An ideal therapy candidate should be highly specific and effective against cancer cells, yet well tolerated by the patient. Now a very promising approach for cancer therapy is under development using oncolytic viruses which naturally target and destroy malignant cells.

Oncolytic virus is a virus that preferentially infects and kills cancer cells. There are several categories of "oncolytic" viruses: wild-type animal viruses that do not typically infect human cells but are cytotoxic to human cancer cells, attenuated mutants of human viruses in which critical genes for virus replication that are dispensable in cancer cells have been deleted or mutated, and viruses that have been attenuated by serial passage in culture, such as most live virus vaccines.



Nature Reviews | Microbiology

Figure 6 Summary of the seven members of oncolytic virus (Cattaneo, Miest et al. 2008).

There are several members of oncolytic virus as shown below (table 2) (Cattaneo, Miest et al. 2008). Oncolytic viruses are effective against a wide variety of human cancers in preclinical models and encouraging results are reported from clinical trials. Oncolytic viruses may also be engineered to deliver therapeutic transgenes. Various mechanisms of antitumoral efficacy of oncolytic virus are shown in table 2 (Wong, Lemoine et al. 2010).

Table 2 Mechanism of antitumoral efficacy of oncolytic virus (Wong, Lemoine et al. 2010).

Mechanism	Examples
1. Direct cell lysis due to viral replication	Adenoviruses Herpes simplex viruses
2. Direct cytotoxicity of viral protein	Adenovirus E4ORF4
3. Induction of antitumoral immunity	
*Nonspecific (e.g., TNF)	Adenovirus (E1A)
*Specific (e.g., CTL response)	Herpes simplex virus
4. Sensitization to chemotherapy and	Adenovirus (E1A)
radiation therapy	Adenovirus (AdTK-RC)
5. Transgene expression	Herpes simplex virus (rRp450)
	Vaccinia virus (GM-CSF)

1.2 Fibroblast Activation Protein

1.2.1 History and Concept

Cancer-associated fibroblasts (CAFs) are the most prominent cell type in the tumor stroma. CAFs are large spindle-shaped mesenchymal cells that share characteristics with smooth-muscle cells and fibroblasts (Alt, Yan et al. 2011). While CAFs are identifiable immunocytochemically based on a combination of different markers, such as the expression of α -smooth muscle actin (α -SMA), vimentin, desmin and fibroblast activation protein (FAP) (Kalluri and Zeisberg 2006; Spaeth, Dembinski et al. 2009; Mifflin, Pinchuk et al. 2011), their origin and functional properties are still undefined (Micke and Ostman 2004; Xing, Saidou et al. 2010; Cirri and Chiarugi 2011).

1.2.2 Structure, Bio-Distribution and Function

FAP, also known as FAP alpha or seprase, is a welldefined marker of CAF and blood vessel-associated pericytes (Kalluri and Zeisberg 2006). It is a 95–kDa type II transmembrane serine protease of 760 amino acids expressed in more than 90% of common human epithelial cancers (Scanlan, Raj et al. 1994; Henry, Lee et al. 2007) as well as in reactive fibroblasts during embryonic development (Niedermeyer, Kriz et al. 2000), in tissues of healing wounds (Mathew, Scanlan et al. 1995), in chronic inflammatory lesions, in cirrhotic liver (Wang, Yao et al. 2008), but not in benign tumors or normal adult tissues (Rettig, Garin-Chesa et al. 1993).

FAP belongs to the post-proline dipeptidyl aminopeptidase family, in which the most closely related member is dipeptidyl peptidase IV (DPPIV/ CD26). CD26 is also a cell surface protein, and is widely expressed in the body (Kelly 2005; Havre, Abe et al.

2008; Pure 2009). The catalytic domain of FAP contains a serine protease consensus sequence. FAP has both dipeptidyl peptidase (Levy, McCaughan et al. 2002; Aertgeerts, Levin et al. 2005) and endopeptidase activity, and has a collagenolytic activity to degrade gelatin and type I collagen (Park, Lenter et al. 1999; Christiansen, Jackson et al. 2007; Aggarwal, Brennen et al. 2008).

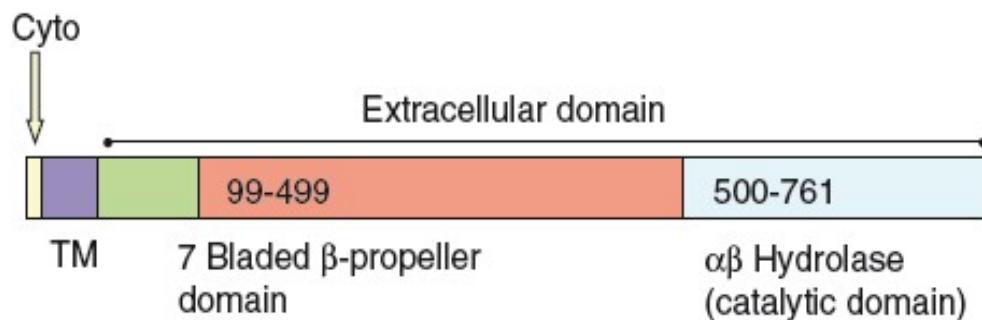


Figure 7 Schematic view of FAP domain structure (Pure 2009). TM means transmembrane.

1.2.3 Clinical Implication of FAP in Patients

Several clinical studies have shown that high level expression of FAP has a relationship with aggressive disease progression and potential development of metastases or recurrence (Iwasa, Jin et al. 2003; Henry, Lee et al. 2007; Cohen, Alpaugh et al. 2008; Dohi, Ohtani et al. 2009). FAP is highly expressed in pancreatic adenocarcinoma with greatest expression immediately adjacent to tumor cells. Higher FAP expression is associated with worse clinical outcome (Cohen, Alpaugh et al. 2008). FAP is consistently expressed in bone and soft tissue tumor cells that are histogenetically related to activated fibroblasts, irrespective of their malignancy (Dohi, Ohtani et al. 2009).

1.2.4 Strategies of Targeting FAP

There are no inhibitors specifically targeting FAP. Some inhibitors that do affect FAP also affect its relative DPPIV or other members in DPP family with the potential clinical side effects since the latter ones are widely expressed in the whole body (Pure 2009; Santos, Jung et al. 2009). LAF237, or vildagliptin, a specific inhibitor of DPPIV, has been developed by Novartis and approved in Europe for treatment of diabetes. Compounds that specifically inhibit FAP have also been described, but their potential to inhibit tumor activity in vivo has not yet been reported. PT100, or talabostat, an inhibitor of multiple members of the DPP family, has been shown to have antitumor and immune-regulatory activities in animal models. PT630, a 'second-generation' inhibitor, is more specific than talabostat, effectively inhibiting FAP and DPPIV but not the intracellular family members due to its lack of cell permeability.

Due to the important role of FAP in stroma, some antibodies targeting FAP have been developed, but to date none have shown clinical potential despite promising results in preclinical studies (Rettig, Su et al. 1994; Mersmann, Schmidt et al. 2001; Cheng, Dunbrack et al. 2002; Scott, Wiseman et al. 2003; Narra, Mullins et al. 2007). F19 is a humanized monoclonal antibody specific for human FAP. It has been proven to be well tolerated in a phase I clinical trial with FAP-positive cancers, but showed no therapeutic efficacy in a phase II trial (Hofheinz, al-Batran et al. 2003; Scott, Wiseman et al. 2003). M036 is a species-cross reactive (human and murine) FAP-specific scAb, which exhibited successfully detection of FAP expression on stroma cells of different human carcinomas as well as on murine host stroma in tumor xenografts, but showed the biologic effects on FAP (Brocks, Garin-Chesa et al. 2001).

1.3 Epithelial Growth Factor Receptor

1.3.1 Concept

The epidermal growth factor receptor (EGFR; ErbB-1; HER1 in humans) is the prototypic member of the class I superfamily of receptor tyrosine kinases (RTKs) and the cell-surface receptor for members of the epidermal growth factor (EGF) family. The EGFR is overexpressed, mutated or dysregulated in many malignancies and is correlated with cancer growth and progression.

1.3.2 Structure, Bio-distribution and Function

EGFR is a 170 kDa protein comprising a ligand-binding region, a single membrane-spanning region and a cytoplasmic intracellular tyrosine kinase containing domain (figure 8) (Harari 2004).

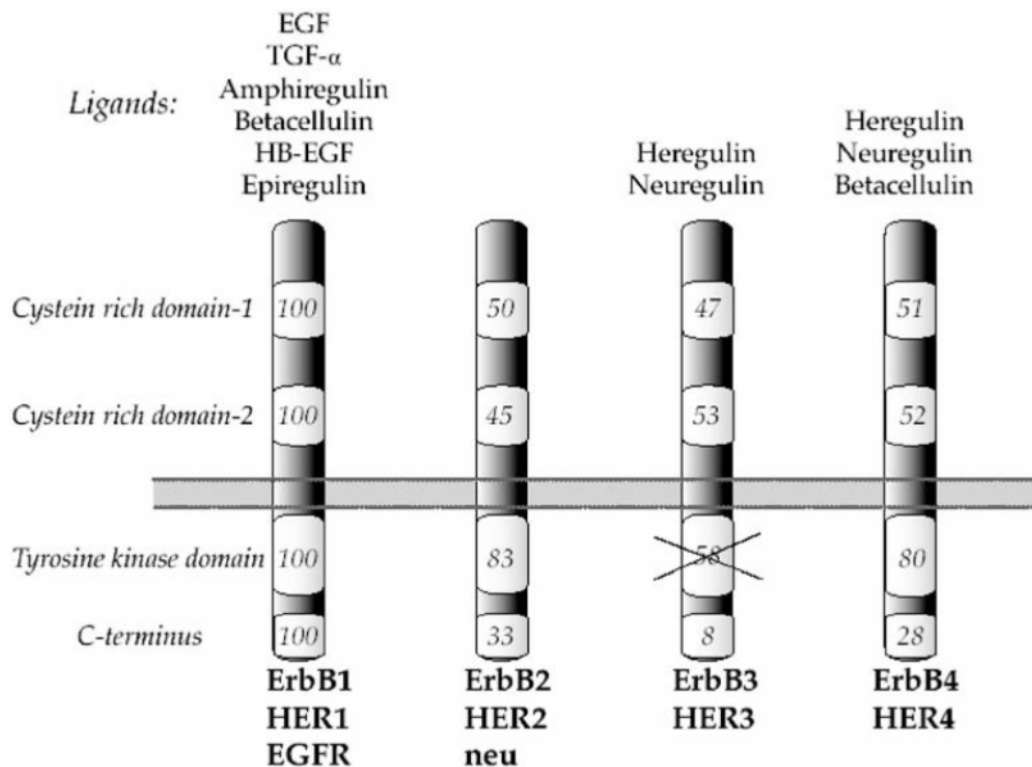


Figure 8 Schematic chart of four members of EGFR family and their ligands (Harari 2004).

EGFR is expressed in various tissues of epithelial, mesenchymal and neuronal origin (Mamot and Rochlitz 2006).

Bound with their distinct ligands, such as EGF, transforming growth factor- α (TGF- α), heparin-binding EGF, amphiregulin, betacellulin, epiregulin and neuregulin G2b, EGFR members form receptor homo or heterodimers followed by phosphorylation of their intracellular tyrosine domain (Watanabe, Shintani et al. 1994; Komurasaki, Toyoda et al. 1997; Wells 1999; Harari 2004). The phosphorylated intracellular sites serve as the stations for a large number of proteins to trigger a cascade of intracellular signaling pathways (figure 9). The integrated intracellular responses to EGFR signaling are multi-directional and pleiotropic, which include mitogenesis, apoptosis,

altered cellular motility, protein secretion and differentiation (Wells 1999; Harari 2004).

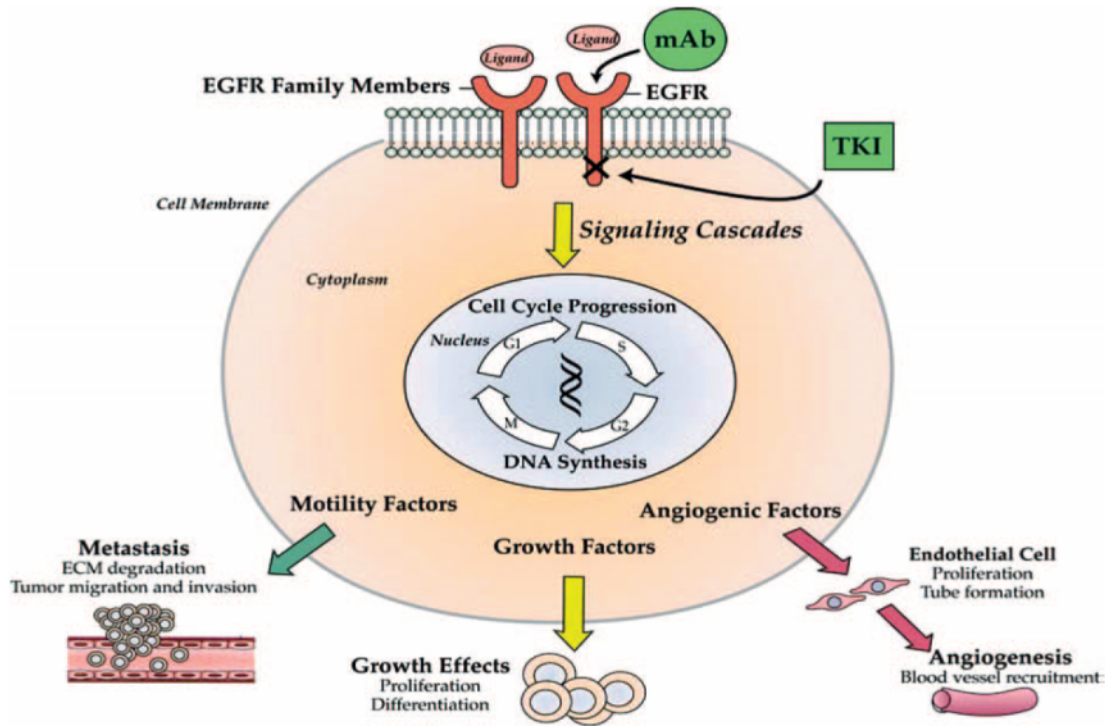


Figure 9 Simplified schematic illustration of the EGFR pathway. The action site for EGFR inhibitors is depicted for mAbs and TKIs (Harari 2004).

1.3.3 Clinical Implication of EGFR in Patients

It is well known that overexpression and dysregulation of EGFR have close correlations with human malignancies, such as bladder cancer, metastatic colon cancer and non-small-cell lung cancer (table 3) (Salomon, Brandt et al. 1995; Nicholson, Gee et al. 2001; Herbst 2002; Mendelsohn and Baselga 2003).

Table 3 Percentage of incidences of overexpression of EGFR in tumors, estimated by tumor type (Harari 2004).

Tumor type	Percentage of tumors
Bladder	31–48
Breast	14–91
Cervix/uterus	90
Colon	25–77
Esophagael	43–89
Gastric	4–33
Glioma	40–63
Head and neck	80–100
Ovarian	35–70
Pancreatic	30–89
Prostate	40–80
Renal cell	50–90
Non-small-cell lung	40–80

1.3.4 Strategies of Targeting EGFR

There are four main strategies for targeting EGFR or blocking its downstream signaling pathways: monoclonal antibodies directly target EGFR, such as *Cetuximab*, *Panitumumab*; small molecules (inhibitors) block tyrosine kinase activation of intracellular domain of EGFR, such as *Gefitinib*, *Erlotinib*; antisense oligonucleotides inhibit EGFR synthesis; antibody-based immunoconjugates for delivery of anticancer agents against EGFR.

1.4 Vascular Endothelial Growth Factor

1.4.1 Concept

Vascular endothelial growth factor (VEGF) is an endothelial cell-specific mitogen *in vitro* and an angiogenic inducer in a variety of *in vivo* models. It is critical for reproductive and bone angiogenesis (Ferrara 2004).

1.4.2 Structure, Bio-distribution and Function

The VEGF receptor family comprises several members (Figure 10): VEGFR-1 (flt-1), VEGFR-2 (KDR flk-1) and VEGFR-3 (flt-4), which consist of seven immunoglobulin-like structures in the extracellular domain, a single transmembrane region, and a consensus tyrosine kinase domain. The accessory receptors neuropilin 1 and neuropilin 2 do not have kinase activity by themselves but enhance VEGFR-2 signaling. The heparan sulfate proteoglycans enhance VEGFR binding and serve as a reserve of VEGF (Hoeben, Landuyt et al. 2004).

The VEGF family currently consists of seven members: VEGF-A, VEGF-B, VEGF-C, VEGF- D, VEGF-E, VEGF-F and PlGF. All of them have a common VEGF homology domain but are preferably expressed in different parts of the body (Hoeben, Landuyt et al. 2004).

VEGF is an important factor with activities in bone marrow and hematopoiesis; enhancement of vascular permeability; improvement of mitogenesis in cells and angiogenesis *in vivo* (Ferrara 2004).

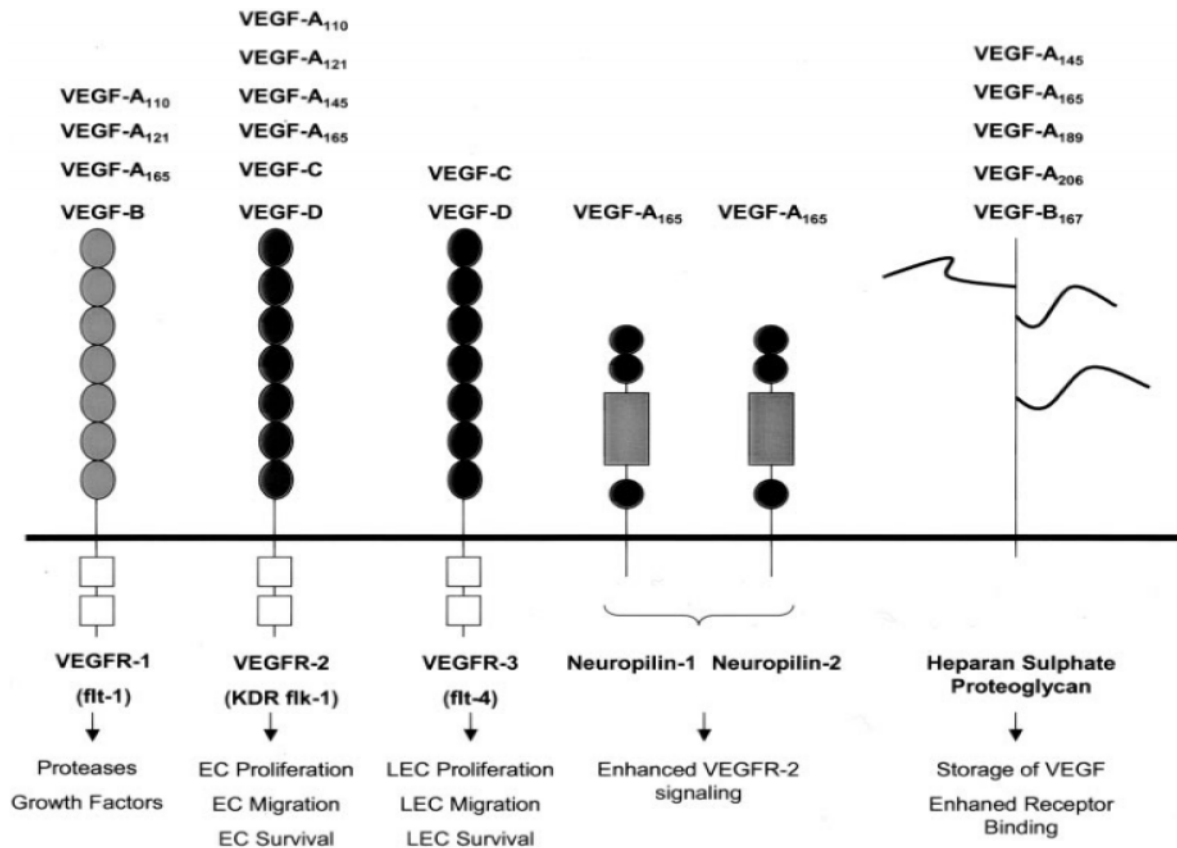


Figure 10 The VEGF receptor family (Hoeben, Landuyt et al. 2004).

1.4.3 Clinical Implication of VEGF in Patients

VEGF has been implicated with poor prognosis in cancers, rheumatoid arthritis, diabetic retinopathy and female reproductive tract, such as polycystic ovary syndrome (Agrawal, Sladkevicius et al. 1998; Tulandi, Saleh et al. 2000; Herbst, Onn et al. 2005; Mercurio, Lipscomb et al. 2005; Pufe, Kurz et al. 2005; Bogaert, Van Damme et al. 2006; Rini and Rathmell 2007).

1.4.4 Strategies of Targeting VEGF

There are two main strategies against VEGF: monoclonal antibody, such as bevacizumab (Avastin) that was approved by the FDA, and antibody derivative ranibizumab (Lucentis); small molecules VEGF: Brivanib alaninate (small molecule TKI: VEGFs, PDGFRs, FGFRs), Aflibercept (recombinant VEGFR fusion protein that binds VEGF A and B, PlGF) (Chang, Garg et al. 2012; Meadows and Hurwitz 2012). Table 4 is the summary of anti-VEGF applications (Chang, Garg et al. 2012).

Table 4 Summary of anti-VEGF applications and properties (Chang, Garg et al. 2012).

Anti-VEGF Agents	Structure	Mechanism of Action	Administration	Efficacy	Side Effects
VEGF antibodies					
- <i>Bevacizumab (Bbv)</i>	Recombinant humanized murine mAb against VEGF-A	Blocks interactions between VEGF-A and receptors (VEGFR-1 and VEGFR-2)	Topical (T) Injection: SC, IO, IV	Partial NV reduction High dose of T comparable to lower dose of SC IO more effective than SC in mice	Epithelial defects (T, SC), subconjunctival hemorrhage (SC), corneal abrasion (IO), corneal stromal edema (IO), RPE tear (IO), retinal detachment (IO), vision loss (IO), lens injury (IO), vitritis (IO), vitreous hemorrhage (IO), endophthalmitis (IO), hypertension (IO), thrombosis (IV)
- <i>Ranibizumab (Rbb)</i>	Fab against all VEGF-A fragments	Blocks the interaction between VEGF-A and receptors (VEGFR-1 and VEGFR-2) *more matured thus higher affinity than Bbv	Injection: Intraocular (IO)	Partial NV reduction	Shorter half-life (may lead to fewer side effects than Bbv, though data not clear) Few studies on corneal NV Uveitis (IO), endophthalmitis (IO), corneal abrasion (IO), vitreous hemorrhage (IO), retinal tear, lens injury (IO), intraocular inflammation (IO), retinal detachment, etc.
- <i>Pegaptanib (Pgb)</i>	RNA aptamer	Blocks the interaction between a specific VEGF-A isoform, VEGF165, and receptors (VEGFR-1 and VEGFR-2)	Injection: Intraocular (IO)	Limited (only binds VEGF165 isoform) Few studies on corneal NV	Reduced risk (limited target) Few studies on corneal NV Endophthalmitis (IO), retinal detachment (IO), lens injury (IO), conjunctival hemorrhage (IO), vitreous hemorrhage (IO), traumatic cataract (IO)
VEGF trap	Fusion of the second domain of VEGFR-1 and the third domain of VEGFR-2 with a human IgG fc fragment	Binds all VEGF-A isoforms and PlGF-1, -2	Injection: S, IO	Partial NV reduction Extended duration in eye *Highest affinity	Hypertension (S), proteinuria (S)
siRNA	Double stranded RNA fragments homologous to target gene (VEGF and its receptors)	Processed by RNAse III (Dicer), fragments incorporated into RNA induced silencing complex (RISC), degrades mRNA sequence-specifically	Intravenous (IV) Subconjunctival (SC)	Targets both the intracellular and extracellular effects of genes Transient effects SC more effective than IV SIRNA-027 human trial completed	Few studies on corneal NV
VEGF Signaling - tyrosine kinase inhibitors	Variable Small molecules	Targets the downstream tyrosine kinase pathway initiated by VEGFR	Orally available	Targets all/most VEGF receptors None FDA-approved for ocular use Pazopanib in clinical trials Sunitinib in animal trials	Few studies on corneal NV Skin toxicity (seen in cancer treatment)

IO = intraocular; IV = intravenous; NV = neovascularization; RPE = retinal pigment epithelium; S = systemic; SC = subconjunctival.

1.5 Vaccinia Virus

1.5.1 Nomenclature

The precise origin of vaccinia virus is unknown due to the lack of records, but it is closely related to the virus that causes cowpox. The original vaccine for smallpox and the idea of vaccination (cowpox) was reported by Edward Jenner in 1796 (Henderson and Moss 1988). The Latin term *variolae vaccinae*, used for Cowpox, is an essential translation of "cowpox-related pox". When it was found that the virus used in smallpox vaccination was not the same as Cowpox virus, a new name "vaccinia" was used for the vaccine-related virus.

1.5.2 Taxonomy and Morphology

Vaccinia virus (VACV) is a large, complex, enveloped virus belonging to the poxvirus family with a linear, double-stranded DNA genome approximately 190 kbp in length that encodes approximately 250 genes. Poxviridae are divided into two subfamilies based on their host range. Entomopoxviridae infects insects and chordopoxviridae infects vertebrates. The subfamily of the chordopoxviridae consists of eight genera: orthopoxviruses, parapoxviruses, avipoxviruses, capripoxviruses, leporipoxviruses, suipoxviruses, molluscipoxviruses and yatapoxviruses (table 5) (Harrison, Alberts et al. 2004). One of the most intensively studied viruses is the vaccinia virus, belonging to the orthopoxviruses.

Table 5 The poxvirus family (Harrison, Alberts et al. 2004).

Subfamily	Genus	Type species
Chordopoxvirinae (vertebrate hosts)	<i>Orthopoxvirus</i>	Vaccinia virus
	<i>Parapoxvirus</i>	Orf virus
	<i>Avipoxvirus</i>	Fowlpox virus
	<i>Capripoxvirus</i>	Sheeppox virus
	<i>Leporipoxvirus</i>	Myxoma virus
	<i>Suipoxvirus</i>	Swinepox virus
	<i>Molluscipoxvirus</i>	Molluscum contagiosum virus
	<i>Yatapoxvirus</i>	Yaba monkey tumor virus
Entomopoxvirinae (insect hosts)	<i>Entomopoxvirus A</i>	Melolontha melolontha entomopoxvirus (MMEV)
	<i>Entomopoxvirus B</i>	Amsacta moorei entomopoxvirus (AMEV)
	<i>Entomopoxvirus C</i>	Chironomus luridus entomopoxvirus (CLEV)

Poxviruses are large DNA viruses which encode a number of envelop and non-envelop proteins like RNA polymerase, transcription factors and with the capability to integrate up to 25 kbp of foreign DNA in their genome (Smith and Moss 1983). The basic infectious form of the poxvirus is the mature virion. The virion has a barrel shape with dimensions of ~360×270×250 nm and the density of the outer layer is comparable to one lipid membrane bilayer. The internal structure of the virion consists of a dumbbell-shaped core and aggregates of heterogeneous material which are called lateral bodies. The inner layer is continuous except for a few channels and has a diameter resembling a lipid membrane. The out layer has a palisade structure that is made of T-shaped spikes that are anchored in the lower membrane. The main components are protein (90%), lipid (5%) and DNA (3.2%). The lipid components of vaccinia virus are predominately cholesterol and phospholipids (Stern and Dales 1974; Sodeik, Doms et al. 1993).

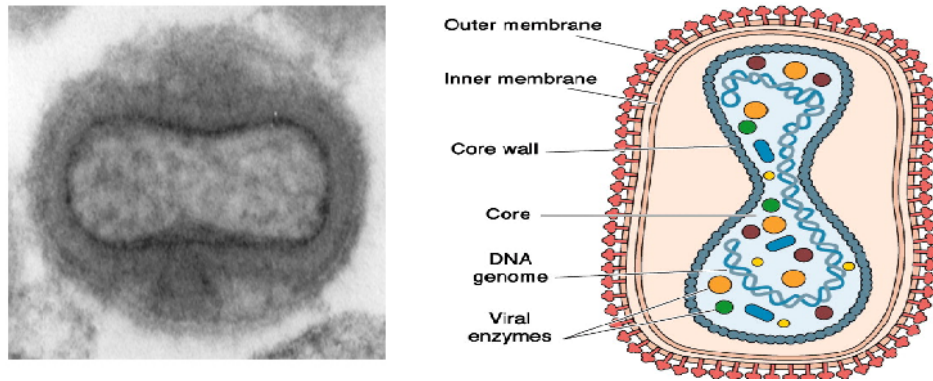


Figure 11 Schematic structure of the vaccinia virus. Morphology of vaccinia virus (left). Transmission electron micrograph of poxvirus virion (right) (from Max-Planck-Institute).

1.5.3 Vaccinia Virus Replication Cycle

One round of infection for most viruses comprises six steps (classical steps): attachment (adsorption), penetration, uncoating, gene expression and genome replication, synthesis of viral mRNA (transcription), synthesis of viral proteins (translation), virion assembly/maturation, release of new infectious virus either by the breakdown of the cell membrane and release of the viruses or "budding" through the cell membrane without necessarily killing the cell.

The life cycle of vaccinia virus follows the classical steps. It is not known exactly how VACV binds the cell membrane. No specific receptor is identified for VACV entry and there are no known cell lines that are completely resistant to VACV entry. After entry, the viral core that contains the necessary proteins for early replication is released into the cytoplasm and transcription and translation start. Vaccinia virus is unique compared to other DNA viruses in that it remains in the cell cytoplasm for the duration of the infectious cycle. Another unusual property of VACV is that it has several virions: intracellular mature virus (IMV), intracellular enveloped virus (IEV),

cell-associated enveloped virus (CEV) and extracellular enveloped virus (EEV). CEV and EEV are basically IMVs with an additional envelope of lipoprotein and have a lower buoyant density than IMV (Blasco and Moss 1992; Smith, Vanderplasschen et al. 2002; Harrison, Alberts et al. 2004).

The replication and assembly of new virus particles is regulated by time-dependent control of gene expression (Rosel and Moss 1985). Figure 12 is the representative picture of the replication cycle of vaccinia virus in one cell (Harrison, Alberts et al. 2004).

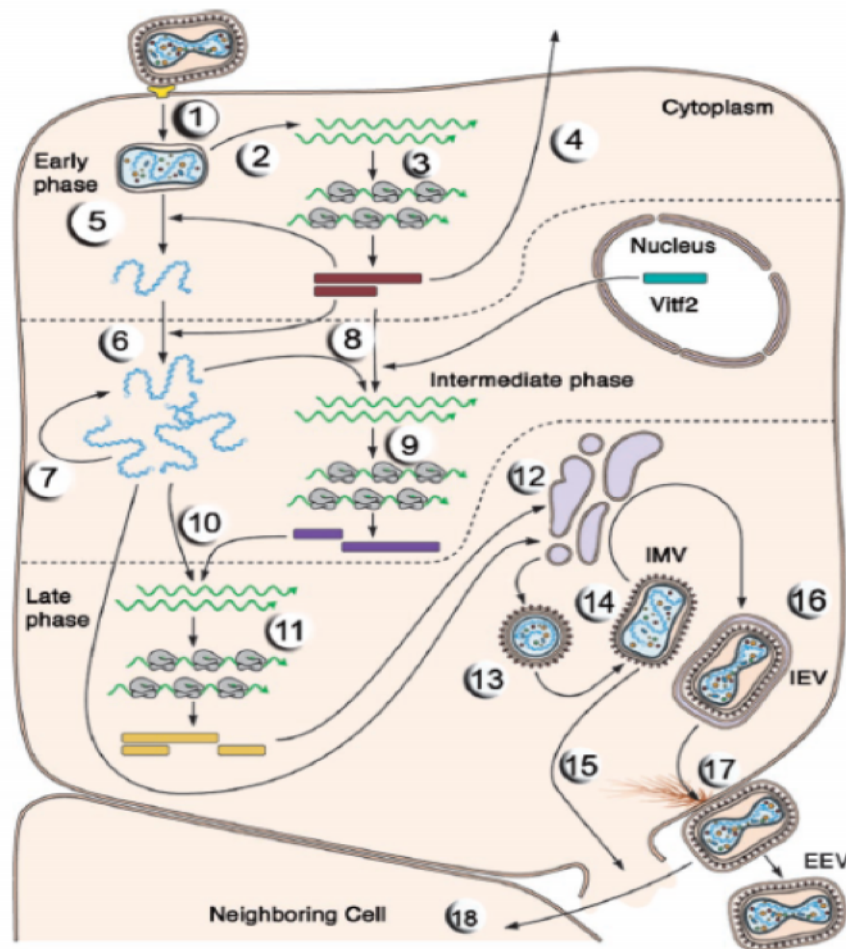


Figure 12 Vaccinia virus life cycle in a single cell (Harrison, Alberts et al. 2004).

1.5.4 Recombinant VACV Used in This Study

The recombinant virus GLV-1h68 is a genetically stable oncolytic vaccinia virus that was constructed by Genelux Corporation (San Diego, CA). It was shown that it can locate, enter, colonize and destroy cancer cells both in cell cultures and in xenograft models (Zhang, Yu et al. 2007). GLV-1h68 was derived from the vaccinia virus Lister strain (LIVP wildtype) and was modified by inserting three expression cassettes into the F14.5L, J2R and A56R loci of the viral genome. They are the Renilla luciferase Aequorea green fluorescent protein fusion gene (*RUC-GFP*), the β -galactosidase gene (*lacZ*) and the β -glucuronidase gene (*gusA*). The *RUC-GFP* fusion protein gene located in the *F14.5L* locus is under control of an early/late promoter whereas the marker gene, β -galactosidase, in the *J2R* locus is under control of the $P_{7.5}$ promoter. Another marker gene coding for β -glucuronidase was inserted into *A56R* locus and is under control of the P_{11k} promoter.

The recombinant viruses GLV-1h282 and GLV-1h442 (figure 13) were derived from GLV-1h68 by replacing the *lacZ* gene in the *J2R* locus with genes encoding anti-fibroblast activation protein, scAb GLAF-5, or anti-EGFRVHHFLAG nanobody, respectively, under the control of P_{SEL} promoters.

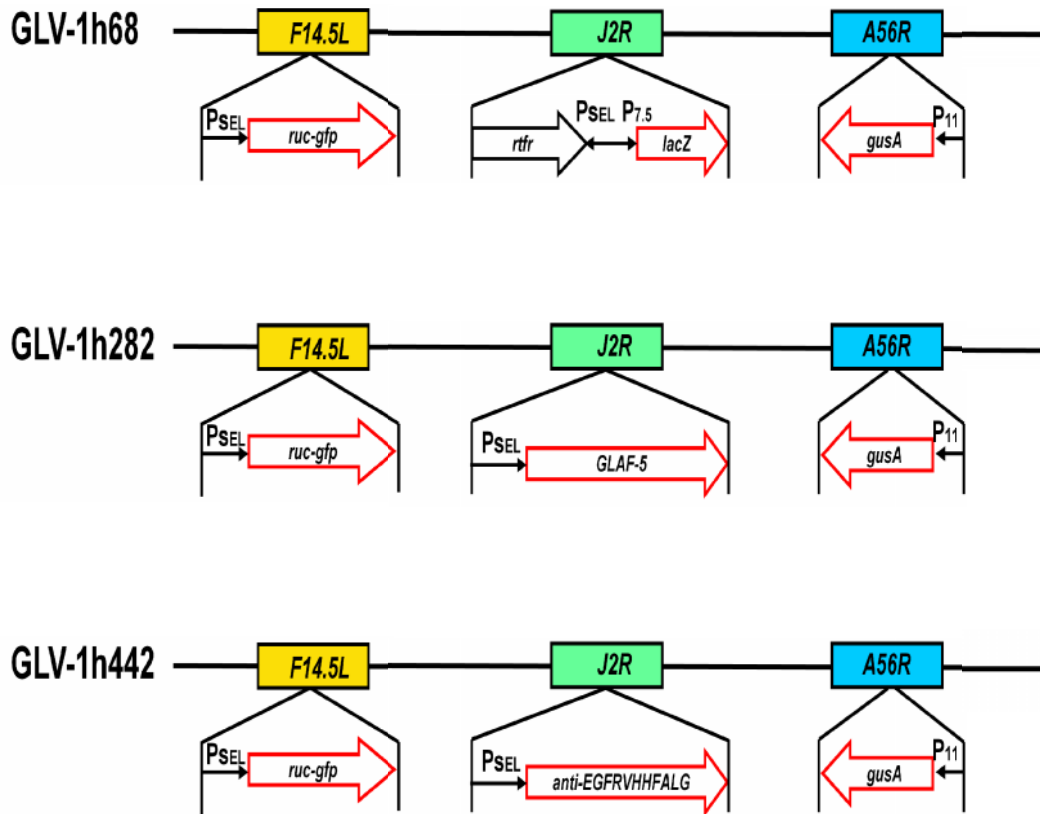


Figure 13 Schematic picture of the new recombinant vaccinia virus GLV-1h282 and GLV-1h442 with GLV-1h68 backbone.

The recombinant virus GLV-1h164 was constructed by inserting into GLV-1h68 the gene encoding the Human Norepinephrine Transporter (hNET) in the *J2R* locus and *GLAF-2* (anti-VEGF scAb antibody) in the *A56R* locus (Chen, Zhang et al. 2009; Frentzen, Yu et al. 2009).

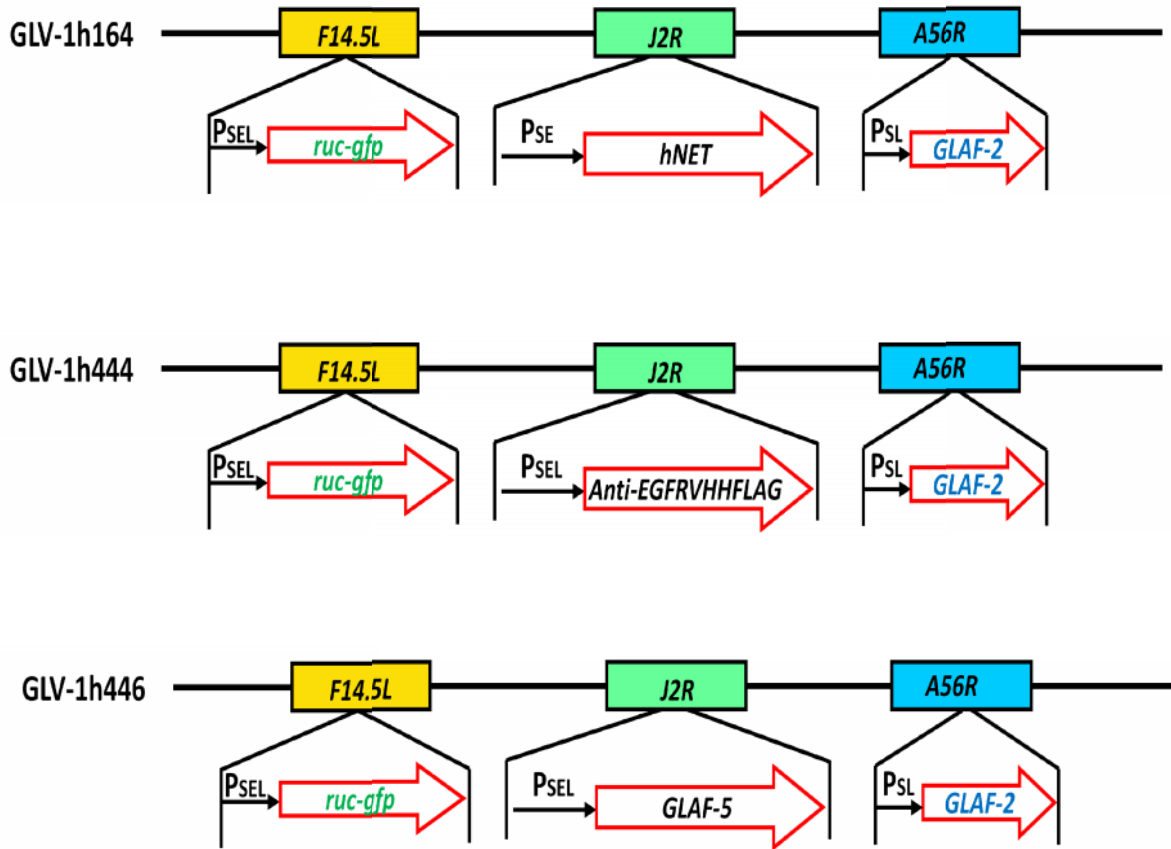


Figure 14 Schematic picture of the new recombinant vaccinia virus GLV-1h444 and GLV-1h446 with GLV-1h164 backbone.

GLV-1h444 and GLV-1h446 are derived from GLV-1h164 by replacing the *J2R* locus with *GLAF-5* (anti-FAP scAb) or *anti-EGFRVHHFALG* nanobody, respectively.

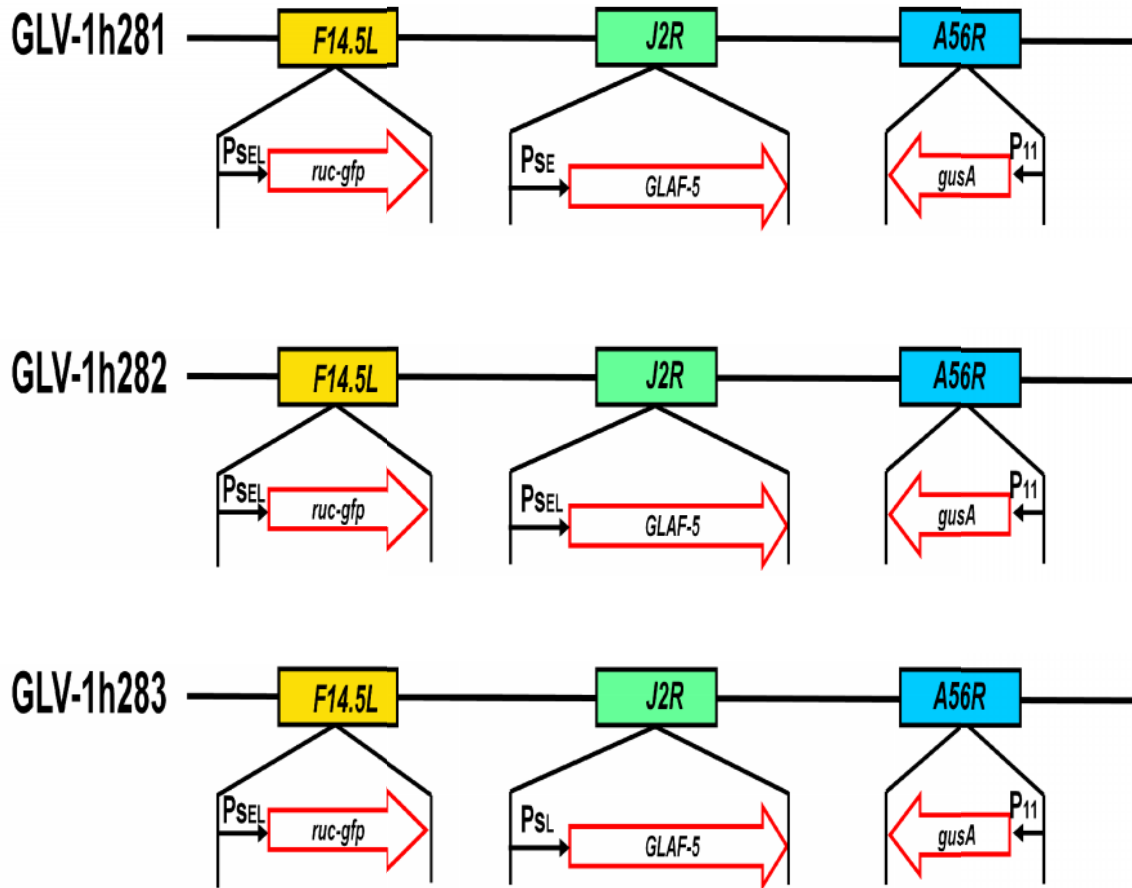


Figure 15 Genomic structures of the new recombinant VACVs expressed anti-FAP scAb under SE, SEL, SL promoters individually.

GLV-1h281, GLV-1h282, GLV-1h283 was derived from GLV-1h68 by replacing the *TFR-LacZ* expression cassette at the *J2R* locus with the *GLAF-5* gene through in vivo homologous recombination, but under SE, SEL, SL promoters individually (figure 15).

1.6 Aims of the Study

Vaccinia virus as the oncolytic virus is an attractive candidate for cancer therapy because of its capability to carry large foreigner genes without comprising its oncolytic activity. Previously our group reported an attenuated live vaccinia virus GLV-1h68, which demonstrated remarkable tumor targeting and oncolytic ability in human tumor xenografts (Zhang, Yu et al. 2007; Yu, Galanis et al. 2009). In addition, preclinical studies demonstrated very promising results of combination virotherapy with chemotherapy or immunotherapy for the treatment and of some cancer types (Frentzen, Yu et al. 2009).

It is well accepted that the stroma in the tumor environment plays a critical role in tumor initiation and development. Here, we conducted experiments to study antitumor therapy with oncolytic virus-mediated virotherapy in combination with antibody-facilitated immunotherapy by utilizing the oncolytic property of VACV to kill tumor cells and the replication property of VACV to continuously produce antibodies which are specifically targeting stroma, such as FAP and (or) VEGF or targeting tumor cells, such as EGFR.

First, the new recombinant VACVs with the respective antibodies were constructed. Second, expression of the antibodies by these recombinant VACVs was tested in cells. Lastly, the effect of overexpression of the antibodies on viral replication efficacy and viral cytotoxicity was evaluated in cells.

The therapeutic efficacy of the new recombinant vaccinia viruses *in vivo* was evaluated. The efficacy of antibody-expressing viruses in tumorous mice was compared with that of the combination therapy with GLV-1h68 plus available commercial antibodies, such as Avastin and Erbitux. The viral toxicity in mice was measured by monitoring the net body weight change. In addition, the viral biodistribution and titers in mouse organs and tumors was evaluated and compared.

In the end, the mechanisms of overexpression of antibodies enhancing antitumor effects were documented, such as their influence on the tumor environment and their change in angiogenesis.

Materials

2.1 Antibodies

Antibody	Source	Manufacturer
anti-CD44	human	BD
anti-CD24	human	BD
anti-LYVE	rabbit	Abcam
anti-Ki67	rabbit	Abcam
anti-CD31	rat	BD
anti-DDDDK	rabbit	Abcam
anti-PECAM-1	goat	Santa Cruz Laboratories
anti-vaccinia A27L	rabbit	Genescript (custommade)
anti- β -actin	mouse	Sigma
anti-mouse IgG peroxidase conjugate	goat	Sigma
anti-rabbit conjugated to HRP	goat	Biorad
anti-fibroblast activation protein	rabbit	Abcam
Phospho-p44/42 MAPK	rabbit	Cell Signaling
Phospho-EGF Receptor (Tyr1068)	rabbit	Cell Signaling
Phospho-EGF Receptor (Tyr845)	rabbit	Cell Signaling

Phospho-EGF Receptor (Tyr1173)	rabbit	Cell Signaling
Rabbit polyclonal IgG	rabbit	Abcam

2.2 Buffers

1 x SDS Buffer:

H ₂ O	83.3 mL
1 M Tris-HCl (pH6.8)	1.0 mL
5 M NaCl	4.0 mL
0.5 M EDTA	0.2 mL
10% SDS	10.0 mL

Before use, add 15 μ L of 10 mg/mL proteinase K and 0.35 μ L β -mercaptoethanol per mL

2 x Triton X-100:

H ₂ O	90.52 mL
0.5 M EDTA	8.0 mL
Triton X-100	1.0 mL

Before use, add 4.8 μ L of β -mercaptoethanol per mL

3.7% Paraformaldehyde:

Paraformaldehyde	18.5 g
PBS	500 mL
Filter through 0.45 micron filter	

40 x Xanthine:

Xanthine	500 mg
NaOH 0.1 N	50 mL
Filter sterilized and store at -20°C	

400 x MPA :

MPA	50 mg
NaOH 0.1 N	5 mL
Filter sterilized and store at -20°C	

670 x Hypoxanthine:

Hypoxanthine	50 mg
NaOH 0.1 N	5 mL
Filter sterilized and store at -20°C	

10 x Gelatin:

NaCl	66.7 g
EDTA	18.6 g
Tris-HCl (pH7.5)	60.5 g
Triton	5 mL
Gelatin	25 g
DdH2O	to 1 L

β -galactosidase Staining Solution:

Solution B	1.5 mL
PBS	0.5 mL
X-Gal	30 μ l

β -glucuronidase Staining Solution:

Solution B	1.5 mL
PBS	0.5 mL
X-Gluc	30 μ L

Citrate Buffer:

Materials

Sodium citrate 0.1 M	4.1 mL
Citric Acid 0.1 mL	9 mL
H ₂ O	450 mL
pH 6	

Crystal Violet Solution:

Crystal violet	1.3 g
Ethanol	50 mL
37% formaldehyde	300 mL
Stir overnight	

Coomassie Staining Solution:

Coomassie Brilliant Blue R-250	0.025 %
Methanol	40 %
Acetic acid	7 %
DdH ₂ O	53 %

Coomassie Distaining Solution:

Methanol	40 %
Acetic acid	7 %

Materials

DdH₂O 53 %

LB Plates:

LB 25 g

H₂O 1 L

Autoclave and pour plates

LB Medium:

LB 25 g

Agar 15 g

H₂O 1 L

Autoclave

Lysis Buffer (tumor or organs):

PBS 50 mL

Protease inhibitor 1 tablet

RIPA Buffer:

NaCl 150 mM

Tris-HCl (pH 7.2) 10 mM

SDS 0.1 %

Materials

Triton X-100	1.0 %
Deoxycholate	1.0 %
EDTA	5 mM

One tablet of Complete Proteinase inhibitors is added to 10 mL RIPA.

For Phosphorylation Western Blot analysis, one PhosSTOP Phosphates Inhibitor Cocktail Tablet is added to 10 mL RIPA

SDS-Loading Buffer:

1 M Tris-HCl pH 6.8	5 mL
Glycerin 20%	10 mL
SDS 4%	20 mL

Solution B:

MgCl ₂	2 mM
K ₃ Fe(CN) ₆	5 mM
C ₆ FeK ₄ N ₆ x 3 H ₂ O	5 mM

Sucrose Solution

Tris-HCl (pH 9.0)	1 mM
Sucrose	according to the concentration

Materials

HyPure Cell Culture dH₂O 1 L

Virus Plaque Overlay Medium:

CMC 15 g

Weighed in 1 L bottle and autoclaved

DMEM 1 L

Antibiotic-antimycotic solution 10 mL

Stir overnight until dissolved

FBS 50 mL

2.3 Cell Lines and Cell Culture Media

A549 cells:	human lung carcinoma (adherent)
CV-1-cells:	green monkey kidney fibroblasts (adherent)
DU145 cells:	human prostate carcinoma (adherent)
FaDu cells:	human hypopharyngeal carcinoma (adherent)
MDA-MB-435:	human breast carcinoma (adherent)

A549 or MDA-MB-435:

RPMI-1640

10% FBS

CV-1:

DMEM

10% FBS

1% Antibiotics-Antimycotics

DU145:

EMEM

10% FBS

1% NEAA

1% Na Pyruvate

FaDu:

EMEM

10% FBS

2.4 Chemicals and Enzymes

<u>Materials</u>	<u>Manufacturer</u>
100 bp DNA Ladder	New England Biolabs
1 kb DNA Ladder	New England Biolabs
β -Mercaptoethanol	Fisher Scientific
3,3',5,5'-Tetramethylbenzidine (TMB) Liquid	
Substrate System for ELISA	Sigma
5-bromo-4-chloro-3-indolyl-b-D-galactopyranoside (X-Gal)	Stratagene
5-bromo-4-chloro-3-indolyl-beta-D-glucuronic acid cyclohexylammonium salt (X-GLCA)	RPI Research Products
6x Orange DNA Loading	Thermo Scientific
Accuprime™ Pfx SuperMix	Invitrogen
Acetic Acid	VWR
Ampicillin	Sigma
Antibiotic-Antimycotic Solution	Cellgro
Benzonase® Nuclease	Novagen
Biorad Protein Assay Standard I	Biorad
Blocker™ Casein in PBS	Pierce
Bromophenol Blue	Aldrich Chemical Company

Materials	Manufacturer
Carboxymethyl Cellulose Sodium Salt	MP Biomedicals
Cadmium Sulfate	Sigma
Casein Blocking Solution	Pierce
Citric Acid	Sigma
Clearslip Mounting Media	IMEB Inc.
Coomassie Brilliant Blue R250	Sigma
Crystal Violet	Sigma
Deoxycholic Acid	Fisher Biotech
Difco™ Agar	BD
Difco™ LB Broth, Miller	BD
DMEM medium 1x	Cellgro
DPBS 1x	Cellgro
EDTA	Fisher Scientific
EMEM medium 1x	Cellgro
Eosin-Y	Richard-Allan Scientific
Ethidium Bromide	Sigma
Fetal bovine serum	Omega Scientific
Formaldehyde	EMD
Formalin 1:10 Dilution, Buffered	Fisher Diagnostics

Materials	Manufacturer
FuGENE [®] Transfection Reagent	Roche
Gelatin	Bio-Rad
Glucose	Cellgro
Glycerol	Fisher Scientific
Hematoxylin QS	Vector
HEPES	Gibco
Holo-Transferrin Human	Sigma
HyClone [®] HyPure [™] Cell Culture Grade Water	Thermo Scientific
Hydrochloric Acid Solution 2N	VWR
Hydrogen Peroxide Solution	Sigma
Tris-HCl	Fisher Scientific
Hypoxanthine	Sigma
Kanamycin	Sigma
Magnesiumchloride	J.T.Baker
Manganese(II)sulfate Monohydrate	Sigma
Methanol, Absolute	Sigma Diagnostics
Modified Mayer's Hematoxylin	Richard-Allan Scientific
Mounting medium	Vector
NuPAGE [®] MOPS SDS 20x Running Buffer	Invitrogen
NuPAGE [®] 20x Transfer Buffer	Invitrogen

Materials	Manufacturer
OmniPur Ethyl Alcohol Pure	EMD
OmniPur® Agarose	EMD
One Shot® TOP10 E. coli	Invitrogen
OPTI-MEM® Medium	Gibco
Pac I	New England Biolabs
Paraplast Tissue Embedding Medium	McCormick Scientific
Paraformaldehyde	Sigma
Phenol:Chloroform:Isoamyl Alcohol 25:24:1	Sigma
Precision Plus Protein™ Standard	Biorad
Proteinase Inhibitor Cocktail Tablets	Roche
PhosSTOP Phosphatase Inhibitor Cocktail Tablets	Roche
Proteinase k	Sigma
Quick T4 DNA Ligase	New England Biolabs
Restriction Enzymes	New England Biolabs
RPMI Medium 1640 1x	Cellgro
Sall	New England Biolabs
S.O.C. Medium	Invitrogen
Sodium Acetate	Fisher Scientific
Sodium Carbonate	Fisher Scientific

Materials	Manufacturer
Sodium Chloride	Fisher Scientific
Sodium Citrate	Fisher Scientific
Sodium Dodecylsulfate (SDS)	Fisher Scientific
Sodium Hydrogencarbonate	Fisher Scientific
Sodium Pyruvate	Cellgro
Sucrose	Sigma
TBE Buffer 10x	Sigma
TMB	Sigma
Trichloroacetic Acid	VWR
Tris (Base)	Fisher Scientific
Tris-Borate-EDTA (TBE) Buffer	Sigma
Triton-X 100	Sigma
Tween-20	Biorad
Xanthine	Calbiochem
Xylene Substitute	Sigma

2.5 Kits

<u>Materials</u>	<u>Manufacturer</u>
Biorad D _C Protein Assay	Biorad
Cell Proliferation Kit II (XTT)	Roche
DNA Clean & Concentrator™ Kit	Zymo Research
DNA-free™ Kit	Ambion
ECL Plus Western Blotting Detection Reagents	GE Healthcare
FLAG® Immunoprecipitation Kit	Sigma
ImmPACT™ DAB Diluent and Chromogen	Vector
Opti-4CN™ Substrate Kit	Biorad
PureLink™ Quick Plasmid Miniprep Kit	Invitrogen
Vectastain ABC Kit Rabbit IgG	Vector
Zero Blunt® TOPO® PCR Cloning Kit	Invitrogen
Zymoclean™ Gel DNA Recovery Kit	Zymo Research

2.6 Laboratory Animals

For *in vivo* experiments, male athymic nude FoxN1 mice were purchased from Harlan. Mice were cared for and maintained in accordance with animal welfare regulations under the approved protocol by the Institutional Animal Care and Use Committee of Explora Biolabs (San Diego Science Center) and of the University of California, San Diego.

The FoxN1 mouse model has an autosomal recessive mutation in the *nu* locus on chromosome 11, which documents hairless phenotype. And its characteristics include dysfunctional rudimentary thymus, T-cell deficient, no generation of cytotoxic effector cells and no graft versus host response, which make this model suitable for oncology, immunology, transplantation and other fields of research (<http://www.harlan.com>).



Figure.1 Phenotype of an athymic nude FoxN1 mouse (<http://www.harlan.com>)

2.7 Laboratory Equipment and Other Materials

<u>Materials</u>	<u>Manufacturer</u>
Balance PL1501-S	Mettler Toledo
Bio Doc-It™ System	UVP
Biosafety Cabinet	The Baker Company Inc.
Cell Culture Cluster 6-well Costar 3516	Corning Inc.
Cell Culture Cluster 24-well Costar 3526	Corning Inc.
Cell Culture Cluster 96-well Costar 3595	Corning Inc.
Cell Culture Flask 75cm ²	Corning Inc.
Cell Scraper	Corning Inc
Cell Spreader	VWR International
Centrifuge Sorvall RC 6 Plus	Thermo
Centrifuge Centra CL2	Thermo
Centrifuge Micro CL 21	Thermo
Combitips Plus 25mL	Eppendorf
Cryotubes 2mL	Nalgene
Digital Caliper	VWR
Digital Dry Bath Incubator	Boekel Scientific
Dish 10cm	Fisher Scientific
Embedding Mold TISSUE-TEK®	IMEB Inc.

Materials	Manufacturer
Falcon 15mL Tubes	BD
Falcon 50mL Tubes	BD
Fluorescence Microscope IX71	Olympus
Heater	VWR International
Hotplate Stirrer 375	VWR Scientific Products
Incubator HERA Cell 150	Thermo Electron Corporation
Incubator Shaker C25	New Brunswick Scientific
Insulin SyringeU-100 29G1/2	BD
MagNA Lyser	Roche
MagNA Lyser Green Beads	Roche
Microfuge Tubes 2.0mL	Avant
Microfuge Tubes Easy Open Cap 1.5mL	Saarstedt
Microplate Reader SpectraMax MS	Molecular Devices
Microscope Cover Glass	Fisher Scientific
Microslides Premium Superfrost®	VWR International
Microwave Carousel	Sharp
Multipipette	Eppendorf
Parafilm Laboratory Film	Pechiney Plastic Packaging
pH Meter Accumet AR15	Fisher Scientific

Materials	Manufacturer
Photometer Biomate3	Thermo Spectronic
Pipet Aid	Drummond
Pipet Tips	VWR International
Pipettes	Rainin
Pipettes 5mL, 10mL, 25mL	Corning Inc.
Power Pac 200	Biorad
Precast NuPAGE [®] Bis-Tris Gel (10% or 12%)	Invitrogen
PVDF Membrane Filter Paper Sandwich 0.2 μ m	Invitrogen
PVDF Membrane 0.45 μ m	GE Healthcare
Rocking Platform	VWR International
Sectioning Machine Leica RM 2125	IMEB Inc.
Slide Staining Set TISSUE-TEK [®] II	IMEB Inc.
Slide Warmer	Barnstaed Labline
Sonifier 450	Branson
Sterile Disposable Scalpel	Sklar Instruments
Syringe 1mL	BD
Syringe Driven Filter Unit Millex [®] -VV PVDF 0.1 μ m	Millipore
Thermocycler Mastercycler Personal	Eppendorf
Tissue Culture Dish 60mm	BD

Materials

Tissue Embedding Center	Reichert – Jung
Tissue Grinder	Kimble
Tissue Processing/Embedding Cassettes with Lid	Simport
Illumatool Tunable Lighting System	Lighttools Research
Vortex VX100	Labnet
Water Bath	Boekel Scientific
Water Bath Isotemp	Fisher Scientific
X Cell Sure Lock™	Invitrogen

Methods

3.1 Generation of Recombinant Vaccinia Viruses (VACVs)

3.1.1 Cloning of Plasmids Encoding anti-EGFRVHHFLAG

VACVs expressed anti-FAP scAb was constructed by Dr. Alexa Frentzen (GLV-1h281, GLV-1h282, GLV-1h283).

VACVs expressed anti-EGFRVHHFLAG (GLV-1h442), anti-VEGF and anti-EGFRVHHFLAG antibodies (GLV-1h444) and anti-VEGF and anti-FAP antibodies (GLV-1h446) were constructed by Ting Huang.

The anti-EGFRVHH nanobody sequence was amplified from the plasmid pGH-anti-EGFRVHH (a kindly provided by Dr. Ying Wang (Shanghai Institute of Immunology, Shanghai Jiaotong University School of Medicine, China), and its nucleotide sequence is identical to that of the published nanobody called EG2 (Bell, Wang et al. 2010; Iqbal, Trojahn et al. 2010). A DDDDK FLAG tag was added in the C terminal for detection and purification of this nanobody. The primers used including FLAG sequence with *Sall* and *PacI* restriction enzyme sites were shown below: Forward: 5'-GTC GAC CCACC ATG GCC CAG GTA AAG CTG GAG GAG TCT-3'; Reverse: 5'-TTA ATT AAT TAC TTG TCG TCG TCA TCC TTG TAG TCT GAG GAG ACG GTG ACC TGG GTC-3'. The primers were synthesized by Integrated DNA Technologies (IDT). PCR in 50 μ L total volume was performed: accuprime™ Pfx Supermix 45 μ L; primer-Forward (10 μ M) 2 μ L; primer-Reverse (10 μ M) 2 μ L; DNA template (50

ng/ μ L) 1 μ L following with this program: 94 °C 2 min and 35 cycles of 94 °C 30 s; 56 °C 30 s; 72 °C 60 s then 72 °C 7 min.

The PCR products were separated on DNA agarose gels and then were purified with the PCR purification Kit (Invitrogen). The blunt PCR product was subcloned into the transfer vector: pCR[®]-Blunt II-TOPO vector (Invitrogen) and the transfer vector was taken up by the chemically competent bacteria (One Shot Chemically Competent *E.coli*, Invitrogen) via transformation. The positive clones were grown on a LB-plate containing 50 μ g/mL Kanamycin and several clones were picked up for overnight bacteria culture in LB_{Kan} medium. One microliter from each overnight culture was used as the DNA template to confirm the positive clone by performing the bacterial PCR. The confirmed clone was isolated and digested with restriction enzymes and the gene product was ligated with the shutter vector pCR-TK-P_{SEL}, resulting in the plasmid pCR-TK- P_{SEL}-anti-EGFRVHHFLAG.

3.1.2 Co-transfection of Plasmids with the Parental Virus GLV-1h68 or GLV-1h164

CV-1 cells grown in 6-well plates were infected with 2×10^4 pfu GLV-1h68 or GLV-1h164. The transfection mixture was prepared with the transfection reagent and 2 μ g plasmids in OPTI-MEM medium. After infection, CV-1 cells were washed and cultured in OPTI-MEM. The transfection mixture was added to the medium and CV-1 cells were incubated for two days until fully infected. The infected cells were harvested and stored at -80 °C.

3.1.3 Plaque Selection

Prior to infection, CV-1 cells seeded in 6-well plates were treated with mycophenolic acid (MPA), hypoxanthine and xanthine one day before the infection. MPA is an inhibitor of purine metabolism and blocks GMP synthesis to interfere with vaccinia virus replication and reduce viral plaque sizes. However the effect can be overcome by the expression of the *E. coli gpt* gene with the presence of xanthine and hypoxanthine. The *gpt* gene was inserted next to the gene of interest and outside of the vaccinia virus flanking regions. The addition of xanthine and hypoxanthine assist to select for the positive vaccinia virus plaques that express XGPRT by single-crossover recombination (Falkner and Moss 1990). Pretreated CV-1 cells with the drugs were infected with 50, 5, 1 μ L of viruses containing cell lysates for 1 h, 2 mL overlay medium was added and the cells were incubated for five days. Six plaques were picked up by aspirating 100 μ L medium around a single plaque and were added into tubes with 500 μ L DMEM medium. These samples were subjected to three cycles of freeze-thaw and were added to CV-1 cells pretreated with the drugs after sonication. After two rounds of plaque selection, MPA, hypoxanthine and xanthine were removed to allow the viruses to undergo the desired double cross-over recombination and the recombinant viruses without the *xgprt* gene can form the plaques. The non-drugs selections were performed three times in CV-1 cells. After the fifth round selection, the plaque lysates were screened for the positive recombination by marker gene expression.

3.1.4 Screening for Marker Gene Expression

The new genes of interest were inserted into the *J2R* locus in which the parental virus GLV-1h68 encodes for the *LacZ* gene and GLV-1h164 encodes for the *hNET* gene. When the parental virus was replaced with a new gene by homologous recombination in that locus, the former gene product will no longer be expressed by the virus. It is a feasible and simple way to test for successful recombination of the targeted gene into the desired locus. Testing the marker gene expression in the

F14.5L (ruc-gfp) and *A56R (beta-glucuronidase)* loci is also easily performed. Generally, a positive homologous recombination in the *J2R* locus, marker gene expression should be positive in the *F14.5L* and *A56R* locus, while marker gene expression was negative in the *J2R* locus.

3.1.5 Screening for GPT

In order to avoid that the viruses only underwent one cross-over recombination which still contained the *gpt* gene, the selected plaques were also performed by screening for *gpt* expression. MPA pretreated CV-1 cells were infected with the selected plaques for five days. The viruses which underwent two cross-over recombination events and lost the *gpt* gene cannot survive in the presence of MPA. They were the candidates of the aimed viruses and would be amplified as Passage 1 stock and verified for the aimed sequence in PCR assay.

3.1.6 DNA Extraction from Viruses

To get Passage 1 stock, 2x 60 mm plates for each virus with 1 mL DMEM2% medium were infected with 200 μ L lysates from the fifth round selection for 1 h and 1 mL DMEM2% medium was added. The stock was stored for 2 days. The total harvest volume was 2.2 mL and 200 μ L was taken for DNA extraction, which was subjected to centrifugation and to the pellet 100 μ L prepGEM Tissue (89 μ L DNA-free water, 10 μ L of 10x buffer Gold, 1 μ L prepGEM) was added, followed by the incubation at 75 °C for 5 min followed by incubation at 95 °C for 5 min, 1 μ L was used as template for the PCR.

3.1.7 Amplification and Purification of Recombinant Viruses

After confirmation of the inserted DNA sequence, amplification and purification of the new VACVs were performed. CV-1 cells grown in T225 flasks were infected with 2×10^6 pfu virus for 2 days until the plaques were observed. The infected cells were harvested. The cell pellets were collected after centrifugation and resuspended in 10 mM Tris-Cl pH9.0. The cell suspensions were mechanically homogenized to release the virus particles from the infected cells. The cell debris were separated by centrifugation and discarded as a pellet. The supernatant containing the virus particles were subjected to equilibrium sucrose gradient centrifugation to separate and purify the virus by the size. The virus band within the gradient was harvested, washed and resuspended in 1 mM Tris-HCl pH9.0 followed by sonication to break viral aggregates and storage at -80°C .

3.2 Virological Methods

3.2.1 Infection of Cells with Vaccinia Virus

Virus aliquots were thawed in the water bath then kept in ice. Prior to infection, virus was subjected to sonication for 30 s in the ice water. This procedure broke the formation of virus aggregates. The medium was aspirated from the cells and the desired amount of virus in culture medium with 2% FBS was added (infection volume was normally 25 μ L per well for 96-well plate; 200 μ L for 24-well plate; 500 μ L for 6-well plate and 60 mm² plate; 10 mL for T225 tissue culture flask). After one hour incubation at 37 °C, 5% CO₂ with gentle agitation every 20 min, fresh culture medium with 2% or 10% FBS was added.

3.2.2 Determination of Viral Titers by Standard Plaque Assay

For standard plaque assay, virus was diluted by 10-times fold serial dilutions. CV-1 cells seeded in 24-well plates with full confluence were infected in duplicates with 200 μ L respective virus stock. Carboxymethylcellulose (CMC) overlay medium was added after 1 h infection. After 48 hours incubation, cells were stained with 250 μ L crystal violet per well for at least one hour at RT. Plates were washed and colorless virus plaques were identified and counted. Virus titers were calculated using the formula as below:

$$\frac{\text{Plaque forming units (pfu)} \times \text{dilution factor}}{\text{Infection volume}} = \text{pfu/mL}$$

3.2.3 Viral Replication Assay

Cells seeded in 6-well plates grown until 90% confluence the next day were infected with an multiplicity of infection (MOI) of 0.01 in respective culture medium with 2% FBS for 1 h in the incubator with gentle agitation every 20 min, followed by adding the fresh medium with 2% FBS. The infected cells were harvested at different time points 1, 24, 48, 72, 96 h after the infection by scraping the cells. Following three times freeze-thaw cycles, serial dilutions of the harvested viruses were tittered by the standard plaque assay in CV-1 cells. Samples were measured in triplicate. “In virology, the concept of MOI is the ratio of infectious agents (e. g. phage or virus) to infection targets (e. g. cell).”

3.2.4 Viral Cell Killing Ability Assay

Cells seeded in 96-well plates were infected with VACVs at an MOI of 0.01 or 1 with 25 μ L infection medium containing 2% FBS. The medium only treated cells were used as the negative control. After one hour, the infection medium was removed and 100 μ L fresh culture medium with 10% FBS was added. Cell proliferation and viability at different time points was measured with Cell Proliferation Kit II (XTT) (Roche) at 450/700 nm. The relative survival rates of cells were calculated with medium treated cells. Four wells were used for each sample.

3.3 Molecular Methods

3.3.1 Polymerase Chain Reaction (PCR)

Polymerase chain reaction (PCR) is a very sensitive and widely used method for DNA amplification. It normally contains the steps: denaturation: separate double-stranded DNA into single-stranded; annealing step: primers bind to the single strands DNA template; elongation: extend the primers to synthesis a complementary strand with abundant dNTPs. The time of elongation is dependent on the size of the DNA fragment, normally 1 min for 1 kb. In our system, PCR reactions were prepared using the AccuPrime™ Pfx Supermix. PCR in 50 µL total volume was performed: accuprime™ Pfx Supermix 45 µL; primer-Forward (10 µM) 2 µL; primer-Reverse (10 µM) 2 µL; DNA template (50 ng/µL) 1 µL following with this program: 94 °C 2 min and 35 cycles of 94 °C 30 s; 56 °C 30 s; 72 °C 60 s then 72 °C 7 min.

3.3.2 Agarose Gel Electrophoresis

Horizontal agarose gel electrophoresis is used for separation of DNA fragment by the size. Choosing agarose concentration is based on the sizes of DNA fragments. The principle is that the greater of the agarose concentration, the easier to separate the small linear DNA molecules. Ethidium bromide (EB) is added to intercalate between the DNA bases and enables visualization of DNA bands by the UV light. The size of DNA fragments is measured in base pairs (bp) and comparable with the DNA ladder.

3.4 Protein Analytical Methods

3.4.1 Preparation of Soluble Protein from Mammalian Cells

Cells grown in the desired format to 95% confluence were infected with VACVs. After 1 h infection, cells were washed and added with the desired medium without FBS. At each time point for harvesting, medium was collected and was spun down to remove the cell lysates and cells were resuspended in PBS then scraped off the wells. After centrifugation PBS was aspirated and the cell pellets were resuspended in RIPA buffer and subjected to sonication to break up cell membrane and extract the protein from the cells. Then cells were removed from degrade DNA with benzonase at 37 °C for half an hour. After that, the samples were centrifuged at 4 °C and stored -80 °C for further analysis.

3.4.2 Protein Quantification

For quantification of the protein concentration, the DC protein assay kit (Bio-Rad) was used according to the instructions of the manufacturer. Standards were prepared in definite amounts of concentration from 0.2, 0.4, 0.6, 0.8, 1.0 mg/mL of lyophilized Bovine Plasma Gamma Globulin (Bio-Rad). Five μL of the standard or samples were pipetted into a 96-well plate followed by adding 25 μL reagent A to each well. Then 200 μL reagent B was added and kept in the dark for 15 min at RT. Absorption was measured at 750 nm using a plate reader and the protein concentration was calculated by setting the absorbance against the equation of the trend line of the standard curve.

3.4.3 SDS-PAGE

Sodium dodecyl sulfate polyacrylamide gel electrophoresis (SDS-PAGE) is a widely used technique to separate protein according to their molecular weight and electrophoretic mobility. SDS is an anionic detergent that denatures proteins and imparts a negative charge to linearize protein.

To perform the SDS-PAGE electrophoresis assay, precast NuPAGE® Bis-Tris gels (Invitrogen) were loaded with 20 µg of protein mixed with SDS loading buffer and Precision Plus Protein Standard (Bio-Rad) was loaded as the protein ladder. The gel chamber was filled with 1x NuPAGE® MOPS Running buffer (Invitrogen). Then the gel electrophoresis was conducted at a voltage of 200 for 55 min.

3.4.4 Transfer Protein to PVDF Membrane (Western blot)

Proteins in a polyacrylic matrix are not detectable for macromolecular ligands such as antibodies and have to be transferred to a membrane. Degraded proteins are transferred to a polyvinylidene fluoride (PVDF) membrane through migration within an ionic gradient. The negatively charged proteins migrate towards a cathode. They bind to the membrane through hydrophobic interaction.

For protein transfer the XCell SureLock™ Mini-Cell with a blot module (Invitrogen) was used. The proteins were blotted on a 0.2 µm PVDF membrane (Invitrogen) or 0.45 µm PVDF (GE healthcare) membranes according to the sizes of the aim protein. The blot was assembled in the following order from cathode to anode: three buffer soaked sponges, buffer soaked filter paper, polyacrylamide gel, membrane, buffer soaked filter paper, three buffer soaked sponges. The inner chamber was filled with 1x NuPAGE® Transfer buffer (Invitrogen) and the outer chamber with cold water for

cooling. The proteins were blotted for 1 h at 15 V (the membrane around 13 cm x 8 cm).

3.4.5 Colorimetric Immunodetection

After half-dry transformation, PVDF membrane was blocked 1x gelatin buffer for 2 h on a shaker at RT followed by incubation with the primary antibody suitably diluted in PBST overnight at 4 °C. The following day, the membrane was washed with TBST 3 x 10 min on a shaker and was incubated with the secondary antibody in a 1:5000 dilution for 2 h at RT. After a final wash of 1 h in TBST, the protein was detected with GE Healthcare Amersham ECL Prime Western Blotting Detection Reagent kit then followed with a colorimetric method the Opti-4CN kit (Bio-Rad).

3.4.6 ELISA

Enzyme-linked immunosorbant assay (ELISA) is a biochemical technique widely used to detect the presence of an antibody or antigen in a sample. A representative protocol to quantify the concentration of GLAF-5 as below: a 96-well plate was coated with the recombinant human FAP at a final concentration of 1 µg/mL for overnight at 4 °C. The next day, the plated was washed and blocked with 200 µL Blocker™ Casein in PBS (Pierce) for 2 h at 37 °C. Then it was washed again and incubated with 50 µL serial diluted positive controls or the samples for 1 h at RT. After that, the plate was washed and incubated with 1:5000 diluted rabbit anti-DDDDK antibody (Abcam, ab21536) for 1 h at RT followed by washing again. Next, it was incubated with HRP-conjugated goat anti-rabbit IgG (Jackson Immuno Research, 111-036-046) for 1 h at RT. Then it was developed using 100 µL 3, 3, 5,

5'-tetramethylbenzidine (TMB, Sigma, T0440) and stopped after sufficient color development by adding 100 μ L 2 N HCl. Absorbance was read in a microplate reader at 450 nm.

3.5 *In Vivo* and *Ex Vivo* Studies

3.5.1 Establishment of Xenograft Tumor Models

Prior to implantation of the tumor cells, the nude mice were kept in the animal room for one week to rest and adjust the new environment when they arrived. Implantation of 5×10^6 A549 lung carcinoma cells, 1×10^7 DU145 or 1×10^7 FaDu in 100 μ L PBS subcutaneously in the upper right hind leg area was carried out with 1 mL syringe. Mice were measured once per week with a digital caliper when the tumors were visible. Length, height and width of the tumors were measured and written down. The tumor volume is calculated using the following formula:

$$\text{Tumor volume (mm}^3\text{)} = \frac{\text{length} \times \text{width} \times (\text{height} - 5)}{2}$$

The weight of mice was weighed with an electronic balance to keep track of any changes of body weight after the tumor cells implantation and treatment with virus.

When tumor volumes reached 400-450 mm^3 , injection with VACVs were performed. A549 or DU145 xenografts were injected with 2×10^6 pfu/ mouse in 100 μ l PBS (5×10^6 pfu/mouse FaDu xenograft) through retro orbital (r. o.) with insulin syringes. The remaining virus was titrated in CV-1 cells to confirm whether the virus titers were identical with the calculated numbers. PBS only treated mice were used as the mock control.

3.5.2 Antibody Injection (Avastin and Erbitux)

For Erbitux treatment, mice were intraperitoneal (i.p.) injected with 12 mg/kg commercial Erbitux (Imclone LLC) diluted with sterile 0.9% NaCl in ddH₂O. Treatments were performed three times a week for 5 weeks starting at one week after the injection.

For Avastin treatment, mice were i.p. injected with 5 mg/kg commercial Avastin (Genetech Inc) diluted with sterile 0.9% NaCl in ddH₂O. Treatments were performed two times a week for 5 weeks starting at one week after the injection.

For Avastin and Erbitux combined therapy, mice were i.p. injected with 5 mg/kg Avastin in the morning of Monday and Thursday and 3 mg/kg Erbitux were i. p. injected in the afternoon of Monday and Thursday for 5 consecutive weeks starting at one week after the virus injection.

3.5.3 Anesthesia and Blood Collection from Orbital Sinus

Laboratory mice were solely anesthetized using isoflurane which is a highly volatile anesthetic with hypnotic and muscle-relaxing effects. Mice were put in a knockout box and a mixture of isoflurane and oxygen was administered to the mice. Isoflurane has a very low distribution coefficient and therefore mice react rapidly on increasing or decreasing concentrations.

3.5.4 Detection of Virus-encoded Marker Gene RUC-GFP Expression

GFP expression within tumors upon inoculation of recombinant vaccinia virus was monitored under blue light using a stereo fluorescence macro imaging system. GFP expression was scored using a four point system: 0) no GFP signal, 1) one spot, 2) two or three local spots, 3) diffuse signal from half the tumor, 4) strong signal from whole tumor.

3.5.5 Tumor and Organ Preparation for Virus Titration

Tumors and organs (testes, bladder, spleen, kidneys, livers, heart, lungs and brain) were dissected, weighed and placed in MagNA Lyser Green Beads tubes (Roche) containing 500 μ l PBS with Proteinase Inhibitor (50 mL PBS with one tablet of Proteinase Inhibitor Cocktail) followed by homogenization at the speed of 6500 for 30 s. After that, the tubes were frozen in liquid nitrogen immediately and kept at -80 °C for long storage. If the weight exceeds 800 mg, additional tube was used for the same organ. Samples were subjected to three cycles of freeze-thaw and sonicate three times for one minute to further break up the virus aggregates. Tubes were combined if the tissues were split into more than one tube. Virus titers were determined by standard plaque assay in CV-1 cells. 10 μ l of organ lysates was added CV-1 cells containing 200 μ l DMEM2%FBS. Tumors were diluted until 10^{-6} and all the dilutions were used for titration.

3.5.6 Histology Analysis of Tumors - Paraffin Embedded Slides

Fresh tumors were cut and fixed with 10% neutral buffered formalin overnight, dehydrated and embedded with paraffin. Five μm sections were cut, dewaxed and stained with H&E. For immunohistochemistry, paraffin-embedded sections were dewaxed and antigen retrieval was performed in 10 μM sodium citrate buffer in a steam cooker. Slides were washed at RT and hydrated in PBS for 10 min. Endogenous peroxidase activity was then quenched with 3% hydrogen peroxidase for 10 min. Sections were then blocked with 10% normal goat serum in PBS containing 1% BSA and 0.1% Tween-20 for 1 h. Endogenous avidin and biotin were blocked using the avidin-biotin kit (Vector Laboratories). Samples were then stained with antibodies against FAP (diluted 1:1000, Abcam); anti-PECAM-1 (diluted 1:200, Santa Cruz Laboratories); vaccinia A27L (diluted 1:1000, Genelux custom-made rabbit polyclonal antibody) and isotype-matched antibodies were used as the negative controls. Incubations were done at 4 °C overnight. Biotinylated secondary antibodies were used with 1:5000 dilution and were detected with horseradish peroxidase using the Vectastain Elite ABC and Vector ImmPact DAB Peroxidase substrate (Vector Laboratories).

3.5.7 Histological Analysis of Tumors - Agarose Embedded Slides

Dissected tumors were fixed directly in liquid nitrogen and stored at -80 °C, frozen tumors were fixed in 30 mL of cold paraformaldehyde (4% in PBS) at 4 °C overnight on a shaker followed by 5 times 30 min wash with PBS to remove all remnants of PFA. Meantime 5% Low Melting Point agarose was melted in a water bath and then

was poured into 6-well plates when the cut side of one tumor was set down on the well. The 6-well plates were put in humidity chamber set to hard them for 1 h at 4 °C. Tumor tissues were cut into 100 µm sections using a VT1200S vibratom and placed directly in 24-well plates with 500 µl PBS. The sections were blocked 5% goat serum for 1 h at RT, followed with the respective diluted primary antibody overnight. The following day specific proteins of interest were stained with the respective diluted primary antibodies and fluorescence-labeled secondary antibodies.

The fluorescent-labeled preparations were examined using a Leica MZ 16 FA Stereo-Fluorescence microscope equipped with a FireWire DFC/IC monochrome CCD camera. Digital images were processed with Photoshop.

Results

4.1 Anti-fibroblast Activation Protein Single Chain Antibody GLAF-5 Encoded by Oncolytic Vaccinia Virus Significantly Increases Antitumor Therapy (Part 1)

4.1.1 Construction of Recombinant VACVs Encoding GLAF-5

To investigate the impact of anti-FAP treatment on tumor growth combined with VACV, three new recombinant VACVs were constructed by replacing the *lacZ* expression cassette with the GLAF-5 expression cassette (**Figure 4.1.1**) at the *J2R* locus of GLV-1h68. GLV-1h281, GLV-1h282, and GLV-1h283 contain anti-FAP scAb GLAF-5 under the control of the VACV synthetic early (PSE), synthetic early/late (PSEL) and synthetic late (PSL) promoters, respectively. The genomic structures of GLV-1h281, GLV-1h282, and GLV-1h283 were verified by PCR and sequencing as well as marker gene expression (**Figure 4.1.1**).

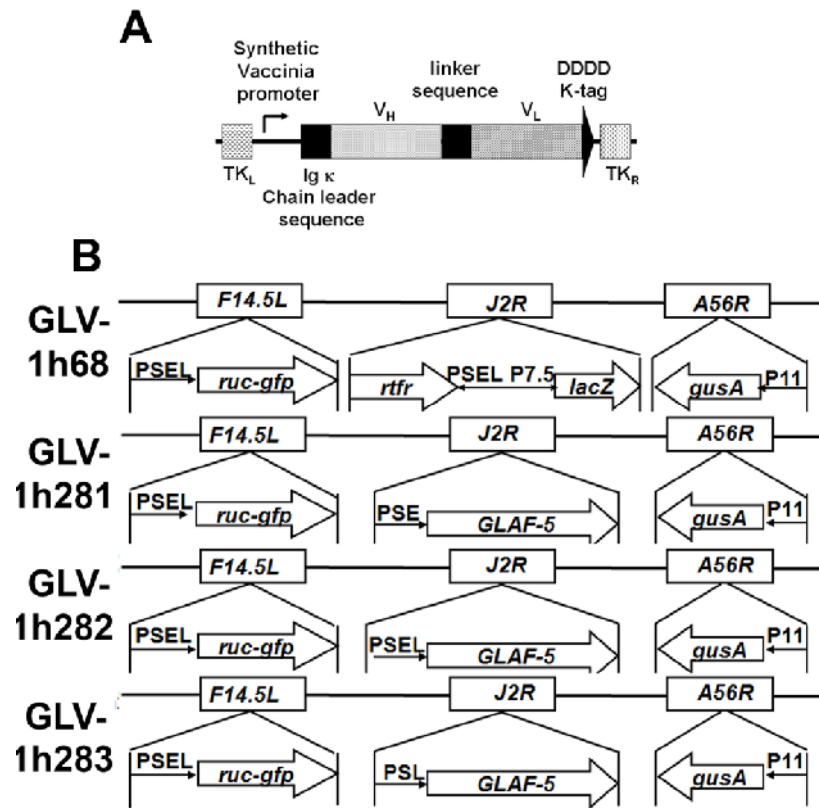


Figure 4.1.1 Structures of VACVs encoding GLAF-5 (A) Schematic representation of the anti-FAP scAb GLAF-5 construct. (B) Genomic structures of the new recombinant VACVs along with their parental virus. GLV-1h281, GLV-1h282, and GLV-1h283 were derived from GLV-1h68 by replacing the *lacZ* expression cassette at the J2R locus with the GLAF-5 expression cassette under the control of the PSE, PSEL, PSL promoters, respectively. All viruses contain *ruc-gfp* and *gusA* expression cassettes at F14.5L and A56R loci, respectively. PSE, PSEL, PEL, P11 and P7.5 are VACV synthetic early, synthetic early/late, synthetic late, 11K, and 7.5K promoters, respectively. *Tfr* is human transferrin receptor inserted in the reverse orientation with respect to the promoter PEL.

4.1.2 Expression of GLAF-5

To evaluate the expression of GLAF-5, human lung carcinoma A549 cells were infected with the individual GLAF-5-expressing VACV strains and the control virus strains GLV-1h68 and GLV-1h108 expressed anti-VEGF scAb GLAF-1 (Frentzen, Yu et al. 2009). Both GLAF-1 and GLAF-5 contain a C-terminal DDDDK sequence to facilitate detection by Western blot and ELISA. Infected cell culture supernatants and cell lysates were analyzed for the presence of GLAF-5 by Western blot analysis.

GLAF-5 was readily detected in both supernatants and cell lysates of A549 cells infected with GLV-1h281, GLV1h282 or GLV-1h283 at the expected size of 30 kDa (**Figure 4.1.2**). As a positive control, GLAF-1 was detected in GLV-1h108-infected samples as the expected (Frentzen, Yu et al. 2009). No protein was detected in mock-infected or parental virus GLV-1h68-infected samples. The expression levels of GLAF-5 were lower in GLV-1h281-infected cell lysates or supernatants than that in GLV-1h282- or GLV-1h283-infected samples, which was consistent with the strength of the promoters driving the expression of GLAF-5.

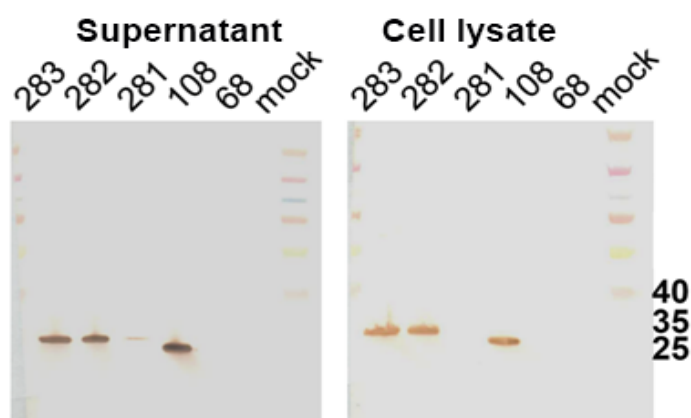


Figure 4.1.2 Expression of GLAF-5 in cancer cells in culture. Western blot analysis of GLAF-5 expression in A549 cells. A549 cells were infected with individual VACV strains at an MOI of

2. Cells and supernatants were harvested at 24 h.p.i. Equal amount of samples were loaded and separated in SDS/PAGE. GLAF-5 and GLAF-1 were detected using anti-DDDDK antibody.

4.1.3 Purification of GLAF-5

To evaluate the purity and function of GLAF-5, it was purified from the supernatant of GLV-1h282-infected CV-1 cells. Briefly, the supernatants were concentrated by centrifugation using centrifugal filter units (Millipore), followed by purification with the FLAG Tagged Protein Immunoprecipitation kit (Sigma). The purification of GLAF-5 was evaluated as the result that single band purity by SDS-PAGE and Coomassie staining (Figure 4.1.3).

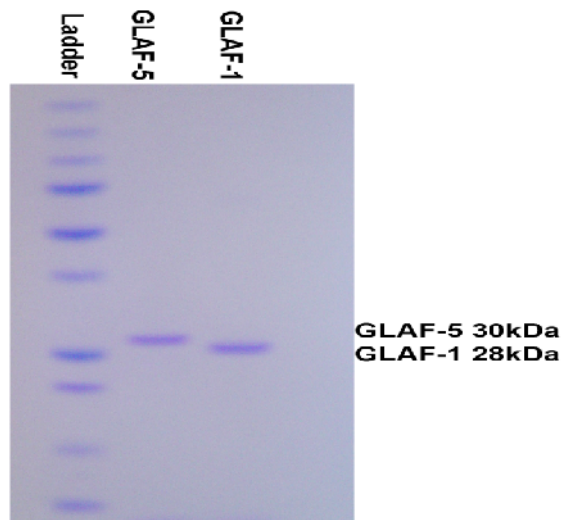


Figure 4.1.3 Purification of anti-EGFRVHHFLAG nanobody. 2 mg GLAF-5 or GLAF-1 were analyzed by SDS-PAGE and Coomassie blue staining of the gel to determine the purity. Purified GLAF-1 as positive control.

The purification of GLAF-5 was verified with Coomassie staining. The concentration of GLAF-5 was determined by Bradford assay and verified by ELISA. **Figure 4.1.4** shows that two-fold diluted GLAF-5 was recognized starting from the concentration of 3.9 ng/mL and the concentration of GLAF-5 was correlated.

GLAF-5 Standard ELISA

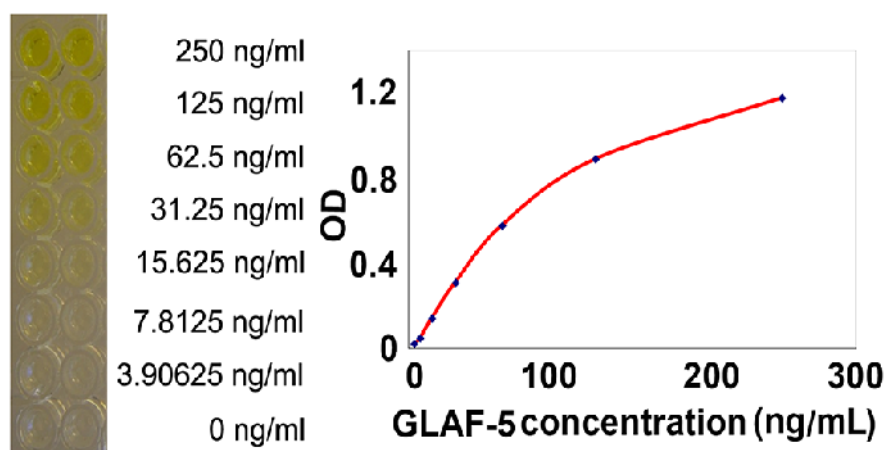


Figure 4.1.4 Concentration of GLAF-5 was verified by ELISA assay. A 96-well plate precoated with the commercial human recombinant FAP overnight, then was added with serially diluted GLAF-5 or the commercial polyclonal antibody against FAP (Abcam), followed by detection with anti-DDDDK antibody.

4.1.4 GLAF-5 Does Not Inhibit DPP Activity of FAP

FAP exhibits DPP (Levy, McCaughan et al. 1999; Park, Lenter et al. 1999; Aertgeerts, Levin et al. 2005) and endopeptidase activities (Edosada, Quan et al. 2006; Christiansen, Jackson et al. 2007; Meadows, Edosada et al. 2007) with the capability of degrading gelatin (Aggarwal, Brennen et al. 2008) and type I collagen in synchrony with other proteinases (Park, Lenter et al. 1999; Christiansen, Jackson et al. 2007). Its substrate(s) in tissues, however, has not yet to be defined. To

investigate whether GLAF-5 was able to block the DPP activity of FAP, a DPP assay was performed. Purified GLAF-5 was serial diluted and combined with commercially available recombinant human FAP (rhFAP) at a concentration of 3.9 ng/mL. The DPP activity of FAP was completely blocked by the commercial polyclonal antibody at the concentration of 4 μ g/well. Interestingly, GLAF-5 did not inhibit the DPP activity, even at the concentration of 4 μ g/well (Figure 4.1.5).

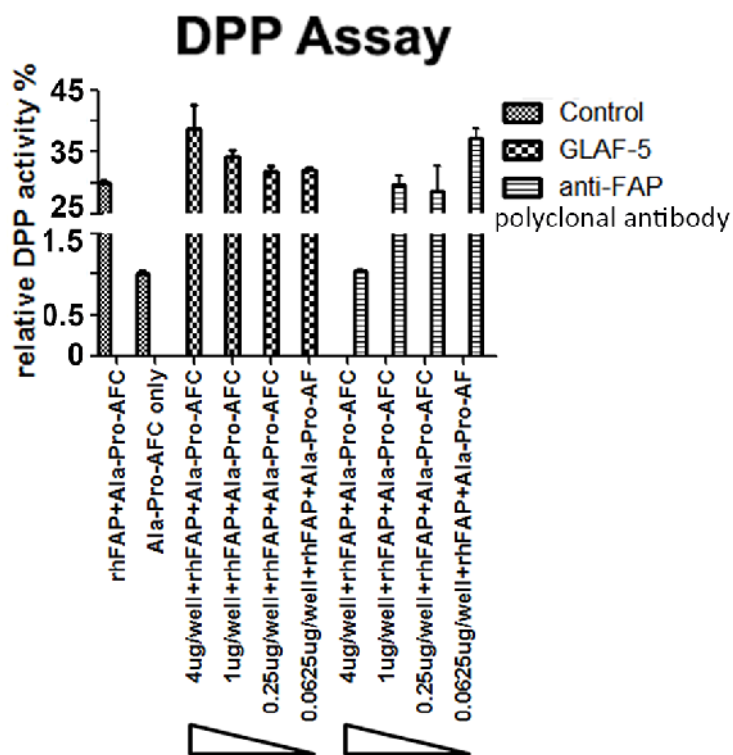


Figure 4.1.5 GLAF-5 does not inhibit the DPP activity of FAP in vitro. The DPP activity of FAP was measured by converting the substrate Ala-Pro-AFC into Ala-Pro and frees AFC. The commercial polyclonal antibody did not inhibit the DPP activity of FAP until the dose increased to 4 μ g/well. Purified GLAF-5 did not inhibit the DPP activity even at the dose of 4 μ g/well.

4.1.5 GLAF-5 Shows Increased Viral Replication Efficiency

To evaluate whether GLAF-5 protein expression altered viral replication efficiency, A549 cells were infected with VACV strains expressed GLAF-5 at an MOI of 0.01 and harvested at the different time points, followed by determination of the viral titers. Unexpectedly GLV-1h281, GLV-1h282 and GLV-1h283 showed significantly enhanced replication efficiency in A459 cells at 24 and 48 hours p.i. in comparison to the parental virus GLV-1h68. At 96 h.p.i., only GLV-1h281 and GLV-1h282 exhibited additive replication efficiency (**Figure 4.1.6**).

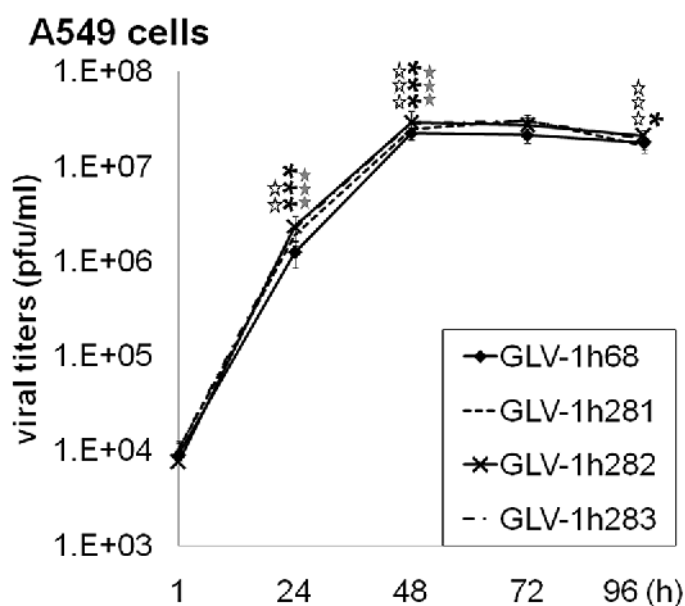


Figure 4.1.6 Expression of GLAF-5 enhances VACV replication efficiency.

Expression of GLAF-5 showed significant enhanced VACVs replication efficiency in A549 cells at an MOI of 0.01. Statistical analysis was performed using one-way ANOVA (** $P < 0.01$, * $P < 0.05$). Stars indicate comparison of the GLV-1h68 group with the groups of GLV-1h281 (open), GLV-1h282 (black) or GLV-1h283 (grey).

4.1.6 GLAF-5 Shows Increased Cell Killing Ability

To assess whether the new VACV strains exhibited a change in viral cell killing efficiency, an XTT assay was performed. Cells were infected at both low (0.01) and high (1) MOIs. The cytotoxicity was determined daily for five consecutive days. **Figure 4.1.7** shows that at an MOI of 1, about 60% of A549 cells died at day 1 and the survival curves for GLV-1h283 and GLV-1h68 were nearly identical, indicating that cells infected with each virus were dying at a similar rate. At an MOI of 0.01, although the survival curves were similar, the percentages of cell survival after infection with recombinant VACVs expressed GLAF-5 were consistently lower than that after infection with GLV-1h68. The difference of the cell survival among GLV-1h68 and all VACV strains expressed GLAF-5 were statistically significant at 72 h.p.i. while GLV-1h281 and GLV-1h282 showed dramatically greater compared to GLV-1h68, indicating that GLAF-5 expressing VACV strains showed overall better cell killing activity. This result was consistent with the higher replication efficiency in A549 cells observed for VACV stains expressed GLAF-5 compared to GLV-1h68. Taken together, VACVs expressed GLAF-5 exhibited superior replication efficiency and cell killing ability than the parental strain, GLV-1h68.

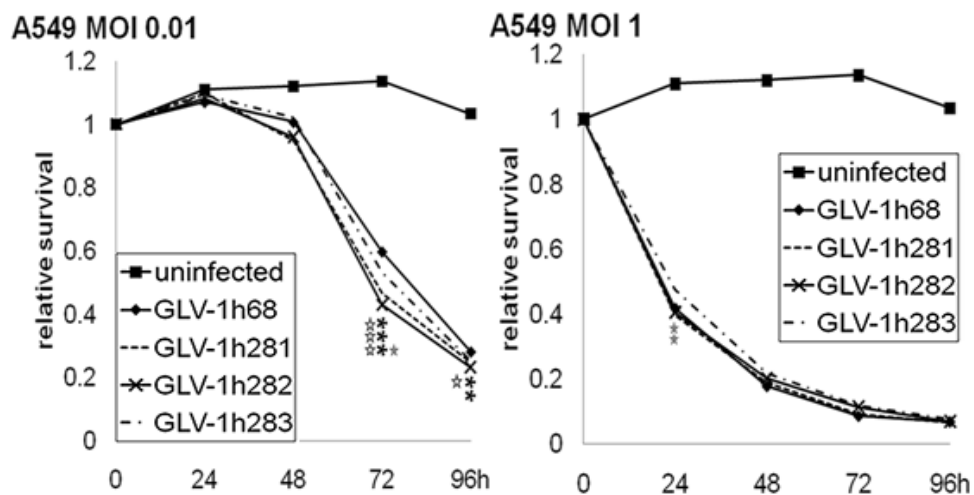


Figure 4.1.7 Expression of GLAF-5 enhances VACV cell killing efficiency.

Expression of GLAF-5 showed significant enhanced VACV-mediated cell killing in A549 cells at MOIs of 0.01 and 1. Statistical analysis was performed using one-way ANOVA (** $P < 0.01$, * $P < 0.05$). Stars indicate comparison of the GLV-1h68 group with the groups of GLV-1h281 (open), GLV-1h282 (black) or GLV-1h283 (grey).

4.1.7 GLAF-5 Enhances VACV-mediated Antitumor effects in “Responder” Tumor Xenograft Models

To investigate the effects of GLAF-5 on VACV-mediated virotherapy, GLV-1h68 and GLV-1h282 were injected intravenously at a single dose into different human tumor xenografts. **Figure 4.1.8 A** shows that, in A549 xenograft mode ($n \geq 7$), tumor growth in the GLV-1h68-treated group exhibited three-phase growth patterns: growth, inhibition and regression, as described previously (Zhang, Yu et al. 2007). In the GLV-1h282-treated group, tumors showed a similar growth pattern. However, tumor growth was delayed and never reached the same volume as in the GLV-1h68-treated group. Significant inhibitory effects on tumor growth were observed after treatment with GLV-1h282 compared to GLV-1h68 at days 7 and 20 p.i. PBS-treated tumors showed exponential growth until mice had to be sacrificed due to tumor burden. Similar results were obtained in the DU145 xenograft model. DU145 tumors shrinkage in the GLV-1h282-treated mice was observed sooner than in the GLV-1h68-treated group (**Figure 4.1.8 B**).

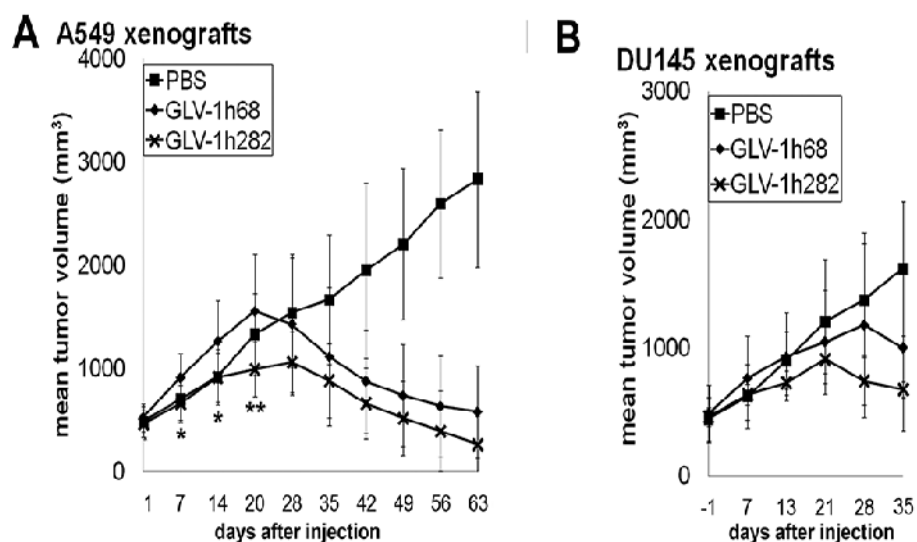


Figure 4.1.8 Expression of GLAF-5 in GLV-1h282-colonized tumors leads to enhanced antitumor effects in responder models. (A) Therapeutic effect of GLV-1h282 on tumor growth in nude mice bearing “responder” human cancer xenografts ($n \geq 7$). Statistical analysis was performed one-way ANOVA (** $P < 0.01$, * $P < 0.05$). Stars indicate comparison of the GLV-1h68 group with the GLV-1h282 group. (B) Therapeutic effect of GLV-1h282 on the “responder” DU145 xenografts ($n=5$).

4.1.8 GLAF-5 Enhances VACV-mediated Antitumor effects in “Non-responder” Tumor Xenograft Model

After demonstrating the enhanced efficacy of GLV-1h282 in “responder” tumor xenograft models, we sought to investigate whether GLV-1h282 could exhibit any therapeutic efficacy in the xenograft models that GLV-1h68 was not able to treat efficiently (“non-responder xenografts”) (Worschech, Chen et al. 2009). FaDu is a human head and neck carcinoma cell which grows aggressively in animal model and FAP was shown to be highly expressed in the stroma of FaDu tumors (Ostermann, Garin-Chesa et al. 2008). The respective VACV strains (5×10^6 pfu/mouse) or PBS as a control were injected retro-orbitally after FaDu tumors ($n \geq 8$) reached 350 mm^3 .

Tumors in the GLV-1h68-treated and PBS-treated group showed almost identical growth patterns, indicating that these tumors did not respond to GLV-1h68-mediated virotherapy (**Figure 4.1.9**). However, tumor size was significantly smaller ($p < 0.05$) at 3 weeks p.i. in GLV-1h282-treated group than in GLV-1h68-treated group.

FaDu xenografts

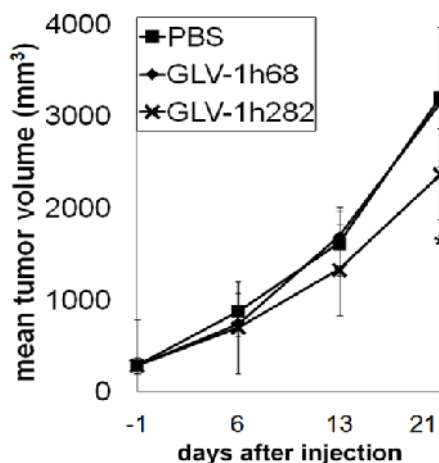


Figure 4.1.9 Expression of GLAF-5 in GLV-1h282-colonized tumors leads to enhanced tumor therapy in non-responder model. Therapeutic effect of GLV-1h282 on the “non-responder” FaDu xenografts ($n \geq 8$). Statistical analysis was performed using one-way ANOVA ($* P < 0.05$). Stars indicate comparison of the GLV-1h68 group with the GLV-1h282 group.

4.1.9 GLAF-5 is Present in Mouse Serum

To determine the expression of GLAF-5 in mice treated with GLV-1h282, blood samples were collected retro-orbitally from mice bearing A549 tumors at 7, 21, 35 days p.i.. The concentration of GLAF-5 was determined by ELISA with FAP-precoated plates. **Figure 4.1.10** shows that GLAF-5 was detectable in the serum of GLV-1h282-injected mice. The concentration of GLAF-5 was higher in the samples

collected at 7 and 21 days p.i. than that collected at 35 d.p.i., which may be due to a decrease in virus replication in companion with tumor shrinkage.

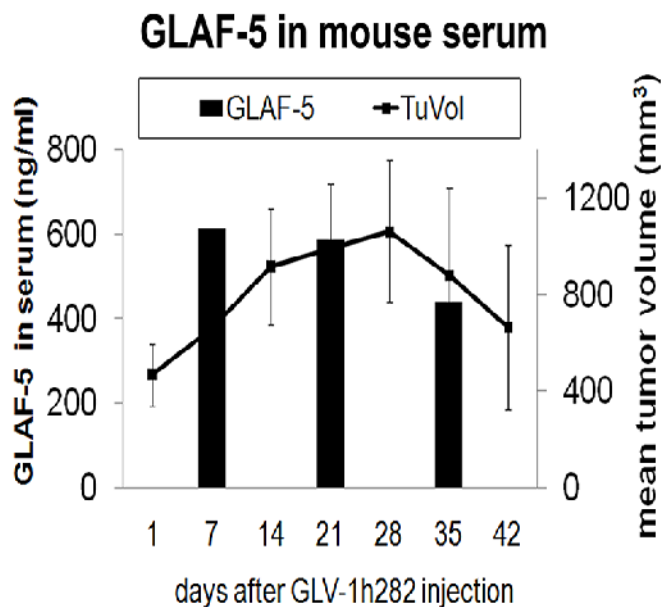


Figure 4.1.10 Detection of GLAF-5 in mouse serum and the changes of tumor volume in mice bearing A549 tumors after treatment with GLV-1h282. Blood samples were taken at 7, 21, 35 days p.i. after treatment with GLV-1h282. The concentration of GLAF-5 in mouse serum was determined by the ELISA with precoated FAP plates. Tumor volume was measured with a digital caliper.

4.1.10 GLAF-5 Does Not Cause Toxicity

The overall toxicity was determined by monitoring the net body weight change of animals. No obvious change in toxicity was observed in these studies, the representative example in A549 model is shown in **Figure 4.1.11**.

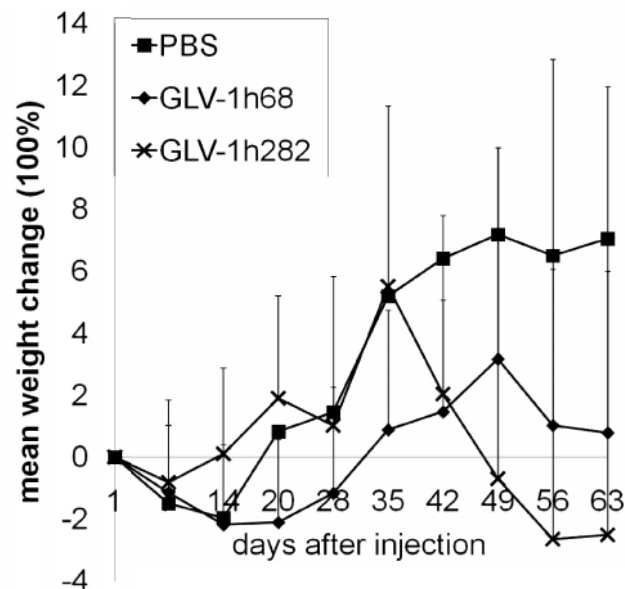


Figure 4.1.11 No significant changes in body weight of mice were observed after VACV treatment. Net body weight of A549 tumor-bearing mice was monitored over time after treatment.

4.1.11 Virally Expressed GLAF-5 Enhances VACV Replication in Tumors

In mice bearing A549 tumors, GLV-1h282-treated tumors showed stronger GFP signals than that of GLV-1h68-treated tumors (**Figure 4.1.12 A**). To further investigate this phenomenon, viral titers in several organs and tumors of VACV treated mice were determined at 14 d.p.i. (n=5) (**Figure 4.1.12 C and Table 4.1.1**). The viral titers of GLV-1h282 in A549 tumors were significantly higher than those of GLV-1h68 (1.63E+9 pfu/tumor of GLV-1h282 vs. 5.98E+8 pfu/tumor of GLV-1h68, $P < 0.01$). No or only minimal amount of virus was detected in healthy organs in mice treated with GLV-1h68 or GLV-1h282 (**Table 4.1.1**).

Similarly, GFP signals and virus distribution in the FaDu tumors xenograft model were analyzed. Bright GFP signals were observed in 8 out of 10 GLV-1h282-treated tumors and 2 out of 8 of GLV-1h68-treated tumors at 21 d.p.i., respectively (**Figure 4.1.12 B and D**). Mice in each group (n=5) were sacrificed at 3, 10 and 21 days p.i. Organs and tumors were analyzed for viral titers. At all time points analyzed, viral titers in tumors were found to be significantly elevated in the GLV-1h282-treated group comparing to GLV-1h68-treated group. Again, no or only minimal amount of virus was detected in healthy organs in mice treated with GLV-1h68 or GLV-1h282 (**Table 4.1.2**). Thus, GLAF-5 significantly enhanced VACV replication in tumors without compromising its safety.

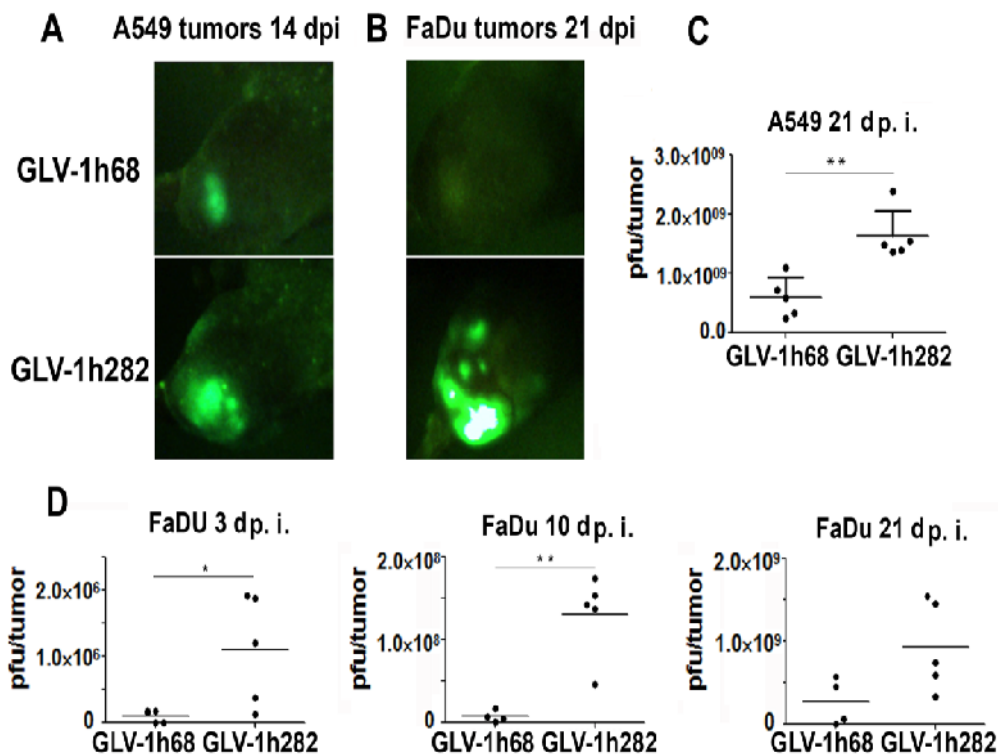


Figure 4.1.12 Virally expressed GLAF-5 enhances VACV replication in tumors than that treated with GLV-1h68. More GFP imaging was visualized in A549 tumors (A) or FaDu tumors (B) with GLV-1h282-treated than that with GLV-1h68 treated. More viral titers in A549

tumors (C) and s (D) treated with GLV-1h282, pfu per tumors (n=5 for A549 and n=5 for FaDu). A549 tumorous mice were injected with GLV-1h68 or GLV-1h282 (2×10^6 pfu/mouse); FaDu tumorous mice were injected with 5×10^6 pfu/mouse. At the aimed time points after injection, mice were scarified and tumors were dissected followed by disruption in homogenization tubes. Viral titers were recovered and titrated in CV-1 cells. Statistical analysis was performed using Student's t Test (** $P < 0.01$), stars indicate comparison of the GLV-1h282 group with GLV-1h68 group.

Table 4.1.1 Expression of GLAF-5 by GLV-1h282 does not alter the biodistribution of the virus in mice.**Viral distribution of GLV-1h68 or GLV-1h282 in A549 tumor-bearing mice at day 14 post infection (pfu/organ or tumor)**

animal No.	GLV-1h68					GLV-1h282				
	1	2	3	4	5	6	7	8	9	10
bladder	0	0	0	0	0	0	0	0	0	0
testes	0	0	0	0	0	0	0	0	0	0
spleen	0	0	1.98E+03	0	0	5.04E+03	4.86E+03	1.46E+03	0	3.31E+03
kidneys	0	0	0	0	0	0	0	0	0	0
liver	0	0	0	0	0	0	0	0	0	0
lungs	0	0	0	0	0	2.72E+03	6.86E+02	5.61E+02	0	5.54E+02
heart	0	0	0	0	0	0	0	0	0	0
brain	0	0	0	0	0	0	0	0	0	0
tumor	3.39E+08	5.86E+08	7.29E+08	2.42E+08	1.09E+09	1.37E+09	1.54E+09	1.48E+09	1.40E+09	2.39E+09
average/tumor	5.98E+08					1.63E+09				

Viral biodistribution of VACVs in “responder” A549-bearing mice at 14 d.p.i. Viral titer in tissue samples, pfu per organ or grams of tumor. To determine the safety of the new VACV GLV-1h282 in mice, A549 tumor-bearing mice (450 mm³) were injected with GLV-1h282 or GLV-1h68 (2×10^6 pfu per mouse). Titers were recovered from different organs and tumors following the protocol (see methods).

Table 4.1.2 Expression of GLAF-5 does not compromise viral safety in GLV-1h282-treated mice in FaDu xenograft model.

Viral distribution of GLV-1h68 or GLV-1h282 in Fadu tumor-bearing mice at day 3 post infection (pfu/organ or tumor)

3 d.p.i.	GLV-1h68					GLV-1h282				
animal No.	1	2	3	4	5	6	7	8	9	10
bladder	0	0	0	0	0	0	0	0	0	0
testes	0	0	0	0	0	0	0	0	0	0
spleen	0	0	0	0	0	4.86E+02	0	0	0	0
kidneys	0	0	0	0	0	0	0	0	0	0
liver	0	0	0	0	0	0	0	0	0	0
lungs	0	0	0	0	0	9.45E+02	0	0	0	0
heart	0	0	0	0	0	0	0	1.47E+03	0	0
brain	0	0	0	0	0	0	0	0	0	0
tumor	0	0	1.81E+05	1.50E+05	1.76E+05	3.71E+05	1.92E+06	1.88E+06	1.28E+05	1.20E+06
average/tumor	1.01E+05					1.10E+06				

Results

Viral distribution of GLV-1h68 or GLV-1h282 in Fadu tumor-bearing mice at day 10 post infection (pfu/organ or tumor)

10 d.p.i.	GLV-1h68					GLV-1h282				
animal No.	1	2	3	4	5	6	7	8	9	10
bladder	0	0	0	0	died at 4 d.p.i	0	0	0	0	0
testes	0	0	0	0		0	0	0	0	0
spleen	0	0	0	0		0	0	0	0	0
kidneys	0	0	0	0		0	0	0	0	0
liver	0	0	0	0		0	0	0	0	0
lungs	0	0	0	0		0	0	0	0	0
heart	0	0	0	0		0	0	0	0	0
brain	0	0	0	0		0	0	0	0	0
tumor	7.60E+06	5.04E+06	1.76E+07	7.58E+05		1.42E+08	1.53E+08	1.74E+08	1.37E+08	4.57E+07
average/tumor	7.75E+06					1.30E+08				

Results

Viral distribution of GLV-1h68 or GLV-1h282 in FaDu tumor-bearing mice at day 21 post infection (pfu/organ or tumor)

21d.p.i.	GLV-1h68					GLV-1h282				
animal No.	1	2	3	4	5	6	7	8	9	10
bladder	0	0	0	0	died at 16 d.p.i.	0	0	0	0	1.44E+04
testes	8.88E+02	0	0	0		0	0	0	0	1.88E+04
spleen	0	0	0	0		0	0	0	0	0
kidneys	0	0	0	0		0	0	0	0	1.25E+03
liver	0	9.52E+03	2.68E+02	0		0	0	2.11E+03	0	0
lungs	0	0	0	0		0	0	0	0	0
heart	0	0	0	0		0	0	0	0	0
brain	0	0	0	0		0	0	0	0	0
tumor	5.76E+08	4.54E+08	5.99E+07	0		5.90E+08	3.35E+08	1.45E+09	7.37E+08	1.54E+09
average/tumor	2.73E+08					9.30E+08				

Kinetics of viral biodistribution of VACVs in “non-responder” FaDu-bearing mice at 3, 10, 21 days p.i. Viral titer in tissue samples, pfu per organ or grams of tumor. To determine the safety of the new VACV GLV-1h282 in mice, FaDu tumor-bearing mice (350 mm³) were injected with GLV-1h282 or GLV-1h68 (5 x10⁶ pfu per mouse). Titers were recovered from different organs and tumors following the protocol (see methods).

4.1.12 Virally Expressed GLAF-5 Reduces Tumor Vascularity and Stromal Cellularity

Therapies targeting FAP inhibited tumor growth partially through suppressing blood vessel angiogenesis (Liao, Luo et al. 2009; Santos, Jung et al. 2009; Fan Cai 2012). To evaluate whether virally expressed GLAF-5 in tumors had effects on tumor angiogenesis, FaDu tumors were excised at 16 d.p.i. and blood vessel density (BVD) in tumors was determined and quantified by staining for CD31 expression (Frentzen, Yu et al. 2009; Liao, Luo et al. 2009). Compared to GLV-1h68-treated group, the BVD in the infected areas of GLV-1h282-treated tumors was 3.8-fold decreased ($P < 0.05$) (**Figure 4.1.13**). In uninfected areas, the BVD in GLV-1h282-treated tumors was 2.1-fold and 2.4-fold lower than in PBS treated ($P < 0.05$) and GLV-1h68-treated ($P < 0.05$) tumors, respectively, suggesting that GLAF-5 suppressed angiogenesis in the FaDu tumors.

Because FAP is a marker of mesenchymal stem cells and plays an important role in regulation of stromagenesis (Kalluri and Zeisberg 2006; Spaeth, Dembinski et al. 2009), we investigated whether GLAF-5 could exhibit a direct effect on tumor mesenchymal stem cells. **Figure 4.1.13 C** shows that expression of GLAF-5 resulted in a 2.3-fold decrease in activated fibroblasts in GLV-1h282-infected areas compared to that in GLV-1h68-infected areas. In uninfected areas, the number of FAP+ cells in GLV-1h282-treated tumors was 2.25-fold and 2-fold lower than in PBS-treated ($P < 0.01$) and GLV-1h68-treated ($P < 0.05$) tumors, respectively.

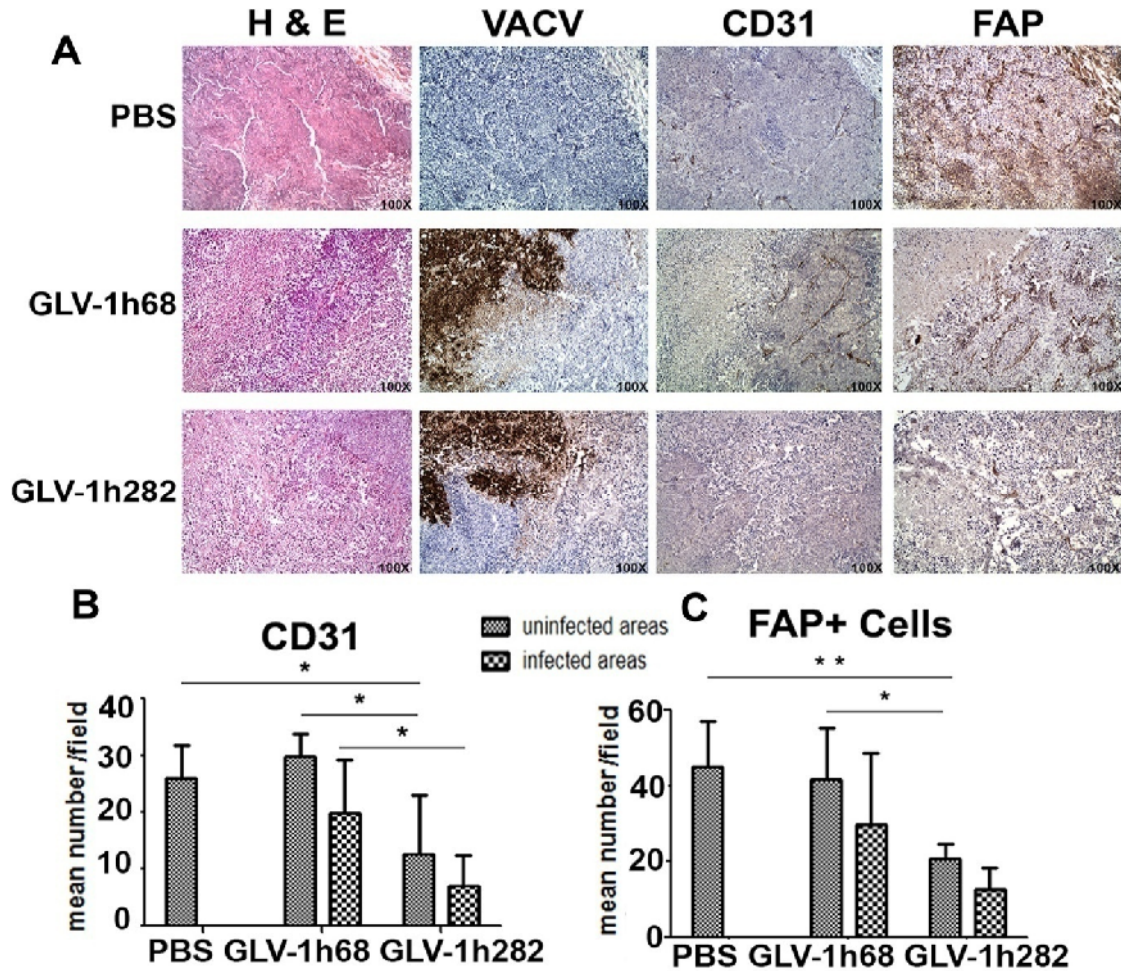
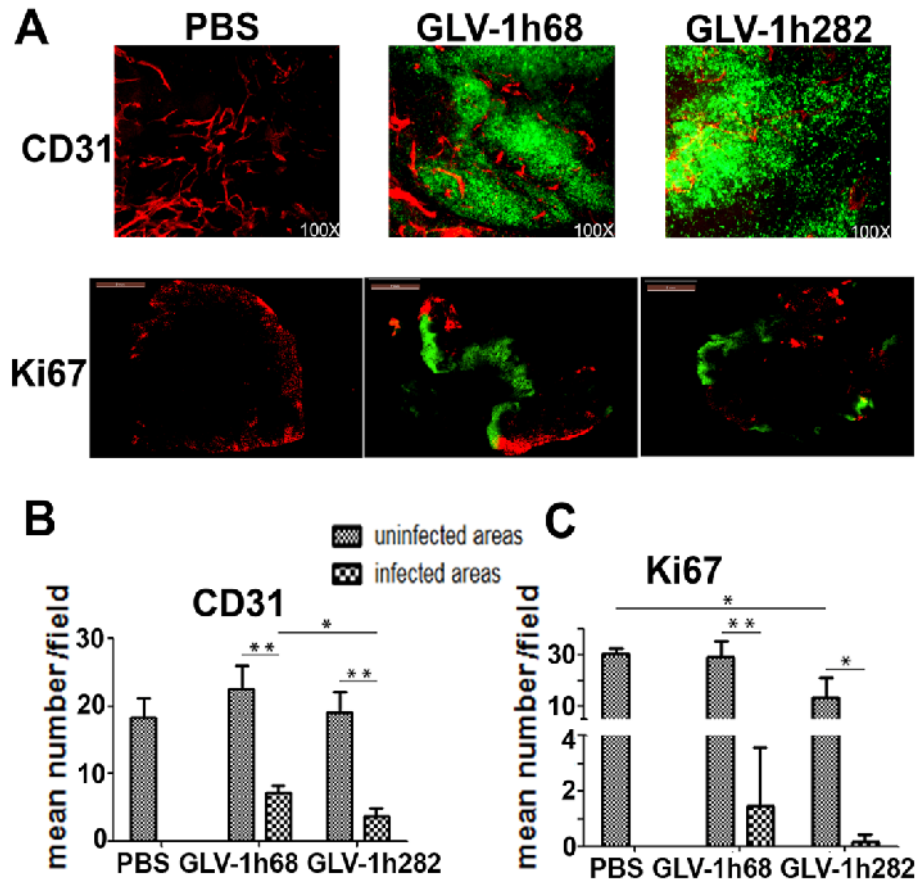


Figure 4.1.13 Expression of GLAF-5 by GLV-1h282 suppresses angiogenesis and FAP+ stromal cells recruitment in FaDu tumors. (A) Immunohistochemical characterization of viral replication, angiogenesis and stromagenesis. Formalin-fixed and paraffin-embedded tumor tissues (n= 4-5 per group) were cut into 5 μ m sections and H&E staining was performed. Adjacent sections were labeled with PECAM-1 for blood vessels, anti-A27L for VACV and anti-FAP for FAP+ stromal cells. Shown are representative areas of tumor sections at 100x magnification. Statistical analysis was performed using Student's t-Test (* $P < 0.05$) (B) Bar graphs show the mean numbers of blood vessels in infected or uninfected areas. BVD was estimated by calculating the number of CD31+ endothelial clusters on 5 non-overlapping fields (100 \times magnification) from 4 or 5 tumors per group. (C) Bar graphs show the mean numbers of FAP+ stromal clusters in infected or uninfected areas by counting 5 non-overlapping fields (100 \times magnification) from 4 or 5 tumors per group. Statistical analysis was performed using Student's t-Test (* $P < 0.05$, ** $P < 0.01$).

In addition, the IHC analysis of DU145 tumors showed a significant reduction in blood vessels and cell proliferation in virus-infected areas after treatment with GLV-1h282 (**Figure 4.1.14**). In GLV-1h282-treated tumors, CD31+ clusters were significantly less than in GLV-1h68-infected tumors ($P < 0.05$). Also, compared to uninfected areas of VACV treated tumors, infection with either GLV-1h68 or GLV-1h282 dramatically reduced BVD ($P < 0.01$ for GLV-1h68-treated group and $P < 0.001$ for GLV-1h282-treated group). Ki67 is a very important marker for evaluating cell proliferation. **Figure 4.1.14 C** shows Ki67+ clusters were significantly decreased in infected areas compared to uninfected areas ($P < 0.01$ for GLV-1h68-treated group and $P < 0.05$ for GLV-1h282-treated group). The expression of GLAF-5 further decreased the number of Ki67+ clusters in both infected and uninfected areas compared to GLV-1h68-treated tumors while no statistically significant change was seen between PBS treated tumors and uninfected areas of GLV-1h68-treated tumors. There was a dramatic difference in BVD between uninfected areas of GLV-1h282-treated tumors and PBS treated tumors ($P < 0.05$).

Taken together, we conclude that expression of GLAF-5 mediated by GLV-1h282 improved tumor oncolysis by significantly reducing tumor vascularity and stromal cellularity and proliferation.



4.1.14 Expression of GLAF-5 in GLV-1h282-localized tumors suppresses angiogenesis and cell proliferation in tumors.

(A) Suppression of blood angiogenesis and cell proliferation ($n=3$). GFP expression of virus-infected cells, CD31 expression (red) or Ki67 positive cells (red) in tumor sections was evaluated. Representative examples are shown. PBS-treated tumors exhibited high proliferation and were highly vascularized, but tumors treated with GLV-1h68 or GLV-1h282 revealed reduced CD31 positive blood vessels and cell proliferation in infected areas. (B) Quantitative analysis of blood vessels was performed by counting CD31+ endothelial cells in eight non-overlapping fields per slide. Statistical analysis was performed using Student's t-Test (* $P < 0.05$). (C) Quantitative analysis of proliferation responses by nuclear expression of Ki67 in eight independent fields per slide. Statistical analysis was performed using Student's t-Test (* $P < 0.05$, ** $P < 0.01$).

4.2. Anti-EGFR Nanobody Encoded by Vaccinia Virus Significantly Enhances Antitumor Therapy (Part 2)

4.2.1 Combined Treatment of GLV-1h68 with Erbitux Enhances Antitumor Therapy in A549 Xenograft Model

Previously, we have shown the enhanced therapeutic efficacy of GLV-1h68 in combination with chemotherapy or immunotherapy (Zhang, Yu et al. 2007; Frentzen, Yu et al. 2009). To evaluate whether the combined treatment with GLV-1h68 and anti-EGFR monoclonal antibody would lead to an additive effect on tumor growth, mice bearing A549 tumors were treated with a single dose of GLV-1h68 or PBS. One group of GLV-1h68 or PBS treated mice was injected intraperitoneally (i.p.) with multiple high dose of Erbitux. The antibody treatment started at one week post injection (p.i.) of GLV-1h68 or PBS and was administered three times weekly for five consecutive weeks (dose reference from (Steiner, Joynes et al. 2007)). **Figure 4.2.1** shows the curve of tumor growth undergoing dynamic change. Tumor growth in the group with Erbitux treatment alone exhibited a similar trend as the PBS group, although tumor sizes were smaller than those of the PBS group. Tumor growth in the GLV-1h68-treated group exhibited the typical three-phase growth pattern as described previously (Zhang, Yu et al. 2007). Tumor sizes exceed those of the PBS group at the beginning, followed by cessation of growth in the middle time period and tumor size regression in the end. Administration of Erbitux to GLV-1h68-treated mice led to significantly increased tumor regression. Thus, the combined use of virotherapy and immunotherapy resulted in more efficient tumor regression than each treatment alone.

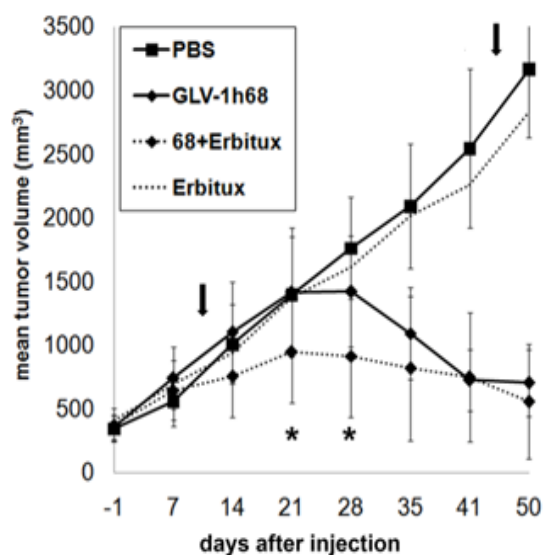


Figure 4.2.1 Treatment of A549 xenograft tumors in mice with GLV-1h68, Erbitux or combination. Mice with A549 tumors ($n \geq 7$) were injected with GLV-1h68 alone (2×10^6 pfu/mouse) or PBS. One group of PBS and GLV-1h68-treated mice was injected intraperitoneally with Erbitux (12 mg/kg, three times weekly for five consecutive weeks) beginning one week after virus injection. Statistical analysis was performed using one-way ANOVA (* $P < 0.05$). Stars indicate the comparison of the GLV-1h68 group with GLV-1h68 plus Erbitux group. The arrows indicate the beginning and end of Erbitux treatment.

4.2.2 Construction of GLV-1h442 Encoding the Anti-EGFRVHHFLAG Nanobody

Encouraged by the enhanced therapeutic efficacy of combined treatment of GLV-1h68 with Erbitux in the A549 xenograft mouse model compared to each treatment alone, the new recombinant VACV encoding anti-EGFRVHHFLAG nanobody was constructed (**Figure 4.2.2**). The plasmid pGH-anti-EGFRVHH contains the sequence of anti-EGFRVHH, which directly targets the extracellular domain of EGFR. The DDDDK FLAG tag peptide was added in the C-terminus of the nanobody for easy

expression, purification and detection. This fusion nanobody cassette was inserted into the *J2R* locus of GLV-1h68 under the synthetic early/late promoter, to produce GLV-1h442.

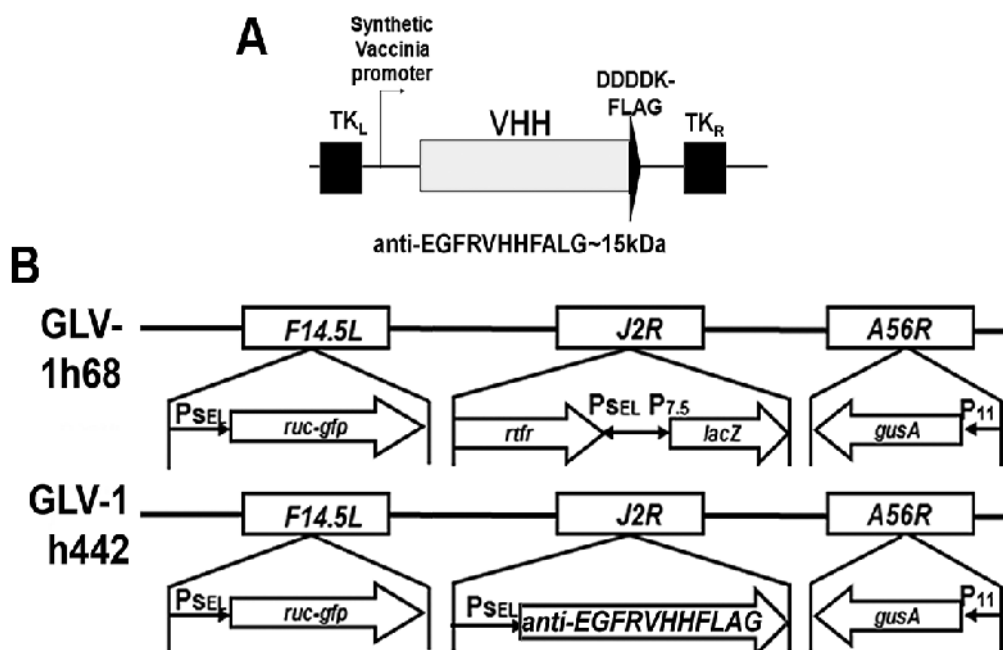


Figure 4.2.2 Expression and purification of anti-EGFRVHHFLAG nanobody in GLV-1h442-infected cells. (A) Schematic of anti-EGFRVHHFLAG nanobody gene construct. (B) VACV constructs and marker genes. GLV-1h68 was used for construction of the modified strain GLV-1h442 expressing anti-EGFRVHHFLAG nanobody. p11, VACV p11 late promoter; pSEL, VACV SEL promoter; p7.5, VACV 7.5K early/late promoter.

4.2.3 Expression of Anti-EGFRVHHFLAG Nanobody in GLV-1h442-infected Cells

The expression of anti-EGFRVHHFLAG nanobody was confirmed in GLV-1h442-infected A549 cells by Western blot analysis (**Figure 4.2.3**). Western blot results of the supernatant and cell lysates from GLV-1h442-infected A549 cells showed a

specific protein band with the expected size of 15 kDa. Samples from GLV-1h282 (VACV encoded anti-FAPFLAG scAb) infected A549 cells were used as a control which showed a protein band around 30 kDa. And no protein was detected in samples from GLV-1h68-infected and uninfected cells.

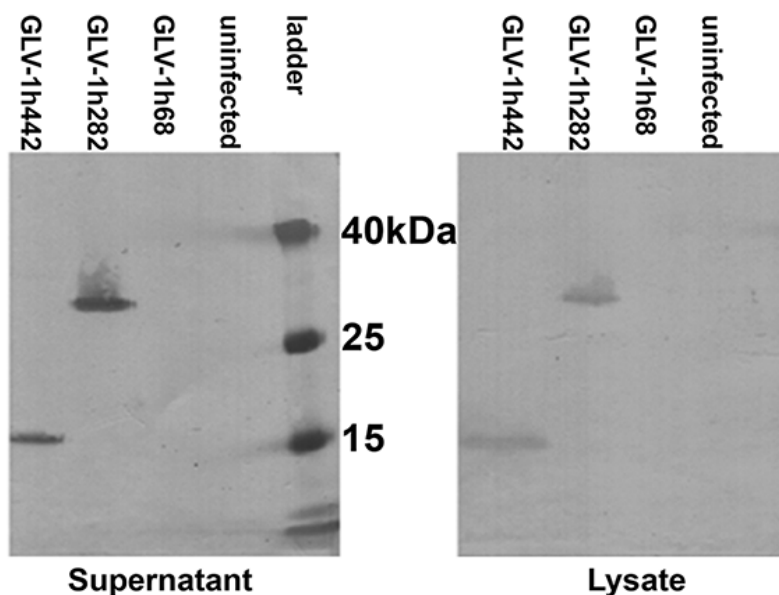


Figure 4.2.3 Expression of anti-EGFRVHHFLAG nanobody in A549 cancer cells after GLV-1h442 infection. Expression of anti-EGFRVHHFLAG nanobody in A549 cancer cells after GLV-1h442 infection. A549 cancer cells were infected with GLV-1h442 at an MOI of 1. The supernatant and cell lysates were isolated and separated by SDS/PAGE. Western blot assay was performed and anti-EGFRVHHFLAG nanobody was detected by anti-DDDDK antibody. Expression of nanobody was shown with the expected size around 15 kDa and GLAF-5 with an expected size around 30 kDa was used as positive control.

4.2.4 Purification of Anti-EGFRVHHFLAG Nanobody

To evaluate the function of the anti-EGFRVHHFLAG nanobody, it was purified from GLV-1h442-infected cells using the FLAG Immunoprecipitation kit. The purified

nanobody was analyzed in increasing amounts by Commassie Blue staining and no non-specific bands were detected (**Figure 4.2.4**).

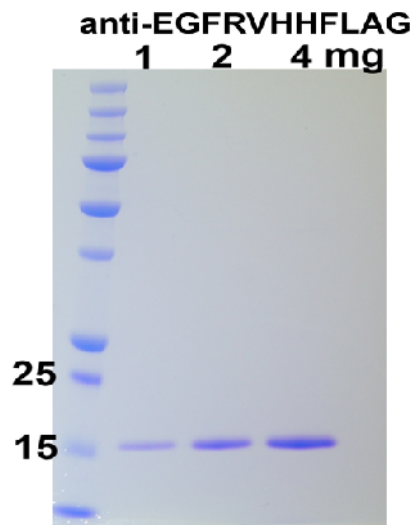


Figure 4.2.4 Purification of anti-EGFRVHHFLAG nanobody. Anti-EGFRVHHFLAG nanobody produced in MDA-MD-435 cells (no EGFR expression) with serum free medium was purified from cell lysates with IP FLAG kit (Sigma). Increasing amount of purified nanobody was analyzed by SDS/PAGE and Commassie blue staining of the gel to evaluate the purity.

4.2.5 Purified Anti-EGFRVHHFLAG Nanobody Decreases Phosphorylation of EGFR in Cells

The purified anti-EGFRVHH nanobody was evaluated for its ability to inhibit EGFR-mediated phosphorylation. Several phosphorylation sites of EGFR were examined. As **Figure 4.2.6** shown, the phosphorylation of EGFR tyrosine kinase site Y845 was inhibited by the higher doses of the nanobody while the phosphorylation of other sites such as Y1045 and Y1173 were not changed. Positive controls used tyrosine kinase inhibitor AG1478 and Erbitux, which inhibited EGF-induced phosphorylation of sites of Y845, Y1045 and Y1173, and EGF alone served as the negative control.

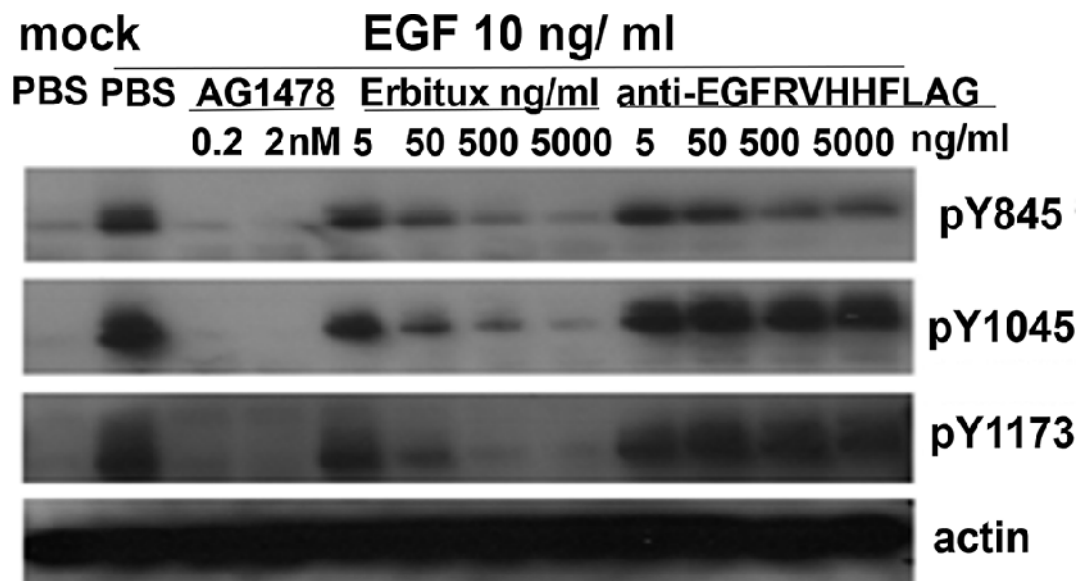


Figure 4.2.6 Anti-EGFRVHHFLAG nanobody blocks EGF-induced phosphorylation of EGFR. Serum starved A549 cancer cells were pretreated with increased doses of Erbitux followed by treatment with purified nanobody or EGFR tyrosine kinase inhibitor AG1478, then EGF was added. EGFR phosphorylation was evaluated in cell lysates by Western blot analysis.

4.2.6 Anti-EGFRVHHFLAG Nanobody Does Not Alter Viral Replication Efficiency

To evaluate the effects of expression of the nanobody on viral replication efficiency and cell killing activity, replication and cell viability assays in cell culture were performed as previously described. As shown in **Figure 4.2.7**, A549 cells were infected with VACVs at an MOI 0.01. GLV-1h442 exhibited a similar replication curve as GLV-1h68.

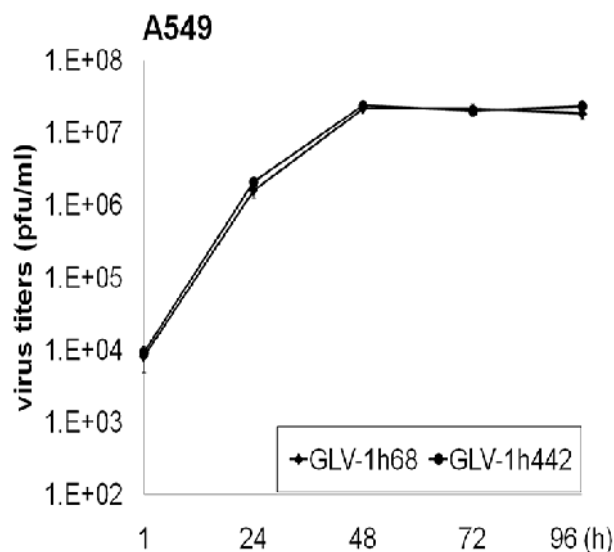


Figure 4.2.7 Virally expressed anti-EGFRVHHFLAG nanobody does not alter viral replication efficiency. Replication efficiency of GLV-1h68 and GLV-1h442 in A549 cancer cells at MOI 0.01. Mean values of triplicates are presented.

4.2.7 Anti-EGFRVHHFLAG Nanobody Does Not Alter Cell Killing Activity

For viral cell killing assay, A549 cells were infected with either GLV-1h68 or GLV-1h442 at low (MOI 0.01) and high (MOI 1) (**Figure 4.2.8**). Cell viability was determined each day following infection for four consecutive days. Cell growth medium treatment was used as the uninfected control. At MOI 1, cell viability decreased immediately after infection and survival curves of the two viruses were almost identical, indicating that cells infected with each virus died at the same rate. However at MOI 0.01, cells continued to grow after infection and started to die after 24 h.p.i. In this case, the cell killing ability of GLV-1h442 was significantly reduced compared to GLV-1h68 ($P < 0.05$). Except for the observations at low MOI, the viral

replication and cancer cell killing ability of GLV-1h442 were not overly affected by the expression of anti-EGFRVHHFLAG nanobody.

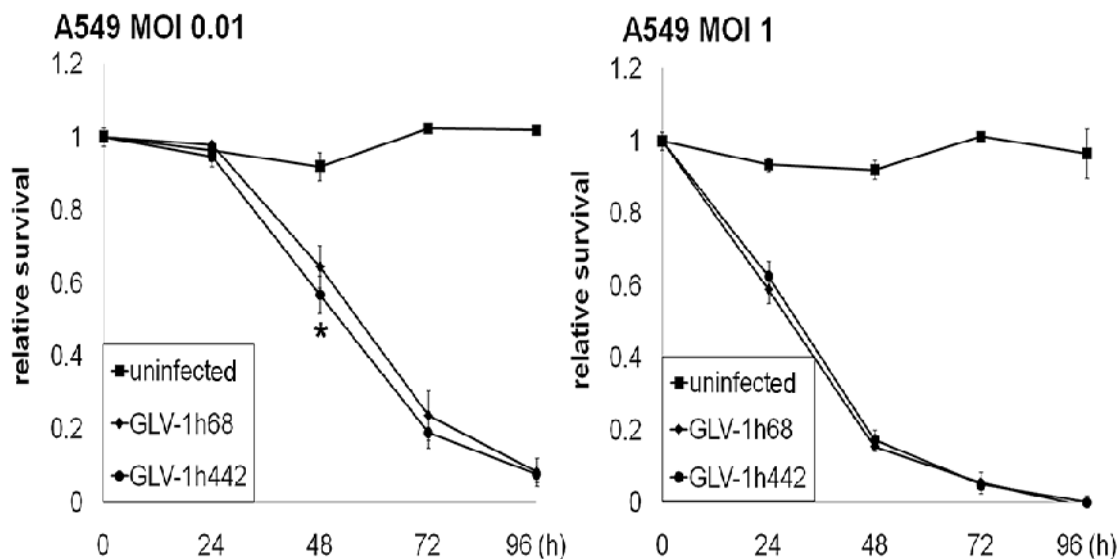


Figure 4.2.8 Virally expressed anti-EGFRVHHFLAG nanobody does not alter cell killing ability. Cell killing ability of GLV-1h68 and GLV-1h442 in A549 cancer cells at MOI 0.01 and MOI 1. Cell viability was determined daily for four consecutive days by XTT proliferation kit. Cell viability before infection was normalized as 1. Mean values of quadruplicates are presented. Statistical analysis was performed using one-way ANOVA (* $P < 0.05$, ** $P < 0.01$) and stars indicate comparison between GLV-1h68 and GLV-1h442.

4.2.8 Anti-EGFRVHHFLAG Nanobody Enhances Antitumor Effects in A549 and DU145 Human Xenograft Models

To investigate the antitumor effects of GLV-1h442 in animal models, mice bearing A549 tumors were injected with PBS or VACVs with or without the combination of Erbitux when the mean tumor size reached 450 mm³. PBS-treated or GLV-1h68-

treated mice were randomly divided into two groups ($n \geq 7$ per group) and one group of each was injected i. p. with Erbitux at 3 mg/kg twice a week for five consecutive weeks starting at 10 d.p.i (**Figure 4.2.9 A**). The tumors kept growing in the PBS-treated group as well as in the PBS combined with Erbitux-treated group. The tumor growth of the GLV-1h68 group also exhibited the typical three-phase pattern as previously described in this study (Zhang, Yu et al. 2007; Yu, Galanis et al. 2009). The tumor sizes of mice treated with GLV-1h68 in combination with Erbitux were smaller than GLV-1h68 alone, but increased rapidly after termination of Erbitux treatment. The combined therapy of GLV-1h68 and Erbitux led to an enhanced inhibition of tumor growth only during the treatment period, while the tumor sizes of mice treated with GLV-1h442 were consistently smaller than the combined therapy of GLV-1h68 and Erbitux or each treatment alone during the entire treatment period. **Figure 4.2.9 B** shows the tumor growth curve of the DU145 xenograft mouse model upon single dose of VACV injection ($n=5$). The average tumor size of GLV-1h442-treated mice was also consistently smaller than that of GLV-1h68-treated mice, though both of them exhibited the typical three-phase growth pattern. Moreover, the starting of tumor shrinkage in GLV-1h442-treated mice was one week earlier than that of GLV-1h68-treated mice, although there was not a significant difference between these two viruses, likely because of the low numbers of mice. Overall, GLV-1h442 exhibited substantial antitumor effects in lung and prostate carcinoma xenograft models.

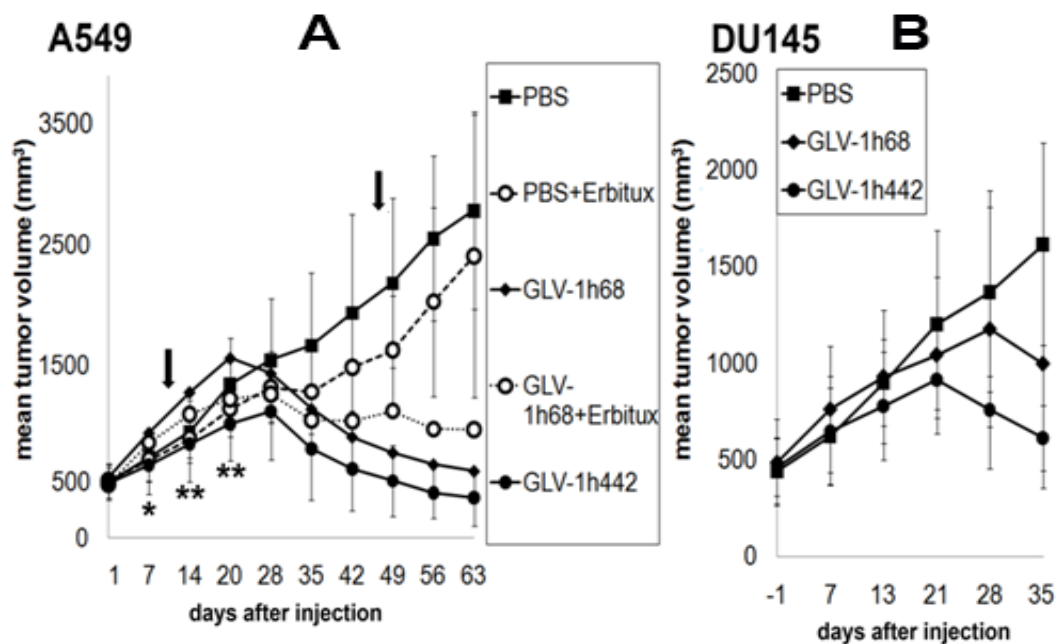


Figure 4.2.9 Virally expressed anti-EGFRVHHFLAG nanobody in GLV-1h442 colonized tumors exhibits enhanced inhibition on tumor growth in xenograft mouse models. (A) Antitumor effects of GLV-1h442 treatment compared to GLV-1h68 with or without Erbitux (i.p., 3 mg/kg, twice a week for five consecutive weeks, starting one week after injection) treatment in mice bearing A549 tumors ($n \geq 7$). Statistical analysis was performed using one-way ANOVA (* $P < 0.05$, ** $P < 0.01$). Stars indicate the comparison between GLV-1h68-treated group and GLV-1h442-treated group. The arrows indicate the beginning and end of Erbitux treatment. (B) Antitumor effects of GLV-1h442 treatment compared to GLV-1h68 treatment in mice bearing DU145 tumors ($n=5$).

4.2.9 Anti-EGFRVHHFLAG Nanobody Does Not Cause Toxicity in A549 and DU145 Human Xenografts

To determine the toxicity of GLV-1h442 which expressing anti-EGFRVHHFLAG nanobody, the change of mouse body weight was monitored weekly. The *in vivo*

toxicity was evaluated based on the change of net body weight during treatment (**Figure 4.2.10**). The overall toxicity of GLV-1h442 was similar to that of GLV-1h68 in both of A549 and DU145 xenograft tumor models.

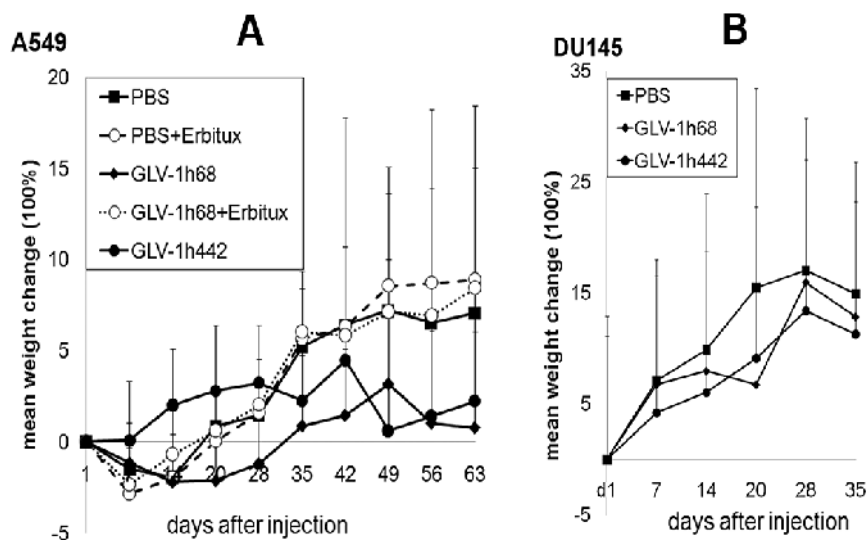


Figure 4.2.10 Mean net body weight changes of GLV-1h442-treated mice compared to GLV-1h68 mice with A549 or DU145 tumors. (A) Mean net body weight change of GLV-1h442 treatment compared to GLV-1h68 with or without Erbitux (i.p., 3 mg/kg, twice a week, for five consecutive weeks, starting at one week after injection) treatment in mice with A549 tumors ($n \geq 7$). (B) Mean net body weight change of GLV-1h442 treatment compared to GLV-1h68 treatment in mice with DU145 tumors ($n=5$).

4.2.10 Virally Expressed Anti-EGFRVHHFLAG Nanobody is Present in Serum of GLV-1h442-treated Mice

To detect anti-EGFRVHHFLAG nanobody in mouse serum, blood samples were collected retro-orbitally from mice bearing A549 tumors after injection of GLV-1h442

at 7, 21 and 35 days p.i. Concentration of anti-EGFRVHHFLAG nanobody was determined in EGFR-precoated plates using a standard curve generated from purified nanobody. Anti-EGFRVHHFLAG nanobody was readily detected in mouse serum at 7 d.p.i. and the concentration reached a maximum at 21 d.p.i. followed by a drop at 35 d.p.i. (**Figure 4.2.11**). The drop in nanobody concentration at 35 d.p.i. corresponded with a decline in tumor size starting at 28 d.p.i.

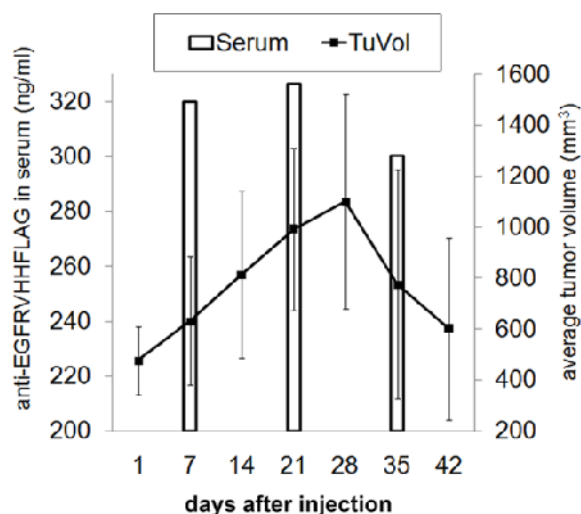


Figure 4.2.11 Expression of anti-EGFRVHHFLAG nanobody in mice serum and alteration of tumor volume in GLV-1h442-treated mice with A549 tumors.

Expression of anti-EGFRVHHFLAG nanobody in mouse serum and change in tumor volume in GLV-1h442-treated mice with A549 tumors. The mouse blood was collected retro-orbitally at 7, 21, 35 days p.i. The expression of anti-EGFRVHHFLAG nanobody was evaluated by ELISA assay with EGFR-precoated plates. Tumor volume was measured by a digital caliper. Each group included four mice.

4.2.11 Virally Expressed Anti-EGFRVHHFLAG Nanobody Does Not Change Viral Distribution

To determine whether the expression of anti-EGFRVHHFLAG nanobody by VACV would affect viral tissue distribution and possible toxicity *in vivo*, mice bearing A549

tumors were sacrificed and organs and tumors were collected by dissection at 14 d.p.i. The viral titers in organs and tumors were determined with standard viral plaque assay in CV-1 cells. **Table 4.2.1** shows that overall titers in tumors were 10^4 to 10^6 logs higher than those found in other organs. Titters in tumors of GLV-1h442-treated mice were about twice higher than those of GLV-1h68-treated mice and GLV-1h68 combined with Erbitux-treated mice. Titters of GLV-1h68 and GLV-1h68 plus Erbitux were not significantly different.

Results

Table 4.2.1 Viral distribution and titers of GLV-1h442 in mice with A549 tumors

Viral distribution of VACVs in A549 tumor-bearing mice at day 14 post infection (pfu/organ or tumor)

animal number	GLV-1h68				GLV-1h68+Erbtux				GLV-1h442			
	19957	20019	20097	20098	20059	20064	20065	20066	20012	20013	20014	20080
bladder	0	0	0	0	0	0	0	0	0	0	3.67E+03	0
testes	0	0	0	3.56E+03	0	2.40E+02	0	0	0	0	4.30E+03	1.05E+02
spleen	2.37E+02	0	0	8.40E+01	0	1.70E+02	0	0	0	0	6.99E+02	4.80E+02
kidneys	0	0	0	0	0	0	0	0	0	0	0	0
liver	0	0	0	0	0	0	0	0	0	0	0	0
lungs	5.40E+02	0	2.68E+02	4.15E+02	0	0	0	0	79.8	0	0	3.40E+02
heart	0	0	0	0	0	0	0	0	0	0	0	0
brain	0	0	0	0	0	0	0	0	0	0	0	0
tumor	6.00E+07	1.70E+07	3.33E+07	5.27E+07	1.82E+06	5.57E+07	7.35E+07	1.50E+07	2.36E+07	1.06E+06	5.58E+07	2.64E+08
tumor average	4.08E+07				3.65E+07				8.61E+07			

Viral tissue distribution and titers of GLV-1h442 in mice with A549 tumors. Viral titers in tumor and organs (pfu per tumor or organ). To determine the distribution of GLV-1h442 *in vivo*, mice with A549 tumors were injected with GLV-1h442 or GLV-1h68 (2 x10⁶ pfu/mouse in 100 µL PBS). Organs and tumors were collected at 14 d.p.i. and homogenized. After three cycles of freeze/thaw and sonication, the viral titers were determined in CV-1 cells by viral plaque assay.

4.2.12 Virally Expressed Anti-EGFRVHHFLAG in GLV-1h442-colonized Tumors Inhibits Cell Proliferation

According to previous study, EGFR was involved in regulation of cell proliferation and apoptosis (Nicholson, Gee et al. 2001). To evaluate the effects of virally expressed anti-EGFRVHHFLAG nanobody on cell proliferation, immunohistochemistry (IHC) staining of Ki67 was performed, which is a maker of cell proliferation. DU145 tumors (n=3) were collected at 36 d.p.i. and processed by standard histology protocol. The extent and location of VACV infection in the tumor sections was evaluated by intensity of GFP. **Figure 4.2.12 A** shows that in PBS-treated tumors most Ki67+ cells were present at the tumor edge. In GLV-1h68-treated tumors, different areas of the tumors could be distinguished as virus-infected and non-infected by GFP fluorescence. In the uninfected areas, the number of Ki67+ cells were similar to that in PBS treated tumors, whereas in infected areas Ki67+ cells were in much greater reduced in number. No Ki67+ cells were found in GLV-1h442-infected areas and only a few Ki67+ cells were present in uninfected areas of GLV-1h442-treated tumors, which was significant less than that in GLV-1h68-treated and PBS-treated tumors (**Figure 4.2.12 B**).

Angiogenesis is also an important factor to evaluate tumor development and involved in regulation of tumor growth according to our previous studies (Frentzen, Yu et al. 2009). Blood vessel density (BVD) was calculated by vessels counting after IHC staining of CD31. **Figure 4.2.12 C** shows that the representative images of BVD in VACV-infected tumors. In uninfected areas, there was no significant difference between VACV-treated tumors and PBS-treated tumors, whereas in infected areas, BVD dramatically decreased after treatment with GLV-1h68 ($P < 0.01$) or GLV-1h442 ($P < 0.001$), although, there was no significant difference between the two VACV-treated groups. Thus, the inhibition of tumor growth by virally expressed anti-

EGFRVHHFLAG nanobody in GLV-1h442 tumors was attributed to suppression of cell proliferation. Nonetheless, expression of the nanobody did not alter the significant reduction in blood vessel density caused by VACV infection.

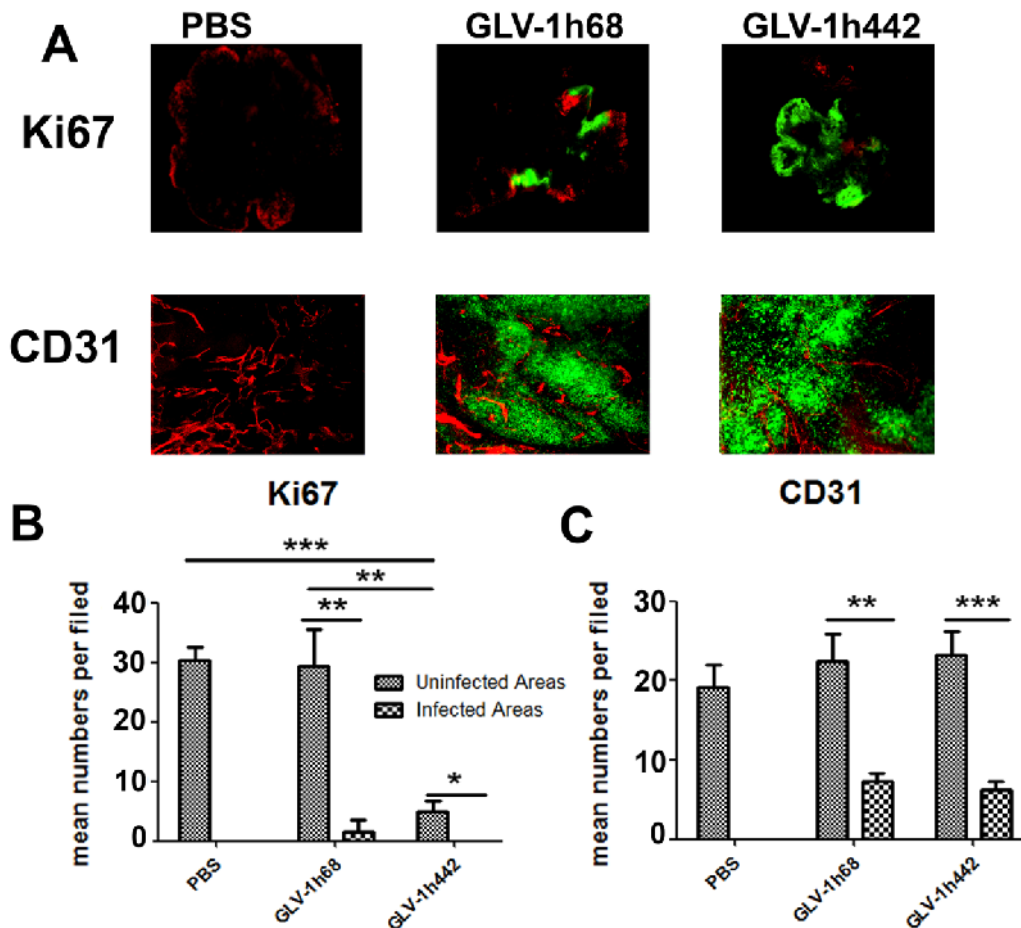


Figure 4.2.12 Virally expressed anti-EGFRVHHFLAG nanobody suppresses cell proliferation rather than angiogenesis in GLV-1h442 colonized DU145 tumors.

Representative images of changes in cell proliferation (A) and blood vessel density (B) are shown. Tumors were dissected at 36 d.p.i. and fixed, sectioned and labeled with anti-human Ki67 antibody for detection of cell proliferation (red) or anti-mouse CD31 antibody for detection of endothelial cells (red). GFP indicated viral infection (green). Quantitative analysis of Ki67+ cells (C) or CD31+ cells (D) in uninfected and infected areas (n=3, 8 non-overlapping fields in uninfected areas and in infected areas from each tumor).

4.3 Expression of Anti-VEGF Antibody Together with Anti-EGFR or Anti-FAP Drastically Enhances Tumor Regression As a Result of Vaccinia Virotherapy (Part 3)

4.3.1 Construction of Two Antibodies Expressing VACVs

We previously showed that VACVs encoded antibody targeting VEGF (GLV-1h108, GLV-1h164) (Frentzen, Yu et al. 2009; Patil, Gentshev et al. 2012; Buckel, Advani et al. 2013), EGFR (GLV-1h442) or FAP (GLV-1h282) significantly enhanced therapeutic effects in human tumor xenograft models compared to their parental virus GLV-1h68. To evaluate whether expressing two antibodies simultaneously in the same virus would exhibit additive benefit in efficacy *in vivo*, two new recombinant VACVs were constructed. The expression cassette for anti-EGFRVHHFLAG or GLAF-5 was inserted into the *J2R* locus of GLV-1h164 under synthetic early/late (SEL) promoter, resulting in GLV-1h444 and GLV-1h446, respectively (**Figure 4.3.1**).

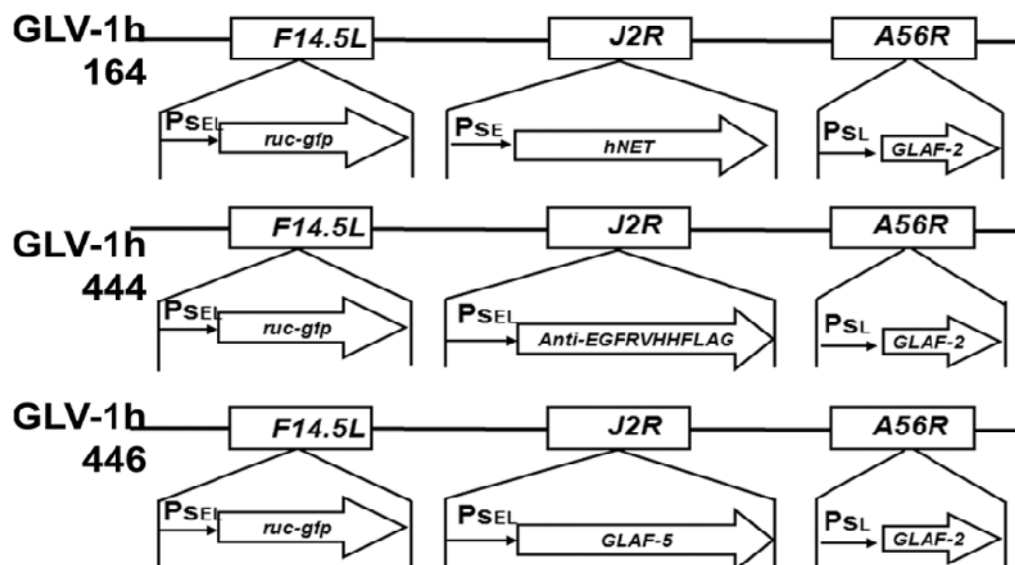


Figure 4.3.1 Genomic structures of the new recombinant VACVs along with their parental viruses. GLV-1h444 and GLV-1h446 were derived from GLV-1h164 by replacing *hNET* expression cassette at *J2R* locus with anti-EGFRVHHFLAG nanobody and GLAF-5 under the control of the PSEL promoter, respectively. All viruses contain *ruc-gfp* expression cassette at *F14.5L* loci. PSE, PSEL, PSL, P11 and P7.5 are VACV synthetic early, synthetic early/late, synthetic late, 11K and 7.5K promoters, respectively.

4.3.2 Expression of Two Antibodies

To determine expression of two antibodies, A549 cancer cells were infected with new VACV strains while the infected supernatant and cell lysates were harvested for Western blot analysis. **Figure 4.3.2** shows the expression of the specific protein bands with the expected sizes. The single chain antibody backbone was able to be recognized using a customized G6 antibody in GLV-1h164-, GLV-1h282-, GLV-1h444- and GLV-1h446-infected samples. Meanwhile, FLAG tag was able to be detected in GLV-1h282-, GLV-1h442-, GLV-1h444- and GLV-1h446-infected samples by anti-DDDDK antibody. The bands from virus-infected samples were all detectable

by anti-A27L antibody which targets the membrane protein A27 in VACV. The amount of samples loaded in the analysis was equally normalized as determined by similar band intensity of actin.

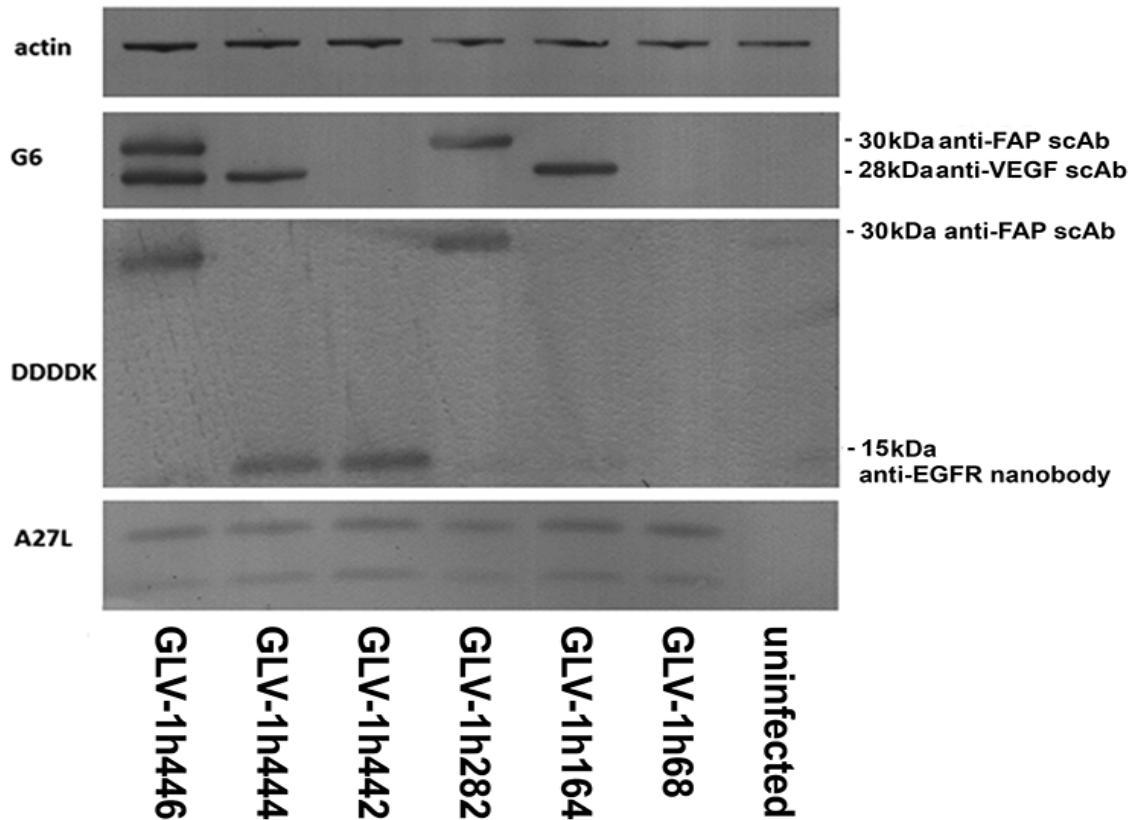


Figure 4.3.2 Expression of antibodies in VACV-infected cancer cells. Western blot analysis of antibody expression in infected A549 cells. A549 were infected with VACVs at an MOI of 1. Samples were harvest at 24 h.p.i. Cell lysates were separated by SDS/PAGE. Western blot analysis was performed with anti-DDDDK antibody targeting FLAG tag, customized G6 antibody targeting scAb backbone, customized anti-A27L antibody targeting membrane protein of VACVs, actin was used as a loading control.

4.3.3 Two Antibodies Expressing VACVs Exhibit Reduced Virus Replication Efficiency

For replication assay, cells were infected with VACVs at a multiplicity of infection (MOI) of 0.01 and harvested at different time points after infection followed by determination of viral titers in CV-1 cells. **Figure 4.3.3** shows the results of representative experiments of viral replication in A549 cancer cells in the early growth phase of 24 to 72 hours post infection (h.p.i.). GLV-1h444 had significantly increased replication efficiency compared to its parental virus GLV-1h442 at 24 h.p.i. ($P < 0.05$). However at 48 h.p.i., GLV-1h444 had significantly reduced replication efficiency compared to GLV-1h164 at 48 h.p.i. ($P < 0.01$) and GLV-1h442 ($P < 0.05$). GLV-1h446 also exhibited significantly lower replication efficiency than GLV-1h164 ($P < 0.001$) and GLV-1h282 ($P < 0.01$) at 48 h.p.i.

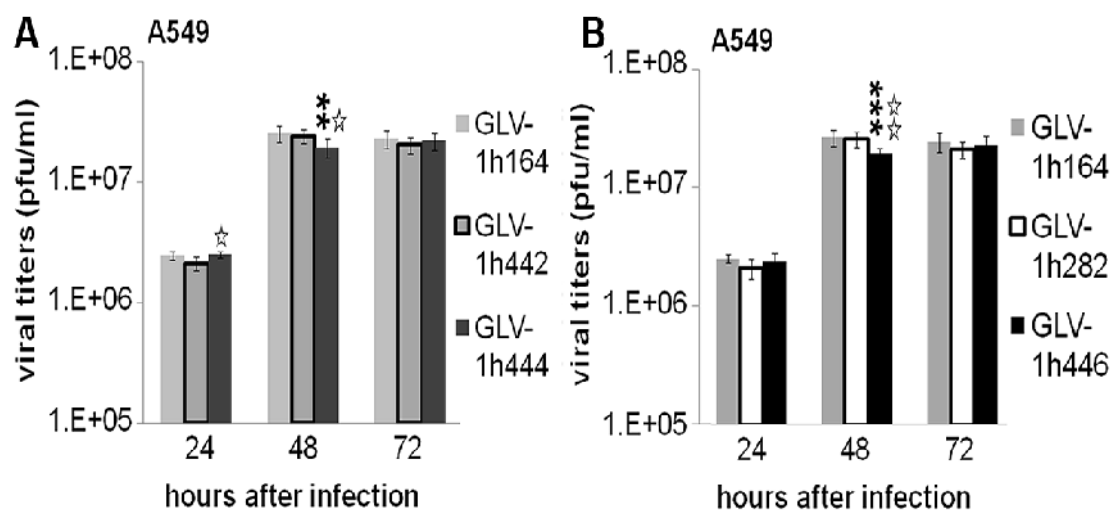


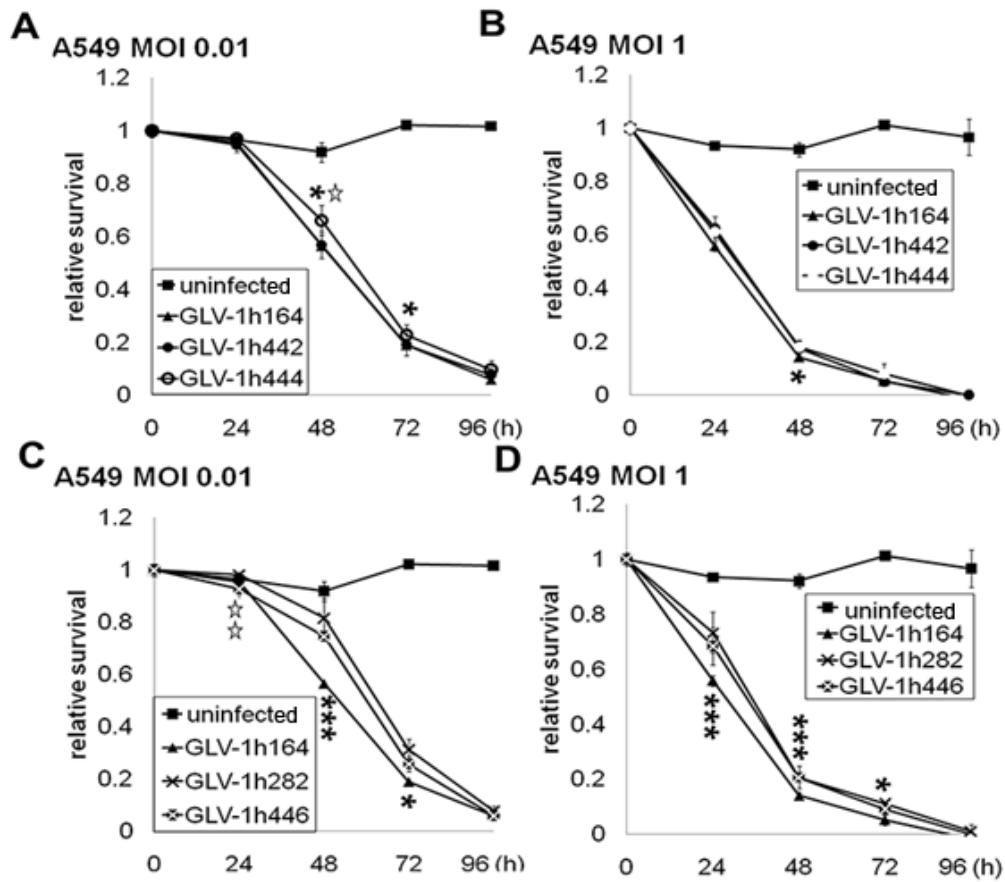
Figure 4.3.3 Comparisons of replication capacity of VACVs in cancer cells.

Replication efficiency of GLV-1h164, GLV-1h442 and GLV-1h444 (A) and GLV-1h164, GLV-1h282 and GLV-1h446 (B) in A549 cancer cells at an MOI of 0.01. Infected cells and supernatant were

collected for determination of viral titers. Statistical analysis was performed using one-way ANOVA (** $P < 0.01$, * $P < 0.05$).

4.3.4 Two Antibodies Expressing VACVs Exhibit Reduced Viral Cell Killing Efficiency

For cell viability, A549 cancer cells were seeded in 96-well plates and infected with each VACV either at a lower MOI (0.01) or at a higher MOI (1) on the next day and then monitored for cell viability for four consecutive days. **Figure 4.3.4 A and C** shows that at the MOI of 0.01, initially the cells continued to grow for 1 day, but declined thereafter. The cell killing efficiency of GLV-1h444 was significantly lower than GLV-1h164 at 48 ($P < 0.05$) and 72 ($P < 0.05$) hours p.i. as well as lower than GLV-1h442 at 48 h.p.i. ($P < 0.05$). At the MOI of 1 (**Figure 4.3.4 B**), cell viability was more rapid than at MOI 0.01 and declined continuously starting at 1 day. GLV-1h444 showed the reduced cell killing efficiency than GLV-1h164 at 48 h.p.i. ($P < 0.05$). **Figure 4.3.4 C** shows the same trend for GLV-1h446 which exhibited dramatically reduced cell killing ability compared to its parental virus, GLV-1h164, at 48 ($P < 0.001$) and 72 ($P < 0.05$) hours p.i. and GLV-1h282 at 24 h.p.i. ($P < 0.01$). At higher MOI of 1, the cells died at a faster rate. By day 3, about 80% of cells were dead (**Figure 4.3.4 B and D**). The viruses expressed the two antibodies appeared to achieve the same endpoint in cancer cell killing at the end, however their killing efficiencies were consistently lower than their parental viruses, which was similar to their replication. Among them, the cell killing abilities of GLV-1h444 and GLV-1h446 were significantly lower than that of GLV-1h164 at 48 h.p.i. ($P < 0.05$) and 24 ($P < 0.001$), 48 ($P < 0.001$), 72 ($P < 0.05$) hours p.i., respectively. Overall, the VACVs simultaneously expressed two antibodies exhibited reduced cell killing efficiency.



Figure

4.3.4 Comparisons of cell killing ability of VACVs in cancer cells. Viability of A549 cells upon infection of VACV with MOI 0.01 (A and C) or MOI 1 (B and D). Medium treated cells were used as control. The amount of viable cells was determined daily for four consecutive days by XTT proliferation kit (Roche). Values are shown as percentage of respective control. Statistical analysis was performed using one-way ANOVA (** $P < 0.01$, * $P < 0.05$).

4.3.5 Two Antibodies Expressing VACVs Reduce Tumor Growth in Human Xenograft Models

To investigate the contribution of two antibodies on tumor progression, two xenograft models of A549 and DU145 were delivered with a single dose of different VACVs. PBS injected tumor-bearing mice were used as negative control. For immunotherapy, a group of PBS and GLV-1h68 injected mice were injected intraperitoneally (i.p.) with the commercially available antibodies Avastin and Erbitux twice a week for five continuous weeks, starting at day 10 (**Figure 4.3.5 A**). Tumors kept growing in PBS treated groups while PBS treatment combined with Avastin and Erbitux led to slower growth for the period of antibody administration whereas followed by faster growth of tumors after terminating the delivery of antibodies at 49 d.p.i. In GLV-1h68-treated mice, tumor growth showed typical three-phases patterns, as described previously (Zhang, Yu et al. 2007): keeping growing at early phase followed by stagnation at the middle phase with tumor regression finally at the late phase. The tumor sizes of mice treated with GLV-1h68 combined with Avastin and Erbitux were smaller than that of GLV-1h68 while the trend was similar to PBS treated groups. The tumor sizes of mice treated with GLV-1h164 and GLV-1h442 were consistently smaller than that of PBS or GLV-1h68-treated groups. However, it was not as small as that of GLV-1h444. And the tumor sizes of GLV-1h444-treated group were significantly smaller than that of GLV-1h442-treated group at 14 and 28 days p.i. ($P < 0.05$). **Figure 4.3.5 B** shows that the tumor sizes of GLV-1h446-treated groups were consistently and significantly smaller than that of its parental viruses of GLV-1h164 treated group at 20 d.p.i. ($P < 0.05$) and GLV-1h282-treated group at days 14, 28, 35 ($P < 0.05$) as well day 20 ($P < 0.01$) p.i. Individual tumor growth curves of A549 tumor-bearing mice are shown in **Figure 4.3.6**.

In the case of the DU145 model (**Figure 4.3.5 C**), tumor growth of the GLV-1h68-treated group also exhibited typical three-phase growth pattern. Tumors kept growing in all mice except GLV-1h444- and GLV-1h446-treated groups which showed consistently slowed or halted tumor growth and the tumor sizes of GLV-1h444-treated group were smaller than that of GLV-1h442-treated group at 13 and 21 days p.i., which exhibited additive efficacy.

Above all, treatment with two antibodies expressing VACVs GLV-1h444 or GLV-1h446 led to stagnation in tumor growth and exhibited the additive efficacy than single antibody expressed VACVs.

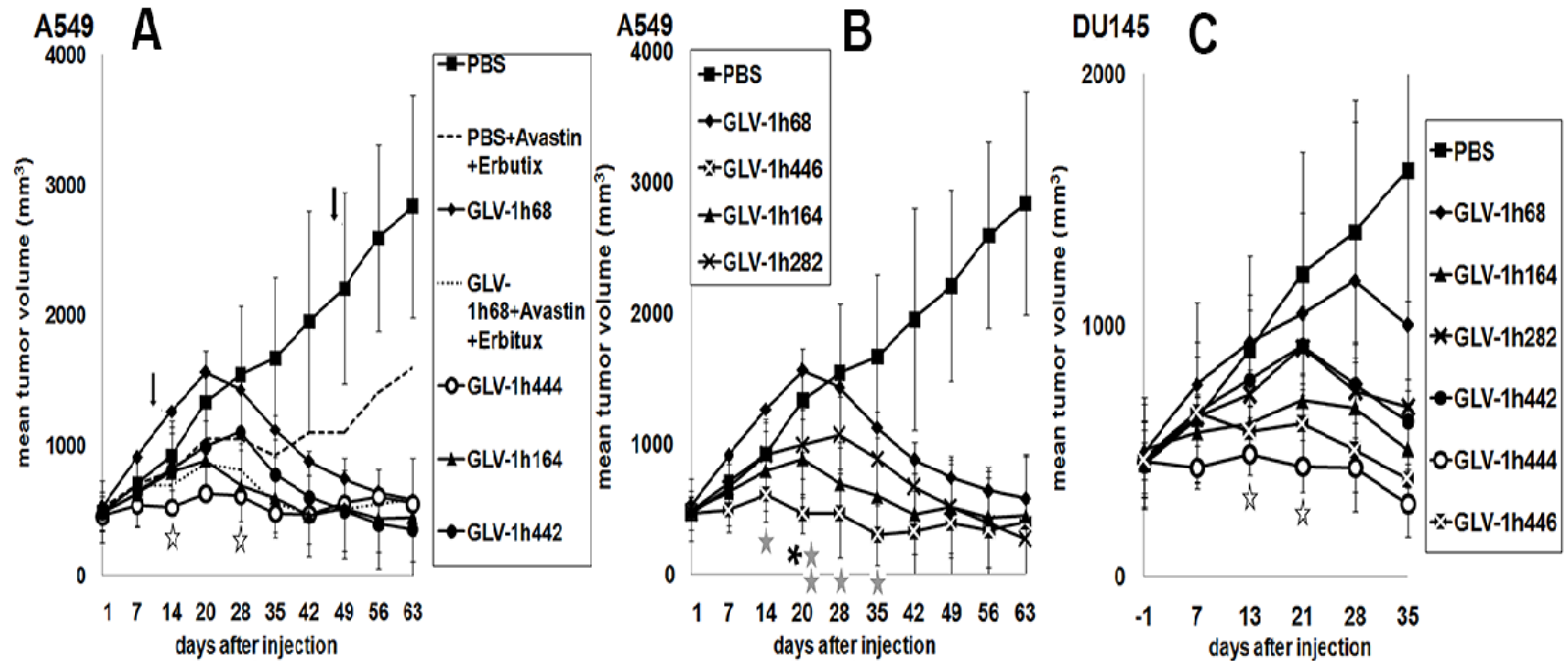


Figure 4.3.5 Two antibodies expressed by VACVs enhance viral antitumor effects in xenograft models. (A-C)

Antitumor effects of VACV strains delivering GLAF-2 and GLAF-5 or GLAF-2 and anti-EGFRVHHFLAG nanobody on tumor growth in A549 tumor-bearing mice (A and B) ($n \geq 7$) or DU145 tumor-bearing mice (C) ($n=5$). Statistical analysis was performed using one-way ANOVA (* $P < 0.05$, ** $P < 0.01$). Stars indicate the comparison among groups of GLV-1h444 and GLV-1h442 (A), groups of GLV-1h446 and GLV-1h164 (black) as well as GLV-1h282 (grey) (B), groups of GLV-1h444 and GLV-1h442 (open) (C). The arrows indicate the start and end of injection of Avastin and Erbitux.

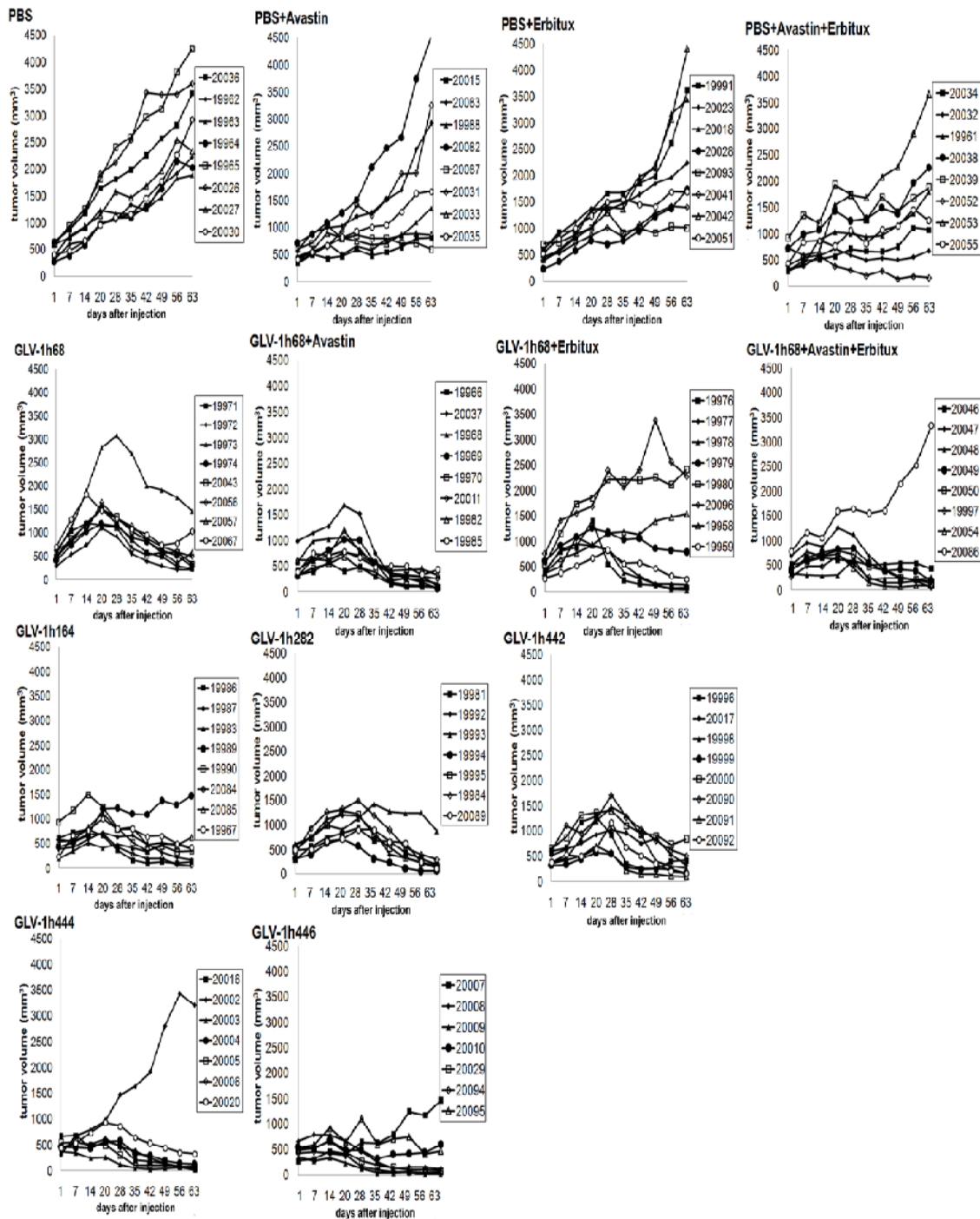


Figure 4.3.6 Individual tumor volume change of A549 tumor-bearing mouse was

monitored after VACV treatment or combined with Avastin and/or Erbitux (n=7-8).

4.3.6 Virally Expressed Antibodies are Detectable in Serum of Mice.

After expression of antibodies in virus-infected cells was confirmed, the presence of antibodies in tumor-bearing mice was also investigated. Serial blood samples were collected retro-orbitally from A549 tumor-bearing mice at 7, 21, and 35 days p.i. All samples were tested for the presence of GLAF-2 by ELISA with VEGF-precoated plates, GLAF-5 with FAP-precoated plates, and anti-EGFRVHHFLAG nanobody with EGFR-precoated plates. **Figure 4.3.7** shows that all three antibodies were detectable at all three different time points. Expression of GLAF-2 was lower in samples from GLV-1h164-injected mice than GLV-1h444- and GLV-1h446-injected mice at 7 and 21 days p.i. The difference was statistically significant between GLV-1h446- and GLV-1h164-treated groups at 21 d.p.i. ($P < 0.001$). This was correlated with lower viral titers in tumors of the GLV-1h164-treated group and higher titers in the GLV-1h446-treated group at 14 d.p.i. (**Table 4.3.1**). Overall, the results indicated that tumor shrinkage at day 35 was preceded by increased expression of antibodies at early stages of treatment (day 7 and 21).

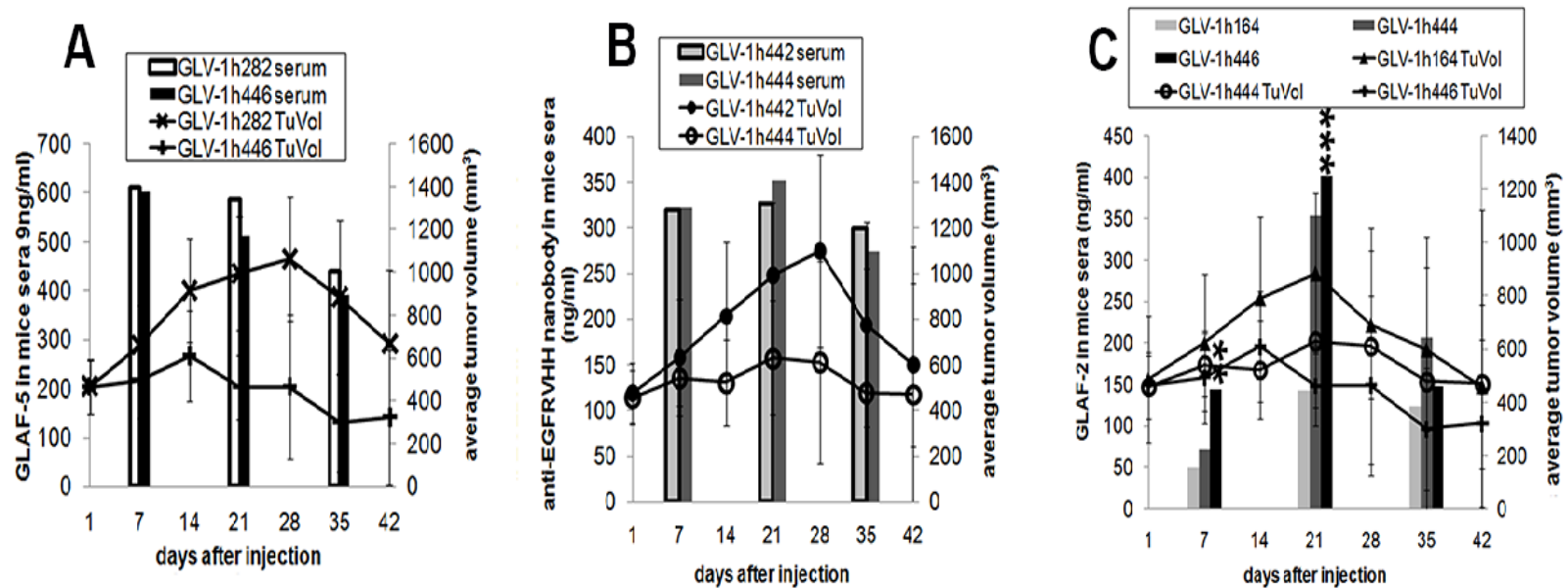


Figure 4.3.7 Detection of antibodies in mouse serum and changes of tumor volume in mice bearing A549 tumors after VACV treatment. (A-C) Expression of antibodies in mouse serum and changes in tumor volume in mice bearing A549 tumors after treatment with VACVs. Blood samples were collected retro-orbitally at 7, 21, 35 days p.i. The concentration of antibodies in mouse serum was evaluated by ELISA assay with precoated FAP, EGFR and VEGF plates, respectively. Tumor volume was measured with a digital caliper. Statistical analysis was performed with Student's t-Test (** $P < 0.01$, *** $P < 0.001$). Stars indicate the comparison between groups of GLV-1h446 and GLV-1h164.

4.3.7 Expression of Two Antibodies by VACVs Does Not Alter Viral Tissue Distribution in Mice

To evaluate the viral toxicity in mice, the changes in net body weight were determined. In the A549 xenograft model, the mean change of net body weight was no more than 10% of initial 30 g weight for any of the VACVs (**Figure 4.3.8 A**). In the DU145 xenograft model, the mean body weight of mice kept increasing slightly after injection of the viruses compared to the base of 21 g (**Figure 4.3.8 B**). Thus, the new VACVs expressed two antibodies did not show evidence of significant toxicity in mice.

The biodistribution analysis of VACVs in different organs or tumors in A549 tumor-bearing mice was performed based on the standard viral plaque assay. **Table 4.3.1** shows that higher viral titers of all virus strains were able to be detected in all tumors and no virus was detected in healthy organs, indicating the viruses were able to specifically target and replicate efficiently in tumors. There were no significant differences of viral titers in tumors between mice treated with two antibody expressing GLV-1h444 and other VACVs or by GLV-1h68 combined with commercially available antibodies. However, viral titers in tumors with treated with GLV-1h446 exhibited significantly higher titers than the parental virus, GLV-1h164 ($P < 0.05$).

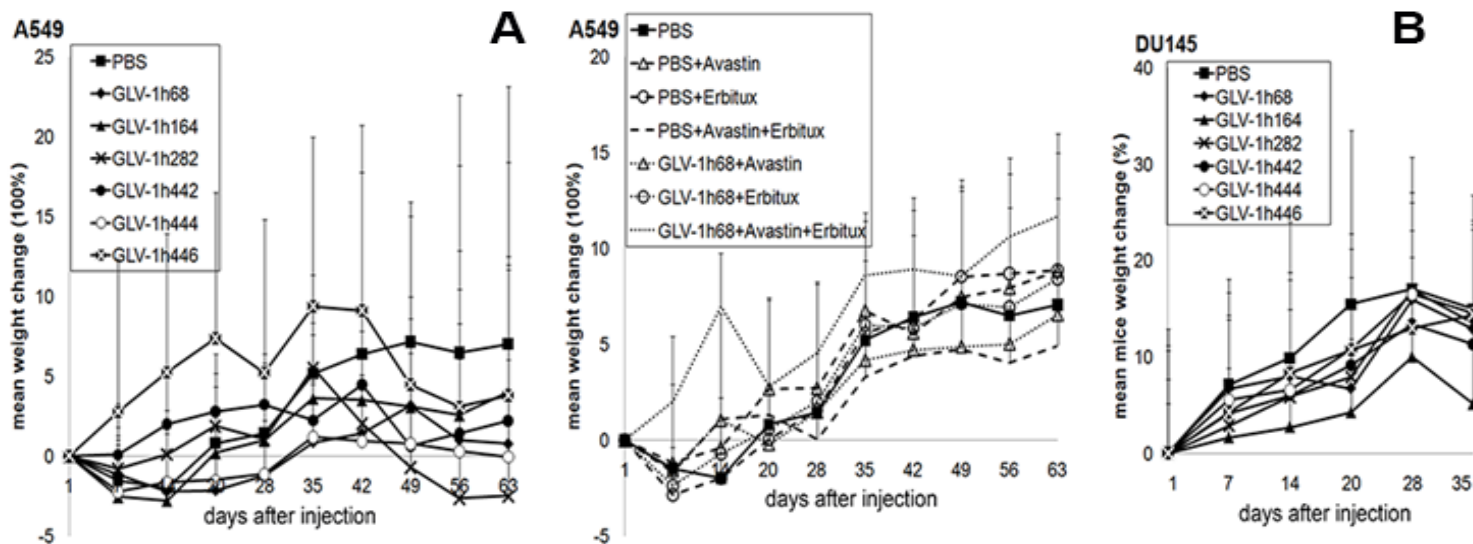


Figure 4.3.8 Changes of mean net body weight of mice were monitored after VACV injection. No significant net body weight change in A549 tumor-bearing mice (A) and DU145 tumor-bearing mice (B). Statistical analysis was performed with one-way ANOVA.

Table 4.3.1 Virally expressed two antibodies do not change viral safety and viral biodistribution in mice.

Viral distribution of VACVs in A549 tumor bearing mice at day 14 post infection (pfu/organ or tumor)

animal No.	GLV-1h68				GLV-1h68+Avastin				GLV-1h68+Erbbitux				GLV-1h68+Avastin+Erbbitux			
	20097	20098	19957	20019	20060	20061	20063	20070	20059	20064	20065	20066	20062	20068	20069	20071
bladder	0	0	0	0	0	0	0	0	0	0	0	0	0	0	0	0
testes	0	3.56E+03	0	0	0	0	0	0	0	2.40E+02	0	0	0	0	0	0
spleen	0	8.40E+01	2.37E+02	0	0	3.47E+01	0	1.38E+02	0	1.70E+02	0	0	0	0	0	0
kidneys	0	0	0	0	0	0	2.80E+03	0	0	0	0	0	0	0	1.10E+02	0
liver	0	0	0	0	0	7.06E+02	0	2.85E+03	0	0	0	0	0	0	0	0
lungs	2.63E+02	4.15E+02	5.40E+02	0	0	0	0	6.98E+02	0	0	0	0	0	0	2.07E+02	0
heart	0	0	0	0	0	0	0	0	0	0	0	0	0	0	0	0
brain	0	0	0	0	0	0	0	0	0	0	0	0	0	0	0	0
tumor	3.33E+07	5.27E+07	6.00E+07	1.70E+07	5.66E+06	9.36E+05	1.70E+06	9.80E+07	1.82E+06	5.57E+07	7.35E+07	1.50E+07	1.08E+07	5.10E+07	5.03E+07	1.90E+06
tumor average	4.08E+07				2.66E+07				3.65E+07				2.85E+07			
stdv	1.94E+07				4.77E+07				3.37E+07				2.58E+07			

animal No.	GLV-1h164				GLV-1h282				GLV-1h442				GLV-1h444				GLV-1h446			
	20072	20073	20074	20075	20076	20077	20078	20079	20012	20013	20014	20080	19960	19975	20044	20045	20021	20022	20024	20025
bladder	0	0	0	0	0	0	0	0	0	0	3.67E+03	0	0	0	2.66E+02	0	0	5.40E+01	2.50E+02	8.19E+01
testes	0	0	0	0	0	0	0	0	0	0	4.30E+03	1.05E+02	0	0	0	0	0	0	0	3.47E+01
spleen	0	0	0	0	3.57E+02	1.73E+02	2.35E+02	0	0	0	6.98E+02	4.80E+02	0	0	0	0	0	3.05E+01	0	8.93E+02
kidneys	0	0	0	0	0	0	0	0	0	0	0	0	0	0	0	0	0	0	0	0
liver	0	0	0	0	0	0	0	0	0	0	0	0	0	0	7.07E+02	0	0	0	0	0
lungs	2.07E+02	0	2.63E+03	2.79E+02	0	0	1.60E+02	0	79.8	0	0	3.40E+02	0	0	0	0	0	3.73E+01	8.70E+01	2.68E+02
heart	0	0	0	0	0	0	0	0	0	0	0	0	0	0	0	0	0	0	0	1.84E+02
brain	0	0	0	0	0	0	0	0	0	0	0	0	0	0	0	0	0	0	0	0
tumor	4.73E+06	3.78E+05	6.66E+06	1.92E+07	9.83E+07	7.28E+07	2.32E+08	3.22E+07	2.36E+07	1.06E+06	5.58E+07	2.64E+08	3.23E+07	6.75E+04	6.99E+07	2.74E+07	4.26E+07	1.70E+07	1.92E+07	2.88E+07
tumor average	7.74E+06				1.09E+08				8.61E+07				3.24E+07				2.68E+07			
stdv	8.06E+06				8.66E+07				1.21E+08				2.87E+07				1.16E+07			

A549 tumor-bearing mice were injected *i.v.* with VACVs (2×10^6 pfu/mouse). A group of mice were intraperitoneal injected with Avastin (5 mg/kg) and/or Erbitux (3 mg/kg) twice weekly for 5 weeks starting from one week after virus injection. Tumors and organs were harvested at 14 d.p.i. Viruses were titrated in CV-1 cells.

4.3.8 Two Antibodies Expressing VACVs Suppress Cell Proliferation.

Expressed antibodies were detectable in serum of mice treated with new recombinant VACVs. To evaluate effects of virally expressed antibodies on tumor progression in the DU145 xenograft model, cell proliferation and angiogenesis were evaluated by staining with anti-human Ki67 and anti-mouse CD31 antibodies, respectively. Infection of VACVs was confirmed by expression of GFP. Representative images of detection of cell proliferation are shown (**Figure 4.3.9**). In uninfected areas, the mean number of Ki67+ cells was dramatically reduced after treatment with two antibodies expressed VACVs compared to PBS or GLV-1h68-treated groups. The mean number of Ki67+ cells from GLV-1h442-treated tumors was the least in uninfected areas. In addition, the mean numbers of Ki67+ cells from GLV-1h444- or GLV-1h446-treated tumors were also significantly less than that of GLV-1h164 treated tumors ($P < 0.05$, $P < 0.01$, respectively). The mean numbers of Ki67+ cells in infected areas were much less than in uninfected areas. In GLV-1h442-treated tumors, no Ki67+ cells were found. There was no significant difference among these groups in infected areas (**Figure 4.3.9 B and C**).

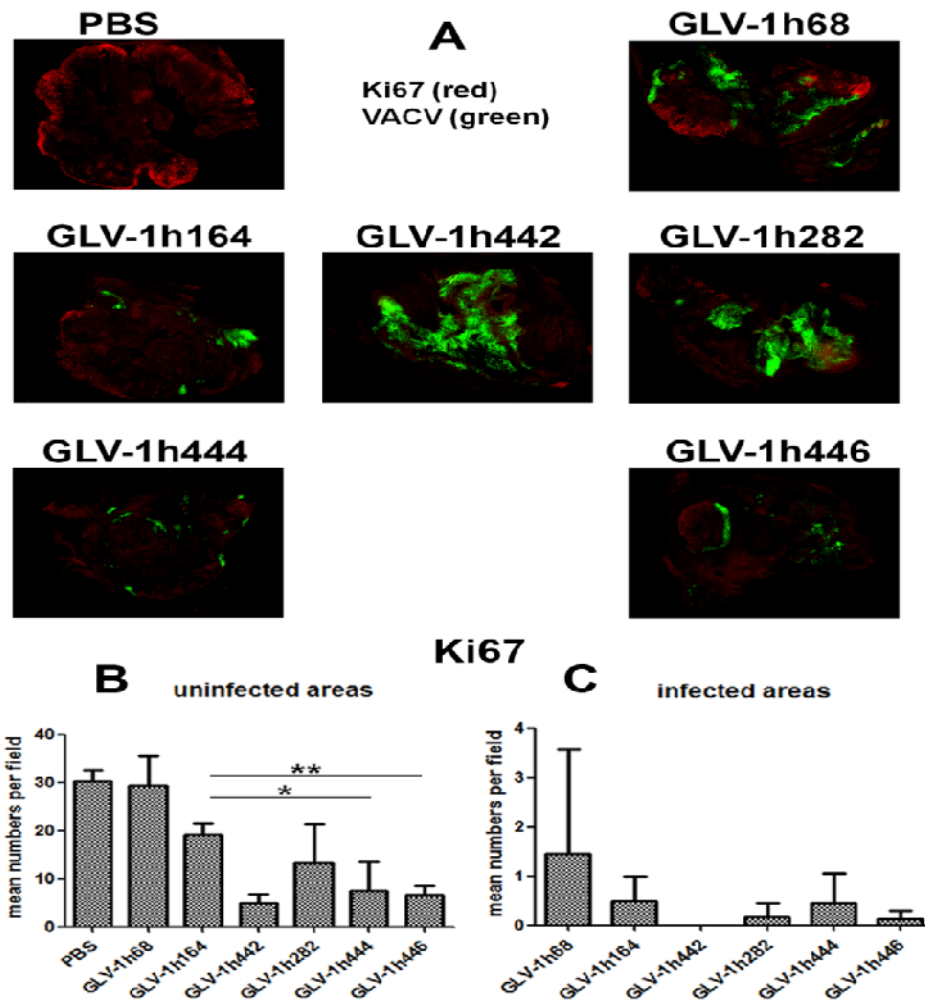


Figure 4.3.9 Two antibodies expressed by VACVs enhance suppression of cell proliferation in VACVs-colonized tumors. (A) Representative images of changes in cell proliferation ($n=3$). Cell proliferation were stained with anti-human Ki67 antibody (red). GFP expression indicates VACV-infection (green). (B and C) Quantitative analysis of cell proliferation in uninfected or infected areas was performed by counting Ki67+ cells on eight independent fields per slide. Statistical analysis was performed with Student's t-Test (** $P < 0.01$, * $P < 0.05$).

4.3.9 Two Antibodies Expressing VACVs Suppress Angiogenesis

Inhibition on angiogenesis in tumors was evaluated by staining with anti-mouse CD31 antibody and representative images of blood vessel staining were shown in **Figure 4.3.10 A**. The overall blood vessel density (BVD) was reduced after VACV treatment in infected areas. **Figure 4.3.10 B and C** show the statistical analysis of the mean numbers of CD31+ cells in virus infected or uninfected areas respectively. There was no significant difference between GLV-1h444- or GLV-1h446-treated tumors and its corresponding parental viruses in uninfected areas. While in infected areas, tumors treated with GLV-1h444 or GLV-1h446 exhibited less BVD comparing to its corresponding parental viruses and there was significant difference between GLV-1h444 and GLV-1h442-treated tumors ($P < 0.01$).

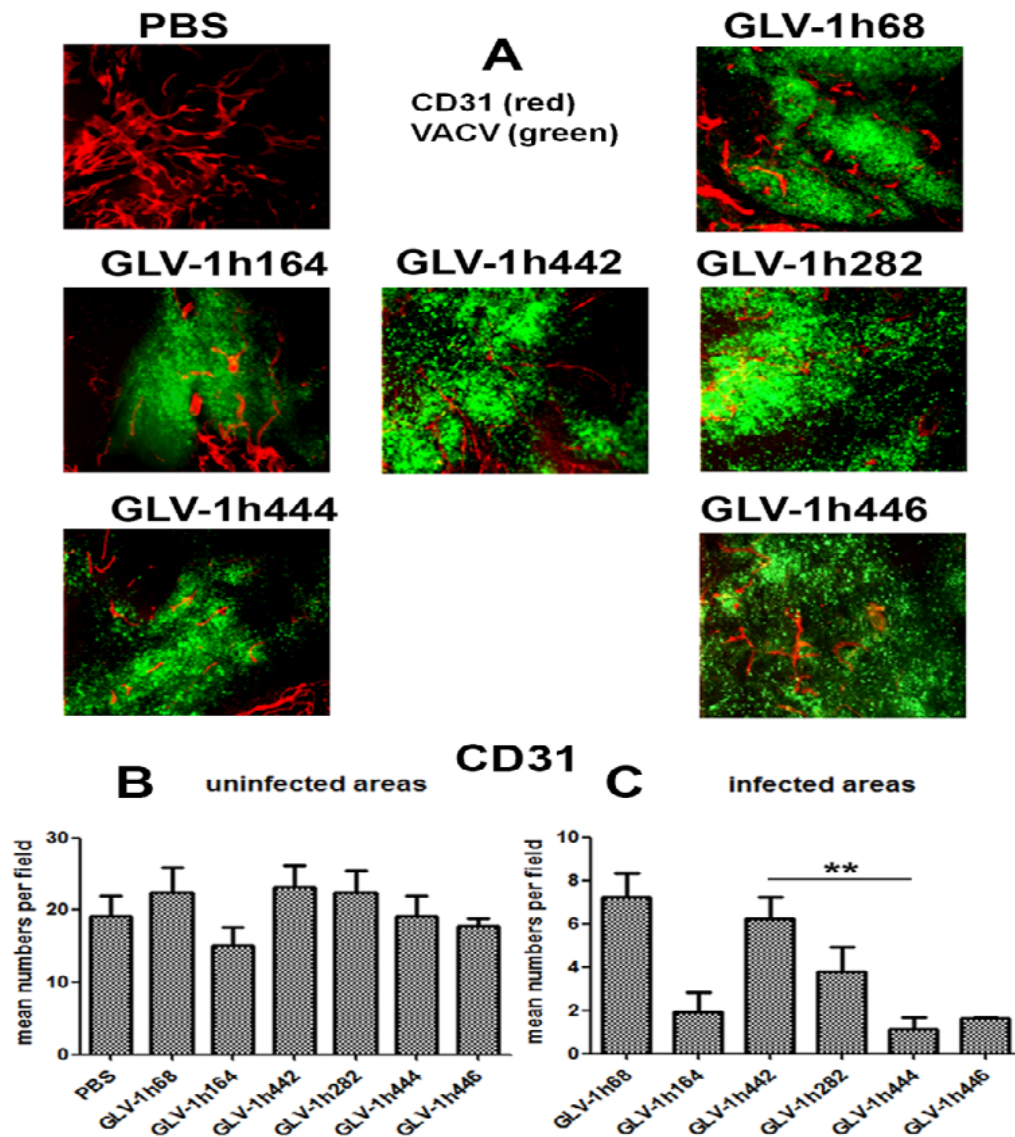


Figure 4.3.10 Two antibodies expressed by VACVs enhance suppression of blood angiogenesis in VACVs colonized tumors. (A) Representative pictures of suppression of blood angiogenesis in DU145 tumors (n=3). GFP expression indicates VACV-infected areas; blood vessels were stained with anti-mouse CD31 antibody (red). (B and C) Quantitative analysis of blood vessel density in uninfected or infected areas was performed by counting CD31+ blood vessels on eight independent fields per slide. Statistical analysis was performed with Student's t-Test (** $P < 0.01$).

Discussion

5.1 Against FAP scAb Encoded by VACV Significantly Enhances Virotherapy

Previously, we showed that GLV-1h68 mediated complete regression in different kinds of xenografts, which are now being tested in phase I/II clinical trials (Zhang, Yu et al. 2007; Chen NG 2010). GLV-1h68 also exhibited enhanced efficacy when combined with immunotherapy, chemotherapy and radiotherapy (Frentzen, Yu et al. 2009; Yu, Galanis et al. 2009; Advani, Buckel et al. 2012). In this study, we show that GLV-1h68 based oncolytic virotherapy can be engineered to express GLAF-5 in cell culture and *in vivo*, which is specifically targeting human and murine FAP in stroma. The virally expressed GLAF-5 increased viral replication and cell killing efficiency in cell culture, enhanced virotherapy *in vivo*, suppressed blood vessel density, cell proliferation and recruitment of MSCs in tumors.

FAP is one of the markers of CAF or MSC and its expression is highly restricted to malignant tumors or wounds in the body (Ostermann, Garin-Chesa et al. 2008; Tran, Chinnasamy et al. 2013), which makes it a promising target of cancer therapy. However, it was recently reported that FAP+ stromal cells are present in a majority of the body and depletion of FAP+ stromal cells caused mouse cachexia and anemia (Roberts, Deonarine et al. 2013; Tran, Chinnasamy et al. 2013). On the contrary, adoptive transfer of FAP-specific T cells *in vivo* demonstrated therapeutic effects on tumor growth without causing adverse effects (Kakarla, Chow et al. 2013) and the anti-FAP antibody sibrotuzumab (F19) was shown to be taken up by tumors but not normal organs in patients (Welt, Divgi et al. 1994; Hofheinz, al-Batran et al. 2003; Scott, Wiseman et al. 2003). Furthermore, no overt developmental defects were seen

in FAP knockout mice (Niedermeyer, Kriz et al. 2000). Hence, FAP is still a rational target for cancer therapy and deserves further study.

The epitope of FAP recognized by M036 is different from that of F19 (Brocks, Garin-Chesa et al. 2001), which was used in preclinical and clinical studies (Park, Lenter et al. 1999; Dohi, Ohtani et al. 2009; Fischer, Chaitanya et al. 2012) and did not show a therapeutic effect in patients (Welt, Divgi et al. 1994; Hofheinz, al-Batran et al. 2003; Scott, Wiseman et al. 2003). The possible therapeutic effects of M036 are still unknown (Brocks, Garin-Chesa et al. 2001). In our study, we show that expression of GLAF-5, containing the complementarity determining regions from M036, increased viral replication efficiency and reduced tumor growth, even though it did not inhibit the DPP activity of FAP (SI figure 1). This indicated that the non-proteolytic activity of FAP was likely involved in stimulating tumor growth, which was consistent with the findings of previous studies (Huang, Simms et al. 2011).

Engineering of the parental virus GLV-1h68 by replacement of *rtfr-lacZ* in the *J2R* locus with the GLAF-5 expression cassette increased viral replication and cell killing efficiency. This was due to the expression of GLAF-5. Viral replication efficiency was inversely proportionate to the transcription/translation burden added to the viral genome, as we previously described (Chen, Yu et al. 2011). In this study, GLAF-5 with one of the three strong promoters (PSE, PSEL, PSL) was inserted into the *J2R* locus of GLV-1h68 to replace the weak promoter (P7.5), which would have negative effects on viral replication. Unexpectedly, GLAF-5 expressing VACVs showed the enhanced replication efficiency, which was attributable to expression of GLAF-5 offsetting the negative effects of viral replication caused by the replacement of stronger promoters. The additive replication efficiency of GLAF-5 was also observed in “responder” and “non-responder” tumors treated with GLV-1h282, which is at least partially attributable to the enhanced virotherapy *in vivo*.

It has been shown that anti-FAP treatment resulted in suppression of blood angiogenesis (Liao, Luo et al. 2009; Santos, Jung et al. 2009). In this study, BVD was significantly reduced in VACV infected areas of tumors compared to uninfected

areas, as was previously shown that virotherapy with GLV-1h68 and its derivatives suppressed angiogenesis in VACV infected areas (Frentzen, Yu et al. 2009). However, GLV-1h282-infected areas of tumors showed an even greater reduction in BVD than in GLV-1h68-infected areas. The difference could be due to the higher viral replication efficiency of GLV-1h282 in tumors compared to GLV-1h68, since no additive effect was observed in uninfected areas of GLV-1h282 compared to tumors treated with PBS or GLV-1h68. In addition, Ki67 staining, a marker for cell proliferation, in uninfected areas of tumors treated with GLV-1h282 was significantly decreased compared to GLV-1h68 or PBS treated tumors. An explanation is that virally expressed GLAF-5 caused changes in the tumor environment, resulting in suppression of cell proliferation.

FAP is a mesenchymal stem cell (MSC) marker (Bae, Park et al. 2008; Spaeth, Dembinski et al. 2009). In the FaDu model, virally expressed GLAF-5 significantly reduced FAP+ stromal cells and CD31+ cells in uninfected areas compared to PBS or GLV-1h68-treated tumors, which demonstrated that virally expressed GLAF-5 modulated the tumor environment and suppressed MSC cells as well as angiogenesis. In addition, CD31+ cells were much less in GLV-1h282-infected areas than in GLV-1h68-infected areas. The phenomena was different in DU145 tumors, since that no significant difference of the numbers of CD31+ cells was observed in uninfected areas of tumors treated with GLV-1h68 and GLV-1h282, which might be due to higher FAP expression in FaDu tumors (Ostermann, Garin-Chesa et al. 2008).

The clinical efficacy of antibody-based immunotherapy is limited by poor penetration and sustained availability of the antibody in tumors. Overcoming these limitations requires that the immunotherapeutic be administered at high doses and at frequent intervals. GLAF-5 was consistently detectable in mouse serum after a single treatment with GLV-1h282 and the continuous biosynthesis of GLAF-5 was accompanied with successful replication of GLV-1h282 *in vivo*. The presence of GALF-5 in the circulation resulted in therapeutic effects in areas of the tumors that were not yet infected with the virus. This was evident by the reduction in Ki67+ cells,

less CD31+ cells and FAP+ cells in uninfected areas of GLV-1h282-treated DU145 tumors or FaDu tumors. Moreover, the expression level of GLAF-5 would be expected to decrease and cease in the later phases of treatment (35 d.p.i) as tumor regression occurs and viral replication in the tumor slows down.

Previous studies raised a safety concern with the depletion of FAP+ stromal cells in which cachexia or other adverse effects were observed in mouse models (Roberts, Deonarine et al. 2013; Tran, Chinnasamy et al. 2013). However, in our system, significant toxicity or abnormal behavior of mice was not observed. Compared to T cell based immunotherapy targeting FAP+ stromal cells (Kakarla, Chow et al. 2013; Tran, Chinnasamy et al. 2013), our strategy has several advantages. First, the administration of an immunotherapeutic by viral expression could be accomplished by a single dose, making it efficient, patient compliant, and economical. Second, the consistent and continuous production of virally expressed GLAF-5 is superior to T cell based therapy, which showed limited therapeutic efficacy partially due to unsuccessful persistence of T cells *in vivo*. Third, virally expressed GLAF-5 targets the FAP protein alone, not the cells expressing FAP, which might avoid adverse effects associated with the disturbance of other functions of FAP+ cells.

In summary, we demonstrate that the oncolytic VACV, GLV-1h282, encoded GLAF-5, significantly enhances anti-tumor therapy in both “responder” and “non-responder” xenograft models through suppression of angiogenesis, cell proliferation and stromagenesis, without causing apparent toxicity. The anti-tumor effects of GLV-1h282 treatment associated with the inhibition of FAP function in stromal cells were similar in strategy to T-cell based methods, but superior in efficacy and safety (Kakarla, Chow et al. 2013; Tran, Chinnasamy et al. 2013).

5.2 Against EGFR Nanobody Encoded by VACV Significantly Enhances Virotherapy

VACV GLV-1h442, engineered to express anti-EGFRVHHFLAG nanobody, specifically colonized and replicated in tumors, resulting in continuous and consistent production of EGFR targeted nanobody demonstrated by presence of anti-EGFRVHHFLAG at early (7 d.p.i.), middle (21 d.p.i.) and late (35 d.p.i.) stages of tumor infection. The highest level of nanobody coincided with higher viral replication (21 d.p.i.) followed by tumor regression at 28 d.p.i. Anti-EGFRVHHFLAG nanobody has the characteristics of small size, enhanced stability, efficient tumor penetration, and low immunogenicity and was applied for *in vivo* molecular imaging. Viral expression of anti-EGFRVHHFLAG nanobody for treatment of EGFR overexpressing carcinomas, producing a continuous source of nanobody, overcomes the limitation of administration of nanobody due to its short *in vivo* half life (41 min) (Gottlin, Xiangrong et al. 2009; Iqbal, Trojahn et al. 2010). As purified from GLV-1h442-infected cells, anti-EGFRVHHFLAG selectively inhibited the phosphorylation of a single EGFR tyrosine kinase site in A549 cells, thus blocking the EGFR-mediated signaling pathway. In contrast, two commercial kinase inhibitors Erbitux and AG1478, blocked phosphorylation of all three EGFR sites. The results may indicate that these agents might recognize different epitopes than anti-EGFRVHHFLAG or have different mechanisms in cell culture. However, *in vivo* multiple dose treatment of Erbitux combined with GLV-1h68 showed less efficient inhibition of tumor growth than single dose treatment of GLV-1h442, which demonstrated that the continuous and consistent production of EGFR targeted nanobody by VACV was more efficacious than multiple administration of monoclonal antibody.

Expression of this nanobody in cancer cells did not significantly alter viral replication and cell killing in cell culture, but it increased replication of VACV in tumors *in vivo* (8.61×10^7 pfu/tumor of GLV-1h442 vs. 4.08×10^7 pfu/tumor of GLV-1h68). The

reason for the higher viral replication was not likely due to EGFR inhibition because no such effect was seen in the GLV-1h68 combined with Erbitux-treated group (3.65×10^7 pfu/tumor of GLV-1h68 plus Erbitux).

A key factor for cancer development is uncontrolled cell growth and EGFR is involved in this process. The mean number of Ki67+ cells in infected and uninfected areas of tumors treated with GLV-1h442 was significantly less than their counterparts treated with GLV-1h68 or PBS. As expected virus infection of proliferating tumor cells causes cell lysis and death, hence a reduction in Ki67+ cells in virus infected areas. Naturally, the effect did not apply to uninfected areas of tumors where the mean number of Ki67+ cells of GLV-1h68-treated tumors was similar to that of PBS-treated tumors. However, the expression of anti-EGFRVHHFLAG nanobody targeting EGFR was able to inhibit cell proliferation in tumors as a function of the rate of replication of GLV-1h442, and the effect spread beyond the areas that were directly infected. Thus, additive effects of infection of tumors with GLV-1h442 and the expression of anti-EGFRVHHFLAG resulted in accelerated tumor growth suppression and greater tumor regression.

Angiogenesis which supports nutrients and structures is another important factor involved in cancer development. As previously described (Frentzen, Yu et al. 2009), BVD was significantly less in infected areas than that in uninfected areas of both GLV-1h68 and GLV-1h442-treated tumors. However, in uninfected areas, no significant difference was found in PBS, GLV-1h68 and GLV-1h442-treated tumors, suggesting that expression of the EGFR targeted anti-EGFRVHHFLAG nanobody had no substantial influence on tumor vascularity. This is consistent with the hypothesis that up-regulation of VEGF is independent of the EGFR signal pathway (Tabernero 2007).

Previous studies of EGFR-targeted nanobodies have shown that inhibition EGFR phosphorylation and cell proliferation in cell culture did not necessarily correspond with tumor regression *in vivo* (Roovers, Laeremans et al. 2007; Tijink, Laeremans et al. 2008; van de Water, Bagci-Onder et al. 2012). In some cases, specific delivery of

nanobodies to tumors was not efficiently achieved by systemic administration possibly because of their accumulation in kidneys and liver, giving rise to concerns of adverse renal and liver effects (Oliveira, van Dongen et al. 2012). In our system, VACV specifically colonized and replicated in tumors to lyse tumor cells in conjunction with production and spread of virally expressed nanobody, suggesting the avoidance of these shortcomings and good prospects for clinical use.

Non-small lung cancer cell line A549 (EGFR wild type, *KRAS* mutated) is moderately responsive to Erbitux (Zhang, Yun et al. 2012), consistent with our results that lower dose of Erbitux did not show efficient therapeutic efficacy in A549 tumors in mice. Additionally, we did not evaluate the therapeutic effects on carcinomas with EGFR mutation. Either of these cases could present a limitation of this treatment strategy. However, GLV-1h442 exhibited enhanced efficacy in both the low EGFR expression model (A549 xenograft mouse model) (Derer, Bauer et al. 2012) and in the high EGFR expression model (DU145 xenograft mouse model) (Dhupkar, Dowling et al. 2010) compared to its parental virus GLV-1h68.

It was reported that Erbitux mediated tumor regression was involved in the innate and adaptive immune systems in a newly developed xenograft mouse model with reconstituted immune cells (Yang, Zhang et al. 2013). It was not clear from our studies whether virally expressed anti-EGFRVHHFLAG nanobody would have an effect on these immune systems. According to previous studies, infection of VACV may change immune environments (Worschech, Chen et al. 2009), activate innate immunity (Zhang, Yu et al. 2007) and lead to accumulation of macrophages (Weibel, Basse-Luesebrink et al. 2013). Furthermore, VACV exhibited preference in replication in cancer stem-like cells (Wang, Chen et al. 2012).

In summary, our results show that GLV-1h442 expressed anti-EGFRVHHFLAG nanobody targeting EGFR enhanced tumor regression in xenograft mouse models and its efficacy was superior to GLV-1h68 alone, Erbitux alone and comparable or better than the combined treatment of GLV-1h68 with Erbitux. We also demonstrated that expression of anti-EGFRVHHFLAG nanobody was detectable *in vivo* after

colonization of tumors with GLV-1h442, which corresponded to inhibition of cell proliferation in tumors. Therefore, we propose that new anticancer strategies combining oncolytic VACV mediated antitumor therapy with therapeutic antibodies expressed by the VACV infected cells is a rational and promising approach for cancer treatment.

5.3 Expression of Anti-VEGF Antibody in Combination with Anti-EGFR or Anti-FAP Dastically Improves Virotherapy

We demonstrate that the new recombinant VACVs, GLV-1h444 and GLV-1h446, expressed antibodies of GLAF-2 combined with either anti-EGFRVHHFLAG nanobody or GLAF-5, significantly enhanced therapeutic efficacy and accelerated tumor regression in two xenograft mouse models as compared to their parental strains expressing either single antibodies or no antibodies

Expression of the two antibodies by GLV-1h444 and GLV-1h446 caused a reduction in viral replication efficiency and cell killing ability. This might be due to the replacement of the weaker promoter (PSE) in GLV-1h164 with the stronger promoter (PSEL) of anti-EGFRVHHFLAG nanobody and GLAF-5 in GLV-1h444 and GLV-1h446 respectively. It has been proven that viral replication efficiency is inversely proportional to the transcription/translation burden in the viral genome (Chen, Yu et al. 2011). The principle also applies to the reduced replication efficiency of GLV-1h444 and GLV-1h446 compared to their parental viruses GLV-1h442 and GLV-1h282, respectively, because again of the replacement of the weaker promoter (P11) with the stronger promoter (PSL). GLV-1h444 and GLV-1h446 showed higher replication efficiency than GLV-1h442 and GLV-1h282 at the early time point (24 h.p.i.) because

there was no influence of the stronger PSL promoter until it was expressed at late time points (24-48 hours p.i.).

High levels of VEGF, EGFR or FAP in patients are associated with poor prognosis of treatment outcome (Nicholson, Gee et al. 2001; Gorrell, Wang et al. 2003; Mamot and Rochlitz 2006; Chang, Garg et al. 2012; Meadows and Hurwitz 2012; Wikberg, Edin et al. 2013). Avastin and Erbitux have shown limited clinical efficacy (Bergers and Hanahan 2008; Karapetis, Khambata-Ford et al. 2008; Alberts, Sargent et al. 2012) despite their promising results in preclinical studies (Manegold 2008; Bennouna, Sastre et al. 2013), which partially could be due to poor penetration and lower tumor targeting of the antibodies *in vivo* after systemic administration (Jain 2001). Oncolytic VACV-mediated virotherapy not only specifically targets and destroys tumor cells but can also produce one or more antibodies by incorporation of expression cassettes into its genome (Zhang, Yu et al. 2007; Frentzen, Yu et al. 2009; Saravia, Zapata et al. 2009). Our data shows that continuous production of antibodies was detectable in serum of mice treated with single or two antibodies expressing VACVs, and the expression was associated with successful replication of VACVs in tumors. Higher expression of antibodies was determined in early phases (7 and 21 days p.i.) followed by lower expression at late phase (35 d.p.i.), which indirectly demonstrated that efficient virus replication resulted in tumor regression later. In addition, expression of GLAF-5 and anti-EGFRVHHFLAG nanobody were higher than GLAF-2, which was correlated with higher replication efficiency of GLV-1h282 and GLV-1h442 compared to GLV-1h164 in tumors (SI table 1). The viral titers of GLV-1h164 expressing anti-VEGF antibody in tumors were almost four-fold lower than that of GLV-1h68 (7.74×10^6 pfu/tumor vs. 4.08×10^7 pfu/tumor, $P < 0.05$). Additionally, the groups treated with Avastin (GLV-1h68 combined with Avastin, 2.66×10^7 pfu/tumor or GLV-1h68 combined with Avastin and Erbitux, 2.85×10^7 pfu/tumor) and GLAF-2 (GLV-1h444, 3.24×10^7 pfu/tumor or GLV-1h446, 2.69×10^7 pfu/tumor) also showed lower viral titers in tumors than GLV-1h68. The results here indicate that the suppression of blood vessels and the reduction of nutrient supplements would reduce tumor growth and viral replication. However, VACVs

expressed EGFR or FAP targeted antibodies showed higher replication efficiency in GLV-1h442 or GLV-1h282-treated tumors (GLV-1h442, 8.61×10^7 pfu/tumor and GLV-1h282, 1.09×10^8 pfu/tumor). The mechanism for this is not clear.

It is well known that cancer progression is due to uncontrolled growth of cells. Suppression of cell proliferation as evidenced by a reduction in Ki67+ cells was observed in tumors. In virus uninfected areas, the mean number of Ki67+ cells was almost the same between PBS and GLV-1h68-treated groups and it was almost ten-fold higher in virus infected areas, indicating that viral oncolysis of tumor cells directly suppressed cell growth when it successfully colonized and replicated in tumors. There was no significant difference in the mean numbers of Ki67+ cells among the groups, which demonstrated that the cell killing ability of VACVs was almost the same. However, in uninfected areas of tumors treated with VACVs expressed antibodies, the mean numbers of Ki67+ cells were much lower than that of GLV-1h68-treated tumors. Among them GLV-1h164 or GLV-1h282-treated tumors was about one third or half of GLV-1h68, which meant blocking of VEGF or FAP would slightly suppress cell proliferation, whereas blocking EGFR significantly reduced cell proliferation, resulting in suppression of tumor growth.

Tumor growth and cancer development also require continuous support of nutrition and structural sustainment from the tumor microenvironment (Pietras and Ostman 2010; Xing, Saidou et al. 2010). Reduction of angiogenesis and blood vessels was observed in antibody expressing VACV infected areas, as previously reported (Frentzen, Yu et al. 2009). The mean number of CD31+ cells in virus infected areas was less than in uninfected areas, which meant viral replication destroyed blood vessels directly. BVD in uninfected areas of GLV-1h164-treated tumors was significantly lower than in GLV-1h68-treated tumors, which proved that VEGF targeted GLAF-2 expressing VACVs spread inside the tumor and suppressed BVD. In virus infected areas, the mean numbers of CD31+ cells in tumors treated with GLAF-2 expressing VACVs and GLAF-5 expressing GLV-1h282 were significantly lower than GLV-1h68-treated tumors, as previously described (Frentzen, Yu et al.

2009). However, there was no dramatic difference in the mean number of CD31+ cells between GLV-1h68 and GLV-1h442-treated groups, indicating that the anti-EGFRVHHFLAG nanobody may not have an effect on BVD.

Overall in our study, VACV mediated suppression of cell proliferation and angiogenesis directly resulting in tumor regression while virally expressed antibody targeting EGFR reduced cell proliferation and GLAF-2 targeting VEGF and GLAF-5 targeting FAP suppressed angiogenesis. Simultaneously expressing two antibodies targeting both cell proliferation and angiogenesis additively destroyed the tumor microenvironment, thus enhancing virotherapy.

In summary, the results presented here show that two antibodies expressed by VACVs significantly improved anti-tumor therapy in human xenograft mouse models through simultaneous suppression of cell proliferation and angiogenesis. This efficacy was superior to their parental viruses, that expressed either no antibodies or single antibodies, and was far superior to treatment with the commercially available antibodies, Avastin and/or Erbitux alone. The VACVs are able to specifically locate and replicate in tumors and continuously produce antibodies, which can circumvent deficiencies of poor tumor penetration and tumor targeting of the commercially available antibodies, thus providing promising candidates for cancer treatment.

5.4 Conclusion

Back to 1889, an English surgeon Stephen Paget raised a hypothesis, named as Paget's Seed and soil hypothesis later, was that he compared the tumor cells with the seed of plants in that both of them "carried in all directions; but they can only live and grow if they fall on congenial soil" (Paget 1889). In the past years, research mainly focusing on the cancer cells and genome-centred models resulted in identification of many oncogenes or tumor suppression genes (Fidler 2003; Mueller and Fusenig

2004), but limited success was achieved for anticancer therapy by the fact that cancer still contributes the second cause of death in the world and with an estimated 12.7 million new cancer cases worldwide in 2008. The partial reason of unsuccessful was due to the overlook of the roles of stroma in cancers, which played an important role in cancer initiation, progression, development, invasion and metastasis. Among them, we chose three directions to be targeted: FAP, EGFR and VEGF.

In recent years, oncolytic virotherapy especially vaccinia virus has emerged as one of the most promising approaches for anti-cancer therapy, offering high selectivity tropism for cancers and little side effects. In our laboratory, GLV-1h68 has been shown to enter, locate in, replicate in and lyse cancer cells in vivo in human xenograft mice models (Zhang, Yu et al. 2007). This virus is currently under phase II clinical trials. We demonstrated that one VACV expressing scAb blocking VEGF (GLV-1h108) significantly enhanced anti-cancer therapy in preclinical trials through decreasing blood vessels in tumor stroma (Frentzen, Yu et al. 2009).

Here, a similar strategy was used to treat cancers by utilizing antibodies expressed by vaccinia viruses. Several new recombinant replication-competent vaccinia viruses were constructed: anti-FAP scAb-encoding VACV (GLV-1h282) and anti-EGFRVHHFLAG nanobody encoding VACV (GLV-1h442) by replacing into the *J2R* locus with the antibody-expression cassettes with GLV-1h68 backbone as well as two- antibodies co-expressing VACVs (GLV-1h444 encodes anti-VEGF and anti-EGFRVHH antibodies; GLV-1h446 encodes anti-VEGF and anti-FAP antibodies) by replacing into the *J2R* locus with the cassettes with GLV-1h164 backbone (anti-VEGF cassette in *A56R* locus). In addition, the experiments were designed to study VACV-mediated and scAb-facilitated oncolytic virotherapy in combination with immunotherapy in virus-colonized tumors.

The inserted cassette sequences were confirmed before the viruses were amplified and purified. Expression of the antibodies in viruses-infected cell lines was tested with FLAG tag or G6 antibody (customized antibody specifically targeting the scAb backbone) as well as were purified using an IP assay kit. Expression of the

antibodies did not have negative effects on viral replication efficacy and viral cell killing ability in several cell lines. To demonstrate the therapeutic efficacy of the new viruses *in vivo*, several types of tumor-bearing mice were delivered with different VACVs with or without combined immunotherapy (Avastin and/or Erbitux) and the changes of the tumor volume and mice body weight were monitored once a week. After the antibody-expressing VACV treatment, the growth of tumor was delayed or inhibited and the volume of the tumor size was significantly smaller than the counterpart of PBS- or GLV-1h68-treated group, which indicating expression of the antibodies led to an enhanced therapeutic effects *in vivo*. The enhancement may be caused by the continuous production of antibodies in colonized tumors. The changes of the body weight of mice injected with antibody-expressing VACV was similar with that of the GLV-1h68-treated mice, which indicated that the new viruses were low toxic for the mice. In addition the virus titers and viral distribution at 14 d.p.i. were also documented. The viral titers in GLV-1h282-treated tumors were significantly higher than that in GLV-68-treated tumors, contributed the enhanced oncolytic efficacy. The viral titers in other VACV-treated or concomitant treated groups of animals (GLV-1h68 with Avastin or Erbitux) were slightly different to that in the GLV-1h68-treated mice. Decrease of the angiogenesis in tumors after antibodies expressing VACVs treatment was also demonstrated by immunohistochemistry staining.

It is well known that continuous tumor growth requires stroma support including neoangiogenesis (Kobayashi and Lin 2006). High level expression of FAP, EGFR and/or VEGF is attributable to the poor outcome of the treatments in patients. Therefore, developing methods of the inhibiting of the expression or function of FAP, EGFR or VEGF is very urgent! There are no available inhibitors exclusively targeting FAP (Pure 2009); antibodies targeting FAP did not exhibit therapeutic success in patients (Hofheinz, al-Batran et al. 2003; Scott, Wiseman et al. 2003) or potential therapeutic application in clinic (Cheng, Dunbrack et al. 2002). In this study, the VACV expressing anti-FAP scAb showed therapeutic efficacy in xenograft-bearing mice through decreasing the angiogenesis in tumors. However the details of the

molecular mechanism are still unknown. GLV-1h68 was shown to be well tolerated in phase I clinical trial and now is under phase II trial. Insertion of an expression cassette into GLV-1h68 offers apparently a promising future in cancer therapy. Erbitux and Avastin are common commercial monoclonal antibodies in the market. However, they showed very promising results in preclinical trials, but limited efficacy and side effects were reported in patients. Erbitux did not significantly affect overall survival rates in metastasized colorectal patients with KRAS wild-type tumors and failed to benefit the patients with less metastasized colorectal cancers (Bokemeyer, Bondarenko et al. 2009; Van Cutsem, Kohne et al. 2009; Gatzemeier, von Pawel et al. 2011). Avastin exhibited limited success in patients when used in the treatment of metastatic colorectal and non-small cell lung cancer patients and may cause high side effects (Quesada, Medina et al. 2007; Sliesoraitis and Tawfik 2011). The deficiency of Avastin and Erbitux may partially be attributable to the slow circulation and poor penetration of the antibodies into the tumor tissue from the blood after systemic treatment or to the heterogeneous biologic and pathologic group in tumor tissues. Thence, high doses and continuous productivity of small size antibodies in oncolytic viruses expressing scAb or nanobody will resolve the problems as well as in combination with virotherapy to perform “multi-target” on stroma and cancer cells simultaneously.

In conclusion, the study here clearly show that the VACV-encoded antibodies (anti-FAP, anti-EGFR, anti-VEGF, anti-VEGF and anti-EGFR as well as anti-VEGF and anti-FAP) significantly improved anti cancer therapy in xenograft models partially due to decreasing angiogenesis in tumor tissues. The efficacy is superior to the treatment with GLV-1h68 alone and with Avastin or Erbitux alone. The expression of the antibodies can be detected in mice sera and tumor lysis. These findings support the assumption that the therapeutic antibody-expressing vaccinia viruses improve an anti-cancer therapy.

References

- Advani, S. J., L. Buckel, et al. (2012). "Preferential replication of systemically delivered oncolytic vaccinia virus in focally irradiated glioma xenografts." Clin Cancer Res **18**(9): 2579-2590.
- Aertgeerts, K., I. Levin, et al. (2005). "Structural and kinetic analysis of the substrate specificity of human fibroblast activation protein alpha." J Biol Chem **280**(20): 19441-19444.
- Aggarwal, S., W. N. Brennen, et al. (2008). "Fibroblast activation protein peptide substrates identified from human collagen I derived gelatin cleavage sites." Biochemistry **47**(3): 1076-1086.
- Agrawal, R., P. Sladkevicius, et al. (1998). "Serum vascular endothelial growth factor concentrations and ovarian stromal blood flow are increased in women with polycystic ovaries." Hum Reprod **13**(3): 651-655.
- Alberts, S. R., D. J. Sargent, et al. (2012). "Effect of oxaliplatin, fluorouracil, and leucovorin with or without cetuximab on survival among patients with resected stage III colon cancer: a randomized trial." JAMA **307**(13): 1383-1393.
- Alt, E., Y. Yan, et al. (2011). "Fibroblasts share mesenchymal phenotypes with stem cells, but lack their differentiation and colony-forming potential." Biol Cell **103**(4): 197-208.
- Bae, S., C. W. Park, et al. (2008). "Fibroblast activation protein alpha identifies mesenchymal stromal cells from human bone marrow." Br J Haematol **142**(5): 827-830.
- Bell, A., Z. J. Wang, et al. (2010). "Differential tumor-targeting abilities of three single-domain antibody formats." Cancer Lett **289**(1): 81-90.
- Bennouna, J., J. Sastre, et al. (2013). "Continuation of bevacizumab after first progression in metastatic colorectal cancer (ML18147): a randomised phase 3 trial." Lancet Oncol **14**(1): 29-37.
- Bergers, G. and D. Hanahan (2008). "Modes of resistance to anti-angiogenic therapy." Nat Rev Cancer **8**(8): 592-603.
- Blasco, R. and B. Moss (1992). "Role of cell-associated enveloped vaccinia virus in cell-to-cell spread." J Virol **66**(7): 4170-4179.
- Bogaert, E., P. Van Damme, et al. (2006). "Vascular endothelial growth factor in amyotrophic lateral sclerosis and other neurodegenerative diseases." Muscle Nerve **34**(4): 391-405.
- Bokemeyer, C., I. Bondarenko, et al. (2009). "Fluorouracil, leucovorin, and oxaliplatin with and without cetuximab in the first-line treatment of metastatic colorectal cancer." J Clin Oncol **27**(5): 663-671.
- Brocks, B., P. Garin-Chesa, et al. (2001). "Species-crossreactive scFv against the tumor stroma marker "fibroblast activation protein" selected by phage display from an immunized FAP-/- knock-out mouse." Mol Med **7**(7): 461-469.
- Buckel, L., S. J. Advani, et al. (2013). "Combination of fractionated irradiation with anti-VEGF expressing vaccinia virus therapy enhances tumor control by simultaneous radiosensitization of tumor associated endothelium." Int J Cancer.
- Cattaneo, R., T. Miest, et al. (2008). "Reprogrammed viruses as cancer therapeutics: targeted, armed and shielded." Nat Rev Microbiol **6**(7): 529-540.

- Chang, J. H., N. K. Garg, et al. (2012). "Corneal neovascularization: an anti-VEGF therapy review." Surv Ophthalmol **57**(5): 415-429.
- Chen, N., Q. Zhang, et al. (2009). "A novel recombinant vaccinia virus expressing the human norepinephrine transporter retains oncolytic potential and facilitates deep-tissue imaging." Mol Med **15**(5-6): 144-151.
- Chen NG, S. A. (2010). "Oncolytic vaccinia virus: a theranostic agent for cancer." Future Virol **5**: 763-784.
- Chen, N. G., Y. A. Yu, et al. (2011). "Replication efficiency of oncolytic vaccinia virus in cell cultures prognosticates the virulence and antitumor efficacy in mice." J Transl Med **9**: 164.
- Cheng, J. D., R. L. Dunbrack, Jr., et al. (2002). "Promotion of tumor growth by murine fibroblast activation protein, a serine protease, in an animal model." Cancer Res **62**(16): 4767-4772.
- Christiansen, V. J., K. W. Jackson, et al. (2007). "Effect of fibroblast activation protein and alpha2-antiplasmin cleaving enzyme on collagen types I, III, and IV." Arch Biochem Biophys **457**(2): 177-186.
- Cirri, P. and P. Chiarugi (2011). "Cancer associated fibroblasts: the dark side of the coin." Am J Cancer Res **1**(4): 482-497.
- Cohen, S. J., R. K. Alpaugh, et al. (2008). "Fibroblast activation protein and its relationship to clinical outcome in pancreatic adenocarcinoma." Pancreas **37**(2): 154-158.
- Cortez-Retamozo, V., M. Lauwereys, et al. (2002). "Efficient tumor targeting by single-domain antibody fragments of camels." Int J Cancer **98**(3): 456-462.
- Dohi, O., H. Ohtani, et al. (2009). "Histogenesis-specific expression of fibroblast activation protein and dipeptidylpeptidase-IV in human bone and soft tissue tumours." Histopathology **55**(4): 432-440.
- Dumoulin, M., K. Conrath, et al. (2002). "Single-domain antibody fragments with high conformational stability." Protein Sci **11**(3): 500-515.
- Edosada, C. Y., C. Quan, et al. (2006). "Selective inhibition of fibroblast activation protein protease based on dipeptide substrate specificity." J Biol Chem **281**(11): 7437-7444.
- Falkner, F. G. and B. Moss (1990). "Transient dominant selection of recombinant vaccinia viruses." J Virol **64**(6): 3108-3111.
- Fan Cai, F. P., Chunting Wang, Zhiyong Li, Shuang Xian, Yuquan Wei. (2012). "Effect of short hairpin RNA targeting of fibroblast activation protein on tumor growth and angiogenesis in a 4T1 murine breast cancer model." 2012 ASCO Annual Meeting from http://www.asco.org/ASCOv2/Meetings/Abstracts?&vmview=abst_detail_view&confID=114&abstractID=92258.
- Ferrara, N. (2004). "Vascular endothelial growth factor: basic science and clinical progress." Endocr Rev **25**(4): 581-611.
- Fidler, I. J. (2003). "The pathogenesis of cancer metastasis: the 'seed and soil' hypothesis revisited." Nat Rev Cancer **3**(6): 453-458.
- Fischer, E., K. Chaitanya, et al. (2012). "Radioimmunotherapy of fibroblast activation protein positive tumors by rapidly internalizing antibodies." Clin Cancer Res **18**(22): 6208-6218.
- Folkman, J., K. Watson, et al. (1989). "Induction of angiogenesis during the transition from hyperplasia to neoplasia." Nature **339**(6219): 58-61.
- Frentzen, A., Y. A. Yu, et al. (2009). "Anti-VEGF single-chain antibody GLAF-1 encoded by oncolytic vaccinia virus significantly enhances antitumor therapy." Proc Natl Acad Sci U S A **106**(31): 12915-12920.

- Gatzemeier, U., J. von Pawel, et al. (2011). "First-cycle rash and survival in patients with advanced non-small-cell lung cancer receiving cetuximab in combination with first-line chemotherapy: a subgroup analysis of data from the FLEX phase 3 study." Lancet Oncol **12**(1): 30-37.
- Gorrell, M. D., X. M. Wang, et al. (2003). "Intrahepatic expression of collagen and fibroblast activation protein (FAP) in hepatitis C virus infection." Adv Exp Med Biol **524**: 235-243.
- Gottlin, E. B., G. Xiangrong, et al. (2009). "Isolation of novel EGFR-specific VHH domains." J Biomol Screen **14**(1): 77-85.
- Hanahan, D. and R. A. Weinberg (2000). "The hallmarks of cancer." Cell **100**(1): 57-70.
- Hanahan, D. and R. A. Weinberg (2011). "Hallmarks of cancer: the next generation." Cell **144**(5): 646-674.
- Harari, P. M. (2004). "Epidermal growth factor receptor inhibition strategies in oncology." Endocr Relat Cancer **11**(4): 689-708.
- Harrison, S. C., B. Alberts, et al. (2004). "Discovery of antivirals against smallpox." Proc Natl Acad Sci U S A **101**(31): 11178-11192.
- Havre, P. A., M. Abe, et al. (2008). "The role of CD26/dipeptidyl peptidase IV in cancer." Front Biosci **13**: 1634-1645.
- Henderson, D. and B. Moss (1988). Smallpox and Vaccinia. Vaccines (3rd ed.). P. SA and O. WA. Philadelphia, Pennsylvania, WB Saunders.
- Henry, L. R., H. O. Lee, et al. (2007). "Clinical implications of fibroblast activation protein in patients with colon cancer." Clin Cancer Res **13**(6): 1736-1741.
- Herbst, R. S. (2002). "Targeted therapy in non-small-cell lung cancer." Oncology (Williston Park) **16**(9 Suppl 9): 19-24.
- Herbst, R. S., A. Onn, et al. (2005). "Angiogenesis and lung cancer: prognostic and therapeutic implications." J Clin Oncol **23**(14): 3243-3256.
- Hoeben, A., B. Landuyt, et al. (2004). "Vascular endothelial growth factor and angiogenesis." Pharmacol Rev **56**(4): 549-580.
- Hofheinz, R. D., S. E. al-Batran, et al. (2003). "Stromal antigen targeting by a humanised monoclonal antibody: an early phase II trial of sibtuzumab in patients with metastatic colorectal cancer." Onkologie **26**(1): 44-48.
- Huang, L., L. O. Gaijkan, et al. (2008). "SPECT imaging with 99mTc-labeled EGFR-specific nanobody for in vivo monitoring of EGFR expression." Mol Imaging Biol **10**(3): 167-175.
- Huang, Y., A. E. Simms, et al. (2011). "Fibroblast activation protein- α promotes tumor growth and invasion of breast cancer cells through non-enzymatic functions." Clin Exp Metastasis **28**(6): 567-579.
- Iqbal, U., U. Trojahn, et al. (2010). "Kinetic analysis of novel mono- and multivalent VHH-fragments and their application for molecular imaging of brain tumours." Br J Pharmacol **160**(4): 1016-1028.
- Iwasa, S., X. Jin, et al. (2003). "Increased expression of seprase, a membrane-type serine protease, is associated with lymph node metastasis in human colorectal cancer." Cancer Lett **199**(1): 91-98.
- Jain, M., S. C. Chauhan, et al. (2005). "Penetratin improves tumor retention of single-chain antibodies: a novel step toward optimization of radioimmunotherapy of solid tumors." Cancer Res **65**(17): 7840-7846.
- Jain, R. K. (2001). "Delivery of molecular and cellular medicine to solid tumors." Adv Drug Deliv Rev **46**(1-3): 149-168.

- Kakarla, S., K. K. Chow, et al. (2013). "Antitumor Effects of Chimeric Receptor Engineered Human T Cells Directed to Tumor Stroma." *Mol Ther*.
- Kalluri, R. and M. Zeisberg (2006). "Fibroblasts in cancer." *Nat Rev Cancer* **6**(5): 392-401.
- Karapetis, C. S., S. Khambata-Ford, et al. (2008). "K-ras mutations and benefit from cetuximab in advanced colorectal cancer." *N Engl J Med* **359**(17): 1757-1765.
- Kelly, T. (2005). "Fibroblast activation protein-alpha and dipeptidyl peptidase IV (CD26): cell-surface proteases that activate cell signaling and are potential targets for cancer therapy." *Drug Resist Updat* **8**(1-2): 51-58.
- Kobayashi, H. and P. C. Lin (2006). "Antiangiogenic and radiotherapy for cancer treatment." *Histol Histopathol* **21**(10): 1125-1134.
- Komurasaki, T., H. Toyoda, et al. (1997). "Epiregulin binds to epidermal growth factor receptor and ErbB-4 and induces tyrosine phosphorylation of epidermal growth factor receptor, ErbB-2, ErbB-3 and ErbB-4." *Oncogene* **15**(23): 2841-2848.
- Levy, M. T., G. W. McCaughan, et al. (1999). "Fibroblast activation protein: a cell surface dipeptidyl peptidase and gelatinase expressed by stellate cells at the tissue remodelling interface in human cirrhosis." *Hepatology* **29**(6): 1768-1778.
- Levy, M. T., G. W. McCaughan, et al. (2002). "Intrahepatic expression of the hepatic stellate cell marker fibroblast activation protein correlates with the degree of fibrosis in hepatitis C virus infection." *Liver* **22**(2): 93-101.
- Liang, W. C., X. Wu, et al. (2006). "Cross-species vascular endothelial growth factor (VEGF)-blocking antibodies completely inhibit the growth of human tumor xenografts and measure the contribution of stromal VEGF." *J Biol Chem* **281**(2): 951-961.
- Liao, D., Y. Luo, et al. (2009). "Cancer associated fibroblasts promote tumor growth and metastasis by modulating the tumor immune microenvironment in a 4T1 murine breast cancer model." *PLoS One* **4**(11): e7965.
- Mamot, C. and C. Rochlitz (2006). "Targeting the epidermal growth factor receptor (EGFR)--a new therapeutic option in oncology?" *Swiss Med Wkly* **136**(1-2): 4-12.
- Manegold, C. (2008). "Bevacizumab for the treatment of advanced non-small-cell lung cancer." *Expert Rev Anticancer Ther* **8**(5): 689-699.
- Mathew, S., M. J. Scanlan, et al. (1995). "The gene for fibroblast activation protein alpha (FAP), a putative cell surface-bound serine protease expressed in cancer stroma and wound healing, maps to chromosome band 2q23." *Genomics* **25**(1): 335-337.
- Meadows, K. L. and H. I. Hurwitz (2012). "Anti-VEGF therapies in the clinic." *Cold Spring Harb Perspect Med* **2**(10).
- Meadows, S. A., C. Y. Edosada, et al. (2007). "Ala657 and conserved active site residues promote fibroblast activation protein endopeptidase activity via distinct mechanisms of transition state stabilization." *Biochemistry* **46**(15): 4598-4605.
- Mendelsohn, J. and J. Baselga (2003). "Status of epidermal growth factor receptor antagonists in the biology and treatment of cancer." *J Clin Oncol* **21**(14): 2787-2799.
- Mercurio, A. M., E. A. Lipscomb, et al. (2005). "Non-angiogenic functions of VEGF in breast cancer." *J Mammary Gland Biol Neoplasia* **10**(4): 283-290.
- Mersmann, M., A. Schmidt, et al. (2001). "Human antibody derivatives against the fibroblast activation protein for tumor stroma targeting of carcinomas." *Int J Cancer* **92**(2): 240-248.
- Micke, P. and A. Ostman (2004). "Tumour-stroma interaction: cancer-associated fibroblasts as novel targets in anti-cancer therapy?" *Lung Cancer* **45 Suppl 2**: S163-175.
- Mifflin, R. C., I. V. Pinchuk, et al. (2011). "Intestinal myofibroblasts: targets for stem cell therapy." *Am J Physiol Gastrointest Liver Physiol* **300**(5): G684-696.

-
- Mueller, M. M. and N. E. Fusenig (2004). "Friends or foes - bipolar effects of the tumour stroma in cancer." Nat Rev Cancer **4**(11): 839-849.
- Narra, K., S. R. Mullins, et al. (2007). "Phase II trial of single agent Val-boroPro (Talabostat) inhibiting Fibroblast Activation Protein in patients with metastatic colorectal cancer." Cancer Biol Ther **6**(11): 1691-1699.
- Nicholson, R. I., J. M. Gee, et al. (2001). "EGFR and cancer prognosis." Eur J Cancer **37 Suppl 4**: S9-15.
- Niedermeyer, J., M. Kriz, et al. (2000). "Targeted disruption of mouse fibroblast activation protein." Mol Cell Biol **20**(3): 1089-1094.
- Nyberg, P., T. Salo, et al. (2008). "Tumor microenvironment and angiogenesis." Front Biosci **13**: 6537-6553.
- Oliveira, S., G. A. van Dongen, et al. (2012). "Rapid visualization of human tumor xenografts through optical imaging with a near-infrared fluorescent anti-epidermal growth factor receptor nanobody." Mol Imaging **11**(1): 33-46.
- Ostermann, E., P. Garin-Chesa, et al. (2008). "Effective immunoconjugate therapy in cancer models targeting a serine protease of tumor fibroblasts." Clin Cancer Res **14**(14): 4584-4592.
- Paget, S. (1889). "The distribution of secondary growths in cancer of the breast." lancet **1**: 571-573.
- Park, J. E., M. C. Lenter, et al. (1999). "Fibroblast activation protein, a dual specificity serine protease expressed in reactive human tumor stromal fibroblasts." J Biol Chem **274**(51): 36505-36512.
- Patil, S. S., I. Gentshev, et al. (2012). "Virotherapy of canine tumors with oncolytic vaccinia virus GLV-1h109 expressing an anti-VEGF single-chain antibody." PLoS One **7**(10): e47472.
- Pietras, K. and A. Ostman (2010). "Hallmarks of cancer: interactions with the tumor stroma." Exp Cell Res **316**(8): 1324-1331.
- Pufe, T., B. Kurz, et al. (2005). "The influence of biomechanical parameters on the expression of VEGF and endostatin in the bone and joint system." Ann Anat **187**(5-6): 461-472.
- Pure, E. (2009). "The road to integrative cancer therapies: emergence of a tumor-associated fibroblast protease as a potential therapeutic target in cancer." Expert Opin Ther Targets **13**(8): 967-973.
- Quesada, A. R., M. A. Medina, et al. (2007). "Playing only one instrument may be not enough: limitations and future of the antiangiogenic treatment of cancer." Bioessays **29**(11): 1159-1168.
- Rettig, W. J., P. Garin-Chesa, et al. (1993). "Regulation and heteromeric structure of the fibroblast activation protein in normal and transformed cells of mesenchymal and neuroectodermal origin." Cancer Res **53**(14): 3327-3335.
- Rettig, W. J., S. L. Su, et al. (1994). "Fibroblast activation protein: purification, epitope mapping and induction by growth factors." Int J Cancer **58**(3): 385-392.
- Rini, B. I. and W. K. Rathmell (2007). "Biological aspects and binding strategies of vascular endothelial growth factor in renal cell carcinoma." Clin Cancer Res **13**(2 Pt 2): 741s-746s.
- Roberts, E. W., A. Deonarine, et al. (2013). "Depletion of stromal cells expressing fibroblast activation protein-alpha from skeletal muscle and bone marrow results in cachexia and anemia." J Exp Med **210**(6): 1137-1151.

- Roovers, R. C., T. Laeremans, et al. (2007). "Efficient inhibition of EGFR signaling and of tumour growth by antagonistic anti-EGFR Nanobodies." Cancer Immunol Immunother **56**(3): 303-317.
- Rosel, J. and B. Moss (1985). "Transcriptional and translational mapping and nucleotide sequence analysis of a vaccinia virus gene encoding the precursor of the major core polypeptide 4b." J Virol **56**(3): 830-838.
- Salomon, D. S., R. Brandt, et al. (1995). "Epidermal growth factor-related peptides and their receptors in human malignancies." Crit Rev Oncol Hematol **19**(3): 183-232.
- Santos, A. M., J. Jung, et al. (2009). "Targeting fibroblast activation protein inhibits tumor stromagenesis and growth in mice." J Clin Invest **119**(12): 3613-3625.
- Saravia, M., G. Zapata, et al. (2009). "Anti-VEGF monoclonal antibody-induced regression of corneal neovascularization and inflammation in a rabbit model of herpetic stromal keratitis." Graefes Arch Clin Exp Ophthalmol **247**(10): 1409-1416.
- Scanlan, M. J., B. K. Raj, et al. (1994). "Molecular cloning of fibroblast activation protein alpha, a member of the serine protease family selectively expressed in stromal fibroblasts of epithelial cancers." Proc Natl Acad Sci U S A **91**(12): 5657-5661.
- Scott, A. M., G. Wiseman, et al. (2003). "A Phase I dose-escalation study of sibtuzumab in patients with advanced or metastatic fibroblast activation protein-positive cancer." Clin Cancer Res **9**(5): 1639-1647.
- Sliesoraitis, S. and B. Tawfik (2011). "Bevacizumab-induced bowel perforation." J Am Osteopath Assoc **111**(7): 437-441.
- Smith, G. L. and B. Moss (1983). "Infectious poxvirus vectors have capacity for at least 25 000 base pairs of foreign DNA." Gene **25**(1): 21-28.
- Smith, G. L., A. Vanderplasschen, et al. (2002). "The formation and function of extracellular enveloped vaccinia virus." J Gen Virol **83**(Pt 12): 2915-2931.
- Sodeik, B., R. W. Doms, et al. (1993). "Assembly of vaccinia virus: role of the intermediate compartment between the endoplasmic reticulum and the Golgi stacks." J Cell Biol **121**(3): 521-541.
- Spaeth, E. L., J. L. Dembinski, et al. (2009). "Mesenchymal stem cell transition to tumor-associated fibroblasts contributes to fibrovascular network expansion and tumor progression." PLoS One **4**(4): e4992.
- Steiner, P., C. Joynes, et al. (2007). "Tumor growth inhibition with cetuximab and chemotherapy in non-small cell lung cancer xenografts expressing wild-type and mutated epidermal growth factor receptor." Clin Cancer Res **13**(5): 1540-1551.
- Stern, W. and S. Dales (1974). "Biogenesis of vaccinia: concerning the origin of the envelope phospholipids." Virology **62**(2): 293-306.
- Taberero, J. (2007). "The role of VEGF and EGFR inhibition: implications for combining anti-VEGF and anti-EGFR agents." Mol Cancer Res **5**(3): 203-220.
- Tijink, B. M., T. Laeremans, et al. (2008). "Improved tumor targeting of anti-epidermal growth factor receptor Nanobodies through albumin binding: taking advantage of modular Nanobody technology." Mol Cancer Ther **7**(8): 2288-2297.
- Tran, E., D. Chinnasamy, et al. (2013). "Immune targeting of fibroblast activation protein triggers recognition of multipotent bone marrow stromal cells and cachexia." J Exp Med **210**(6): 1125-1135.
- Tulandi, T., A. Saleh, et al. (2000). "Effects of laparoscopic ovarian drilling on serum vascular endothelial growth factor and on insulin responses to the oral glucose tolerance test in women with polycystic ovary syndrome." Fertil Steril **74**(3): 585-588.
- Van Cutsem, E., C. H. Kohne, et al. (2009). "Cetuximab and chemotherapy as initial treatment for metastatic colorectal cancer." N Engl J Med **360**(14): 1408-1417.

-
- van de Water, J. A., T. Bagci-Onder, et al. (2012). "Therapeutic stem cells expressing variants of EGFR-specific nanobodies have antitumor effects." Proc Natl Acad Sci U S A **109**(41): 16642-16647.
- Wang, H., N. G. Chen, et al. (2012). "Oncolytic vaccinia virus GLV-1h68 strain shows enhanced replication in human breast cancer stem-like cells in comparison to breast cancer cells." J Transl Med **10**: 167.
- Wang, X. M., T. W. Yao, et al. (2008). "Fibroblast activation protein and chronic liver disease." Front Biosci **13**: 3168-3180.
- Watanabe, T., A. Shintani, et al. (1994). "Recombinant human betacellulin. Molecular structure, biological activities, and receptor interaction." J Biol Chem **269**(13): 9966-9973.
- Weibel, S., T. C. Basse-Luesebrink, et al. (2013). "Imaging of intratumoral inflammation during oncolytic virotherapy of tumors by 19F-magnetic resonance imaging (MRI)." PLoS One **8**(2): e56317.
- Wells, A. (1999). "EGF receptor." Int J Biochem Cell Biol **31**(6): 637-643.
- Welt, S., C. R. Divgi, et al. (1994). "Antibody targeting in metastatic colon cancer: a phase I study of monoclonal antibody F19 against a cell-surface protein of reactive tumor stromal fibroblasts." J Clin Oncol **12**(6): 1193-1203.
- Wikberg, M. L., S. Edin, et al. (2013). "High intratumoral expression of fibroblast activation protein (FAP) in colon cancer is associated with poorer patient prognosis." Tumour Biol.
- Wong, H. H., N. R. Lemoine, et al. (2010). "Oncolytic Viruses for Cancer Therapy: Overcoming the Obstacles." Viruses **2**(1): 78-106.
- Worschech, A., N. Chen, et al. (2009). "Systemic treatment of xenografts with vaccinia virus GLV-1h68 reveals the immunologic facet of oncolytic therapy." BMC Genomics **10**: 301.
- Xing, F., J. Saidou, et al. (2010). "Cancer associated fibroblasts (CAFs) in tumor microenvironment." Front Biosci **15**: 166-179.
- Yang, X., X. Zhang, et al. (2013). "Cetuximab-mediated tumor regression depends on innate and adaptive immune responses." Mol Ther **21**(1): 91-100.
- Yu, Y. A., C. Galanis, et al. (2009). "Regression of human pancreatic tumor xenografts in mice after a single systemic injection of recombinant vaccinia virus GLV-1h68." Mol Cancer Ther **8**(1): 141-151.
- Zhang, H., S. Yun, et al. (2012). "A dual-targeting antibody against EGFR-VEGF for lung and head and neck cancer treatment." Int J Cancer **131**(4): 956-969.
- Zhang, Q., Y. A. Yu, et al. (2007). "Eradication of solid human breast tumors in nude mice with an intravenously injected light-emitting oncolytic vaccinia virus." Cancer Res **67**(20): 10038-10046.

Abbreviations

%	percent
°C	degree Celsius
α-SMA	alpha smooth muscle actin
μg	microgram
μL	microliter
μm	micrometer
BF	bright field
BSA	bovine serum albumin
CAF	cancer associated fibroblast
CCD	charge-coupled device
CEV	cell-associated enveloped virus
cm ²	centimeter square
CMC	carboxymethylcellulose
CO ²	carbon dioxide
CPE	cytopathic effect
ddH ₂ O	double-distilled H ₂ O
DMEM	Dulbecco's modified Eagle's medium
DNA	deoxyribonucleic acid

Abbreviations

dpi	days post injection
ds	double-stranded
EDTA	diaminoethanetetraacetic acid
EEV	extracellular enveloped virus
ELISA	enzyme-linked immunosorbant assay
EMEM	Eagle's minimal essential medium
EGFR	epidermal growth factor receptor
FAP	fibroblast activation protein
FBS	fetal bovine serum
g	grams
GFP	green fluorescent protein
h	hours
H ₂ O ₂	hydrogen peroxide
HCl	hydrochloric acid
hpi	hours post infection
hpt	hours post treatment
HRP	horseradish peroxidase
IEV	intracellular enveloped virion
IMV	intracellular mature virus
IV	immature virion

Abbreviations

IP	immunoprecipitation
i.p.	intra peritoneal
i.v.	intravenous
kb	kilobase
kDa	kilo Dalton
mg	milligram
min(s)	minute(s)
mL	milliliter
mm	millimeter
mM	millimolar
mm ³	cubic millimeter
mRNA	messenger RNA
MOI	multiplicity of infection
MPA	mycophenolic acid
MRI	magnetic resonance imaging
MVA	modified vaccinia virus
N ₂	nitrogen
NaOH	sodium hydroxide
NEAA	non-essential amino acids
ng	nanogram

Abbreviations

NLS	nuclear localization sequence
nm	nanometer
NMWL	nominal molecular weight limit
PBS	phosphate buffered saline
PCR	polymerase chain reaction
PDT	photodynamic therapy
PET	positron emission tomography
PFA	paraformaldehyde
pfu	plaque forming units
pg	picogram
pH	potential hydrogenii
PI	propidium iodide
PMSF	phenylmethylsulfonyl fluoride
PVDF	polyvinylidene difluoride
RNA	ribonucleic acid
r.o.	retro-orbital
rpm	rounds per minute
RPMI	Roswell Park Memorial Institute medium
RT	room temperature
RT-PCR	reverse transcriptase polymerase chain reaction

Abbreviations

Ruc	<i>Renilla</i> luciferase
scAb	single chain antibody
SDS-PAGE	sodium dodecyl sulfate polyacrylamide gel electrophoresis
sec or s.	second
TRITC	tetramethylrhodamine isothiocyanat
UV	ultra violet
VEGF	vascular endothelial growth factor
WB	Western blot
w/v	weight per volume

Publication

Master:

- 1. Ting Huang[#]**, Wei Wang[#], Mael Bessaud[#], Peijun Ren, Jun Sheng, Huajie Yan Jing Zhang, Xin Lin, Yongjin Wang, Francis Delpeyroux, Vincent Deubel
Evidence of Recombination and Genetic Diversity in Human Rhinoviruses in Children with Acute Respiratory Infection. PLOS ONE, 2009 Jul 27;4 (7):e6355
(# Authors contributed equally)
New York Times reported
<http://www.nytimes.com/2009/11/17/health/17real.html? r=0>

Ph.D:

- 2. Ting Huang**, Huiqiang Wang, Nanhai Chen, Alexa Frentzen, Boris Minev, Joseph Cappello, Aladar A. Szalay
Expression of Anti-VEGF Antibody Together with Anti-EGFR or Anti-FAP Drastically Enhances Tumor Regression as a Result of Vaccinia Virotherapy
(*Nature Medicine*, submission)

Curriculum Vitae

Name: Ting Huang
Date of Birth: 03.03.1983
Place of Birth: Jiang Su, China
Nationality: China
Address: 3076 Via Alicante K
La Jolla, CA 92037, USA

Education:

09/2001-06/2005 Undergraduate study in YangZhou University
09/2005-06/2009 Graduate study in Institut Pasteur of Shanghai, Chinese Academy of Sciences

Current Status:

Since 2/2010 Ph.D candidate in AG Szalay of Julius-Maximilians-Universität Würzburg and Genelux Corporation, San Diego, USA

Ting Huang, 2013

Acknowledgements

First I would like to thank my doctoral father Prof. Dr. A. Szalay to give me the great opportunity to take these interesting and important projects with his smart suggestions, guidance and encouragements for the past three and half years.

Second, I want to thank all the members in the laboratory of “AG Szalay” from University of Wuerzburg for their helpful cooperation when I was in Germany. Many thanks to Ms. Johanna Langbein-Laugwitz, Dr. Jochen Strizker, Dr. Julia Strom, Dr. Barbara Härtl, PD Dr. Ivaylo Gentshev and especial appreciation to Dr. Marion Adelfinger for her kind and nice help of printing my thesis, to Prof. Dr. Grummt for his advice, help and critical proof-reading of my Ph.D thesis. Also, I would like to thank Ms. Farah Badbanchi for her kind treat and encouragement.

Third, I also want to appreciate all the members in Genelux Corporation in San Diego for their help, support and the great teamwork environment they provide for me. Sincere thanks are given to Dr. Alexa Frentzen for her guidance and advice, Dr. Nanhai G. Chen for his guidance, suggestions and critical proof-reading of all of my manuscripts, Dr. Qian Zhang for her helpful advice and Dr. Joseph Cappello for his critical revision of my manuscripts and thesis. In addition, I appreciate Mr. Terry Trevino, Mr. Jason Aguilar and Ms. Melody Jing for their technical support, and Ms. Camha Hoang for her assistance. I also would like to thank Dr. Ying Wang (Shanghai Jiaotong University, China) to provide the plasmid pGH-anti-EGFRVHH for us.

Forth, I would like to thank Prof. Dr. Krohne for his review of my thesis and being as my second reviewer.

Fifth, I am very grateful for the financial support from the fund of Genelux Corporation.

Acknowledgements

The last, I want to appreciate all my families, my parents and my husband for their kind and warm support. I cannot go through the challenges, difficulties and get my Ph.D finally without their encouragement.

Erklärung gemäß § 4 Absatz 3 der Promotionsordnung der Fakultät für Biologie der Julius-Maximiliansuniversität Würzburg:

Hiermit erkläre ich, die vorgelegte Dissertation selbständig angefertigt zu haben und keine anderen als die von mir angegebenen Quellen und Hilfsmittel verwendet zu haben.

Des Weiteren erkläre ich, dass die vorliegende Arbeit weder in gleicher noch in ähnlicher Form bereits in einem anderen Prüfungsverfahren vorgelegen hat.

Zuvor habe ich neben dem akademischen Grad „Master of Natural Science Microbiology, Graduate University of CAS“ keine akademischen Grade erworben oder zu erwerben versucht.

Die vorliegende Arbeit wurde von Prof. Dr. A. A. Szalay betreut.

Würzburg, den _____

Ting Huang